

**Design of Novel Antigen-Specific Immunotherapies for the Treatment of  
Autoimmune Disorders**

Copyright 2017

Chad James Pickens

Submitted to the graduate degree program in Pharmaceutical Chemistry and the  
Graduate Faculty of the University of Kansas in partial fulfillment of the  
requirements for the degree of Doctor of Philosophy.

---

Chairperson Dr. Cory Berkland

---

Dr. C. Russell Middaugh

---

Dr. William Picking

---

Dr. Thomas Tolbert

---

Dr. Thomas Prisinzano

Date Defended: June 29<sup>th</sup>, 2017

The Dissertation Committee for Chad James Pickens certifies that  
this is the approved version of the following dissertation:

**Design of Novel Antigen-Specific Immunotherapies for the Treatment of  
Autoimmune Disorders**

---

Chairperson Dr. Cory Berkland

Date Approved: June 29<sup>th</sup>, 2017

## **Abstract**

Autoimmune disorders are a challenging problem for both afflicted patients and pharmaceutical scientists, since they involve one of the most complex biological systems – the immune system. A dysregulation of antigen recognition is at the center of autoimmune disorders, and can occur in a variety of host tissues throughout the body. Further complicating these diseases is the high degree of variability in terms of clinical manifestation. Traditional therapies for autoimmune disorders, such as corticosteroids or immunomodulators, generally focus on symptom suppression or slowing disease progression rather than treating the underlying cause, which is rarely fully understood. New approaches to treatments in which a disease-causing autoantigen is known seek to leverage antigen specificity through the development of antigen-specific immunotherapies (ASIT).

In this research, we explore different novel approaches to ASIT focused on chemical conjugation, including the design and development of a new therapeutic class, antigen-drug conjugates (AgDCs). By reversing the paradigm of antibody-drug conjugates (ADCs), AgDCs exploit the directing effect of the autoantigen towards diseased cell populations, coupled with the immunomodulatory effects of a small molecule drug. Soluble Antigen Arrays (SAgAs) focus on disrupting immune recognition at the immunological synapse by conjugating autoantigen on a multivalent polymer support. Polymer-drug conjugates also present a unique opportunity as a depot delivery system with the potential for targeted applications. The strategies presented here carry an overarching goal to increase therapeutic specificity while limiting off-target effects, in an attempt to develop improved treatments with better efficacy and safety profiles for patients.

## Acknowledgements

I would first like to thank my advisor, Cory Berkland, for providing guidance, intellectual freedom and flexibility throughout my time in graduate school. I would also like to thank the department of Pharmaceutical Chemistry at KU for providing me with the opportunity to learn from intellectual leaders in the field, who have shared their knowledge and experience with me, and to the faculty members who participated in my dissertation and oral exam committees: Teruna Siahaan, Tom Tolbert, Russ Middaugh, Bill Picking, Wendy Picking, and Tom Prisinzano. I am grateful for the support of the Howard Rytting pre-doctoral fellowship and the NIH dynamic aspects of chemical biology training grant for financial support during my training. I would specifically like thank Tom Prisinzano, Audrey Lamb, and Paul Hanson for their leadership, guidance, and helpful discussions along the way.

The research presented here would not be possible without contributions from many other scientists. In chapter 3, Matt Christopher has been my primary collaborator and contributed *in vivo* and *in vitro* assay data, in addition to improving my understanding of immunology and the mechanisms behind disease. In chapter 4, Brittany Hartwell was my collaborator and co-author, contributing bioassays, *in vivo* data, and an endless pursuit of scientific understanding. Martin Leon has also been a key contributor throughout my research as a fellow synthetic chemist, providing countless hours of discussion, data review and ideas. Lorena Antunez has provided me with the opportunity to expand my training in protein chemistry through work not covered in this dissertation. Melissa Pressnall has been a valuable contributor to my research, allowing me to focus on compiling this dissertation while contributing necessary stability data.

I would also like to thank the many other scientists that contributed to my research or education during my time in graduate school: Brad Sullivan, Josh Sestak, Chris Kuehl, Nabil

Alhakamy, Laura Northrup, Connor Dennis, Nashwa El-Gendy, Sinkome (Kim) Tima, Sawlee (Ben) Saosathan, Danny Griffin, Jian Qian, Jimmy Song, Shara Thati, Stephanie Johnson, Jeanie Salash, Sam Peterson, and Bailey Brooks, Justin Douglas, Sarah Neuenswander, Rupesh Bommana, Ishan Shah, Ryan Moulder, Peter Kleindl, Brian Kopec, Indira Prajapati, and Derek White. Additionally, I would like to thank my undergraduate research advisor, John Keana (University of Oregon), for guidance and training in my scientific pursuits, and Marshall Crew, Ryan Minikis, and Sanjay Konagurthu (Agere Pharmaceuticals) for rapid and extensive training in the pharmaceutical industry. I would also like to thank Paul Walsh and Justin Pennington for providing me with an internship opportunity at Merck during my graduate training. My sincere thanks goes to the many friends and mentors in both industry and academia that I have made along my journey.

Finally, I would like to thank my family for their love and support throughout my life. To my parents, Jim and Margie, my brother, Jesse, and sister-in-law, Uyen, thank you for all you have done, it wouldn't have been possible without you.

## Table of Contents

<b>CHAPTER 1: Introduction to Autoimmune Disorders and Current Treatment Approaches</b>	<b>2</b>
1.1. Introduction to autoimmune disorders	2
1.2. Current treatment approaches for autoimmune disorders	3
1.3. Antigen-specific immunotherapy (ASIT)	4
1.4. Clinical precedence of immune cell targeting using ASIT co-delivery: antibody-drug conjugates (ADCs)	5
1.5. Overview of dissertation	6
<b>CHAPTER 2: Introduction to Bioconjugation via Azide-Alkyne Cycloaddition: Challenges, Considerations, and Limitations</b>	<b>11</b>
2.1. Introduction	11
2.2. Azide-Alkyne Cycloaddition Reaction	11
2.3. Amidation using <i>N</i> -Hydroxysuccinimidyl (NHS) Esters	15
2.4. Thioether Formation to Install Azide and Alkyne Groups	17
2.5. Solid-phase peptide synthesis	18
2.5.1. Amino acid mimics	18
2.5.2. Heterobifunctional linkers	19
2.6. Metabolic labeling methods	20
2.6.1. Amino acid mimics	21
2.6.2. Post-translation modifications	22
2.6.3. Nucleic acids and other anchors for live cell bioconjugation	23
2.7. Payload molecules for modulating biomolecule function	24
2.8. Challenges associated with bioconjugates	26
2.8.1. Synthetic and analytical considerations	26
2.8.2. Biological consequences of solubility	29
2.8.3. Linker stability	30
2.8.4. Conjugation site and loading	32
2.9. Conclusions and Future Directions	33
<b>CHAPTER 3: Antigen-Drug Conjugates as a Novel Therapeutic Class for Antigen-Specific Autoimmune Disorders</b>	<b>35</b>
3.1. Introduction	35
3.2. Materials and Methods	37
3.2.1. Synthetic procedures	38
3.2.1.1. Synthesis of DBCO-functionalized Rhodamine B (Rhod-DBCO)	38
3.2.1.2. Synthesis of azide-functionalized dexamethasone (Dex-N <sub>3</sub> )	39

3.2.1.3. Synthesis of azide-functionalized doxorubicin (Dox-N <sub>3</sub> ).....	40
3.2.1.4. Synthesis of DBCO-functionalized DM1 (DM1-DBCO) .....	41
3.2.1.5. Synthesis of PLP <sub>139-151</sub> -Rhodamine B (PLP <sub>139-151</sub> -Rhod) .....	42
3.2.1.6. Synthesis of PLP <sub>139-151</sub> -Doxorubicin (PLP <sub>139-151</sub> -Dox).....	43
3.2.1.7. Synthesis of PLP <sub>139-151</sub> -Dexamethasone (PLP <sub>139-151</sub> -Dex).....	44
3.2.1.8. Synthesis of PLP <sub>139-151</sub> -Mertansine (PLP <sub>139-151</sub> -DM1) .....	45
3.2.1.9. Synthesis of PLP <sub>139-151</sub> -Monomethyl auristatin E (PLP <sub>139-151</sub> -MMAE).....	46
3.2.2. Analytical characterization .....	47
3.2.3. Drug release and stability studies .....	47
3.2.4. Determination of IC <sub>50</sub> in EAE splenocytes .....	48
3.2.5. In vivo studies in EAE mice .....	48
3.3. Results and Discussion.....	49
3.3.1. Therapeutic design, rationale, and drug selection .....	49
3.3.2. Synthetic strategy and optimization .....	50
3.3.3. Characterization of conjugates and intermediates .....	53
3.3.4. Stability and release kinetics .....	57
3.3.5. Efficacy studies .....	58
3.3.6. AgDCs uniquely combine two therapeutic approaches.....	60
3.4. Conclusion.....	61

**CHAPTER 4: Multivalent Soluble Antigen Arrays Exhibit High Avidity Binding and Modulation of B Cell Receptor-Mediated Signaling to Drive Efficacy Against Experimental Autoimmune Encephalomyelitis..... 63**

4.1. Introduction .....	63
4.2. Materials and Methods .....	66
4.2.1. Synthesis of alkyne-modified Pennsylvania Green (Penn Green-Alk).....	67
4.2.2. Synthesis of azide-functionalized hyaluronic acid (HA-N <sub>3</sub> ).....	68
4.2.3. Synthesis of Soluble Antigen Arrays .....	69
4.2.4. Analytical Characterization of Soluble Antigen Arrays.....	70
4.2.5. Cell Culture .....	71
4.2.6. Flow Cytometry Binding Assay .....	71
4.2.7. Calcium Flux Signaling Assay .....	72
4.2.8. Fluorescence Microscopy .....	72
4.2.9. Preclinical EAE Study in Mice.....	73
4.2.10. Statistical Analysis .....	74
4.3. Results and Discussion.....	75
4.3.1. Structural design of click soluble antigen arrays.....	75
4.3.2. Analytical characterization of click soluble antigen arrays.....	76
4.3.3. Flow Cytometry Binding Assay .....	82

4.3.4. Calcium Flux Signaling Flow Cytometry Assay.....	86
4.3.5. Fluorescence Microscopy .....	88
4.3.6. Preclinical EAE Studies .....	91
4.4. Conclusion.....	95
<b>CHAPTER 5: Hyaluronan-Dexamethasone Conjugate as a pH-Sensitive Drug Delivery System .....</b>	<b>99</b>
5.1. Introduction .....	99
5.2. Materials and Methods .....	101
5.2.1. Synthesis of azide-functionalized dexamethasone (Dex-N <sub>3</sub> ) .....	101
5.2.2. General procedure for the synthesis of alkyne-functionalized hyaluronic acid (HA-Alk) .....	103
5.2.3. General procedure for the synthesis of HA-dexamethasone conjugates (HA-Dex)..	103
5.2.4. Analytical Characterization of HA-Dexamethasone Conjugates .....	104
5.2.5. Determination of Dex conjugation .....	105
5.2.6. Drug release studies.....	106
5.3. Results and Discussion.....	106
5.3.1. Therapeutic design and rationale.....	106
5.3.2. Synthesis and characterization of conjugates and intermediates.....	107
5.3.3. Drug release kinetics .....	115
5.4. Conclusions .....	117
<b>CHAPTER 6: Conclusions and Future Directions .....</b>	<b>119</b>
6.1. Introduction .....	119
6.2. Summary of dissertation chapters .....	119
6.3. Future directions.....	122
6.3.1. Continuing AgDC development .....	122
6.3.1.1. Tuning MS AgDCs to alter drug release or therapeutic potency.....	122
6.3.1.2. Adapting to other therapeutic areas .....	123
6.3.2. Continuing SAgA development .....	124
6.3.3. Diagnostic assays: capturing antigen-specific cells or antibodies.....	125
6.4. Conclusions .....	127



**CHAPTER 1:**  
**INTRODUCTION TO AUTOIMMUNE DISORDERS AND**  
**CURRENT TREATMENT APPROACHES**

## **CHAPTER 1: INTRODUCTION TO AUTOIMMUNE DISORDERS AND CURRENT TREATMENT APPROACHES**

### **1.1. Introduction to autoimmune disorders**

Autoimmune disorders are a dysfunction of the immune system, and the National Institutes of Health (NIH) estimate that autoimmune disorders affect more than 23.5 million Americans with more than 80 currently documented diseases. The adaptive immune response is dependent on recognition of target antigens, and autoimmune disease occurs when the body fails to maintain tolerance toward self-antigens.<sup>1</sup> These self-antigens can be present in a number of host tissues in various organs, leading to diseases such as multiple sclerosis (MS), myasthenia gravis, diabetes mellitus type 1, and myocarditis.<sup>2</sup> Autoimmune reactions are highly complex and variable, relying on a network of interacting cells and biomolecules to shape downstream responses. While the immune system has both central and peripheral tolerance mechanisms to prevent immune reactions to native antigens,<sup>1</sup> autoimmunity can still occur and require therapeutic intervention.

One of the most prevalent autoimmune disorders is MS, a chronic inflammatory and demyelinating disease leading to significant neurological disability in patients, with symptoms including cognitive impairment, motor or sensory disturbances, weakness, pain and fatigue.<sup>3</sup> A major challenge in MS is the heterogeneous clinical presentation of disease, generally correlating with the hallmark white matter lesions of the central nervous system (CNS).<sup>4-5</sup> While full elucidation of the pathogenic mechanisms behind MS is not complete, the current understanding is that myelin sheath proteins that insulate axons in the CNS likely act as the autoantigens which propagate the immune response. Proteolipid protein (>50%) and myelin basic protein (15%) are the most abundant protein components of CNS myelin,<sup>6</sup> and have been successfully used to induce a chronic demyelinating condition in a murine model of MS, experimental autoimmune encephalomyelitis (EAE).<sup>7-8</sup> Recruitment of peripheral immune cells across the blood-brain barrier

in response to CNS myelin autoantigens is a major therapeutic target for MS, although treatments continue to evolve as our mechanistic understanding progresses.<sup>9-10</sup>

## **1.2. Current treatment approaches for autoimmune disorders**

Immunomodulatory agents and hyposensitization therapy are the two general treatment strategies clinically evaluated for autoimmune disease. Immunomodulatory agents have been effective, but suffer from systemic action and subsequent global immunosuppression, which can increase the vulnerability to opportunistic infections in immunocompromised patient populations.<sup>11</sup> In addition to general immunosuppressants, transport inhibitors and inhibitors of immune cell activation also exist, with the general drawback of lacking antigen specificity. Importantly, immunomodulators used to treat autoimmune disorders generally target symptom suppression or reduction of disease progression, and do not substantially halt or reverse disease.<sup>12-13</sup> Hyposensitization therapy involves multiple administrations of antigen in low but increasing doses and has proven effective at inducing immune tolerance to allergens through modulation of T cell and B cell responses,<sup>14</sup> but have shown minimal efficacy in clinical trials for autoimmune disease.<sup>11</sup> Related to hyposensitization therapy is the use of antigen mimics, which have the potential to provide a ‘decoy’ effect for the immune system, distracting antigen-specific immune cells from attacking host tissues.<sup>11</sup> Of these overall strategies, a pressing need exists to improve treatments by exploiting antigen specificity.

### **1.3. Antigen-specific immunotherapy (ASIT)**

By combining the specificity of hyposensitization therapy with the potency of immunomodulatory drugs, the potential to achieve a synergistic effect necessary to induce antigen-specific immune tolerance in autoimmune disease exists, giving rise to antigen-specific immunotherapy (ASIT). Successfully piloted in several models of autoimmune disease,<sup>15-16</sup> the strategy of co-administering a drug and autoantigen provides a unique approach to treating autoimmune disorders. Furthermore, ASIT has implications in both the treatment and prophylaxis of disease,<sup>17</sup> and the potential to obviate the need for extended treatment schedules, which often lead to decreased patient compliance.

Two general strategies for ASIT exist, co-administration and co-delivery, each with their own advantages and drawbacks. Co-administration benefits from simplicity - the components do not require co-formulation and can even employ different routes of administration, easing the formulation and regulatory burden during development. This permits for the utilization of two currently approved products without the need for additional clinical development. However, effective treatment of disease may require spatiotemporal regulation of both entities, which can be difficult to ensure in the absence of a mechanism to promote co-localization.<sup>11</sup> While the treatments may provide a synergistic effect, it is possible that the addition of a delivery vehicle would result in improved therapeutic efficacy.

Co-delivery has distinct advantages over co-administration by eliminating potential variability in trafficking of the components due to differences in molecular properties or routes of administration, and can potentiate an inflammatory response rather than the desired tolerogenic response.<sup>11</sup> In the absence of a delivery vehicle, it can be difficult to maintain the desired therapeutic specificity of this approach, however, when co-delivery vehicles such as micelles,

polymers, or liposomes are included in the formulation, the heterogeneous nature of the composition brings added challenges in terms of reproducibility and analysis. The alternative is chemical modification, linking the drug molecule to the carrier with a stable covalent bond, which greatly enhances the probability of achieving the necessary spatial and temporal regulation without the need for additional excipients or formulation approaches. While the delivery vehicle and covalent modification strategies have seen both clinical and commercial success,<sup>18-19</sup> chemical conjugation has the potential to provide a better defined chemical entity when compared to those encapsulated in a delivery vehicle,<sup>20</sup> and is the focus here.

#### **1.4. Clinical precedence of immune cell targeting using ASIT co-delivery: antibody-drug conjugates (ADCs)**

Covalent modification of potent drugs to biomolecule carriers has exhibited significant interest in recent years with the commercialization of the first antibody-drug conjugates (ADCs), yielding a surge in clinical development.<sup>19,21</sup> ADCs exploit the specificity of the antibody carrier for cancerous cells, in conjunction with the high potency of their cytotoxic payloads. Upon internalization of the ADC, the drug is able to act inside the cancerous cells, while limiting the off-target effects commonly associated with administration of the small molecule drug alone. ADCs are a comparable approach to ASIT, with a slight reversal in roles. In ADCs, the drug-linked antibody targets cell surface antigenic receptors. In the ASIT concept, the antigen is responsible for providing specificity by targeting cell surface antibody receptors, with the co-delivered drug providing the therapeutic effect.

In some cases, installation of cleavable linker systems between the antibody and drug that respond to environmental stimuli present near the intended site of action, such as low pH,

oxidation/reducing conditions, or enzymatic cleavage, can aid in the targeted delivery of the drug. In other cases, the drug may still be active while conjugated to the antibody carrier. A number of different attachment strategies have been proposed<sup>18, 22-25</sup> to enable each approach, with continued development leading to improved ADCs with increased therapeutic windows and safety profiles.<sup>19</sup> While the complexity and therapeutic heterogeneity have produced manufacturing and analytical hurdles, the clinical outcomes seen with ADCs warrant their continued advancement.<sup>21, 26-27</sup> Simply put, ADCs have greatly impacted cancer treatment and established the foundation for future development of novel bioconjugates with implications across the disease landscape.

## 1.5. Overview of dissertation

The focus of this dissertation is on developing novel therapeutics for the treatment of autoimmune disorders, using bioconjugation chemistries to accomplish this task. The concentration of the research presented here is on the design, synthesis, characterization, and stability of these conjugates. Work conducted by other graduate student researchers is included as a proof of concept in *in vitro* or *in vivo* systems, and credited as appropriate here and at the time of publication.

Chapter 2 highlights a powerful conjugation chemistry, the azide-alkyne cycloaddition (AAC) reaction. While the catalyzed version of this reaction was only presented in 2001, a SciFinder search shows 5913 publications using the search term “azide alkyne cycloaddition” in the first 15 years (2001-2016), underlining the reaction’s importance to scientists in many different fields. Parallel to this development is the increasing commercial availability of drugs, probes and other functionalized molecules bearing azide and alkyne moieties for facile access to complex conjugates. The focus of this chapter is to provide an overview of the AAC reaction, chemistries

appropriate for installing azide and alkyne handles on a variety of different molecules, and the common challenges and limitations of the chemistry with key design considerations when constructing therapeutic bioconjugates. This covers the functionalization of small molecules, proteins, peptides, polymers, as well as their subsequent conjugates, and provides the basis for the chemistry employed throughout the rest of the dissertation. This will serve as the basis for a review article to be submitted to ACS Bioconjugate Chemistry.

Chapter 3 focuses on the development of a novel class of compounds, antigen-drug conjugates (AgDCs). By reversing the paradigm of the emerging class of ADCs, AgDCs permits repurposing of this approach for different therapeutic indications. Most current ADCs employ an antibody specific for cell-surface antigens expressed on cancer cells, linked to a potent toxin for the targeted killing of cancerous cells. This approach provides greatly reduced off-target effects when compared with administering the drug alone, and enables the clinical application of payload toxins which are too potent for use as an individual treatment strategy. Utilizing the same targeting concept that the antibody provides, AgDCs link therapeutic molecules to peptide autoantigens in an effort to target antibody receptors present on offending immune cells responsible for disease. Importantly, AgDCs are a platform approach, expandable to a variety of antigen-specific autoimmune disorders. The goal of this work is to present this innovative therapeutic platform applied to the autoimmune disease MS, to promote the development of more efficacious immunotherapies with improved safety profiles and patient outcomes.

Chapter 4 presents an extension of research conducted previously in the Berkland group as an alternative approach to the treatment of antigen-specific autoimmune disorders, termed Soluble Antigen Arrays (SAgAs).<sup>28-29</sup> A key event involved in immune response is the formation of the immunological synapse (Figure 1), requiring co-stimulation of signals present on an antigen-

presenting cell (APC) and a T cell, which triggers a cascade of downstream reactions that result in an inflammatory response and tissue damage.

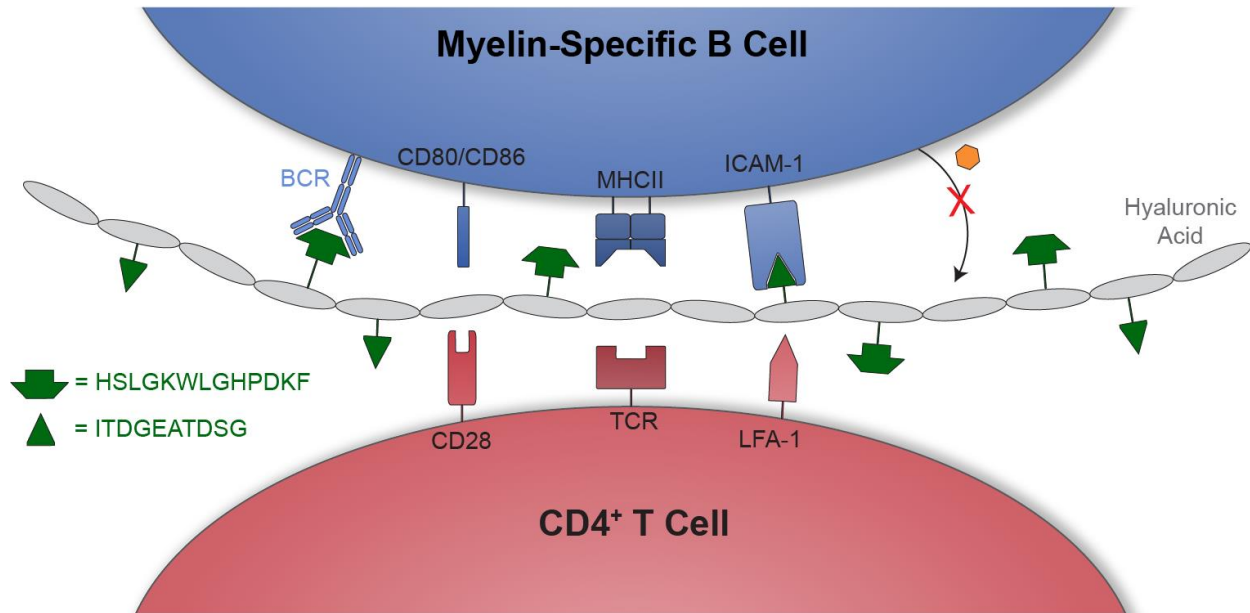


Figure 1: Proposed mechanism of action of SAgA therapeutics, with a particular focus on the immunological synapse.

In this case, a polymeric support of hyaluronic acid co-grafted with a MS peptide autoantigen, proteolipid protein (PLP<sub>139-151</sub>), and a portion of intercellular adhesion molecule derived from CD11a<sub>237-246</sub> (LABL) should effectively disrupt immune response. Mechanistic studies<sup>30</sup> support the hypothesis that receptor clustering induced by SAgA treatment can be an effective method of suppressing immune activation. The initial approach employed an acid-sensitive oxime bond between the polymeric support and peptides, and this work focused on modifications to the linkage to achieve a non-cleavable variant with improved aqueous stability. The hydrolytically stable version, termed ‘clickable’ Soluble Antigen Arrays (cSAGAs), showed improved efficacy<sup>31</sup> in experimental autoimmune encephalomyelitis (EAE), a murine demyelinating model used to mimic MS in humans.



Chapter 5 focuses on the development of a bioconjugate as a monotherapeutic replacement of two approved treatments which are currently co-administered and suffer from decreased efficacy due to poor patient compliance. Cataract surgeries frequently require the use of viscoelastic agents such as hyaluronic acid to maintain the integrity of the corneal endothelium, a monolayer of cells serving as an active fluid pump system and barrier. The current standard of care is phacoemulsification, widely known to cause corneal endothelial cell loss (ECL), which can be limited through the use of viscoelastic agents to stabilize the anterior chamber and limit damage by free radicals. Additionally, the management of post-operative intraocular inflammation through the use of anti-inflammatory agents is common, requiring frequent administration of topical solutions for extended periods of time. This chapter targets the development of a conjugate of hyaluronic acid linked to the anti-inflammatory compound dexamethasone as an extended release version to increase patient outcomes following cataract surgeries, particularly in elderly patient populations where compliance can be a concern.

Chapter 6 presents the conclusions from this dissertation research, with a particular focus on areas of improvement for the therapeutic bioconjugates presented, including ideas on expansion of the approaches to new indications and applications. The hope is that this chapter can present a guide for future scientists to improve or expand upon this work, creating new treatments with improved safety profiles and patient outcomes. The ideas contained in this chapter are a blend of many scientific fields, from chemistry and biology to engineering and immunology, thereby requiring cross-functional scientists to accomplish challenging problems.

**CHAPTER 2:**  
**INTRODUCTION TO BIOCONJUGATION VIA AZIDE-**  
**ALKYNE CYCLOADDITION: CHALLENGES,**  
**LIMITATIONS, AND CONSIDERATIONS**

## **CHAPTER 2: INTRODUCTION TO BIOCONJUGATION VIA AZIDE-ALKYNE CYCLOADDITION: CHALLENGES, CONSIDERATIONS, AND LIMITATIONS**

### **2.1. Introduction**

With the recent surge in the development of therapeutic bioconjugates, synthetic chemists have worked in parallel with biochemists to identify strategies for improving the specificity of the chemical modification. As the field of antibody-drug conjugates continues to emerge, chemical modifications with increasing specificity aide in enhancing bioconjugate homogeneity, therapeutic index, and other pharmacokinetic parameters, resulting in a safer and more effective treatment option for the patient. While historically, the construction of bioconjugates has employed numerous different chemistries, the focus of this chapter will be on the [3+2] cycloaddition reaction between an azide and an alkyne, with chemistries and methods appropriate for installation of these functionalities on proteins, peptides, polymers, small molecules, and cellular components *in vivo*.

There are a number of published reviews and protocols that cover various approaches to conjugating small molecules to biomolecules in a selective fashion.<sup>32-34</sup> While these reviews provide an excellent background on the implementation of these chemistries, the practical challenges and limitations of utilizing these chemistries in terms of relevant physiochemical properties of the conjugate will be discussed here. The reaction schemes presented in this section focus on the use of commercially-available reagents for both functionalization and conjugation.

### **2.2. Azide-Alkyne Cycloaddition Reaction**

The formation of 1,2,3-triazoles was first studied by Huisgen in the 1960's,<sup>35</sup> but was later adapted to the copper-catalyzed azide alkyne cycloaddition (CuAAC) variant, developed

independently by the groups of Sharpless<sup>36</sup> and Meldal<sup>37</sup> in 2002. The addition of a copper catalyst preferentially formed the regiospecific 1,4-substituted triazole under mild reaction conditions and at rates  $10^6$ - $10^7$  greater than the mixture of 1,4- and 1,5-substituted products in the absence of copper, which also necessitated the use of elevated reaction temperatures (Figure 2). Further work has shown that ruthenium complexes are capable of catalyzing the regioselective formation of 1,5-substituted triazoles.<sup>38-39</sup> A number of reviews,<sup>33</sup> protocols,<sup>34</sup> and mechanistic studies<sup>40-41</sup> are available to provide further insight into the unprecedented reactivity of these molecules.

The triazole ring is similar in both electronic properties and topology to a peptide bond, exhibiting a bond distance of  $\sim 5.0$  Å as compared to 3.9 Å in the amide bond,<sup>42</sup> and is stable under common biological stresses, including oxidizing or reducing conditions, enzymatic degradation, or pH. Facile synthesis of the triazole ring, in addition to its stability and chemical properties has been a significant driver of its implementation in bioconjugation applications. Outside of a biological system, however, the triazole ring has been reported to revert back to the parent azide and alkyne components under ultrasonication for 2 hours.<sup>43</sup>

An initial surge in the application of the CuAAC reaction has identified a few drawbacks, primarily associated with the use of copper. The active catalytic species is  $\text{Cu}^{1+}$ , but readily converts back to a more stable  $\text{Cu}^{2+}$  in solution, requiring *in situ* formation of  $\text{Cu}^{1+}$  using  $\text{Cu}^{2+}$  and excess reducing agent. Commonly, this reducing reagent is sodium ascorbate, and together with an active  $\text{Cu}^{1+}$ , have been shown to promote the oxidation of histidine and arginine residues.<sup>44</sup> These unintended side reactions have led to the introduction of accelerating ligands to both limit degradation of these amino acids, in addition to accelerating the rate of the CuAAC reaction.<sup>40, 45</sup> Compounds like aminoguanidine are useful as a surrogate in cases where the biomolecule contains

arginine. Additionally, the toxic effect of copper on cells limits its use in cell based assays where long-term viability is a concern.

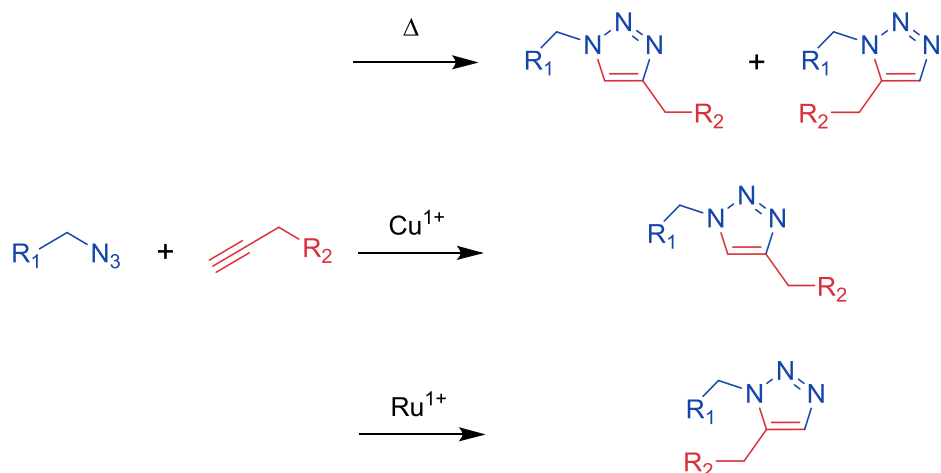


Figure 2: General reaction scheme for the azide-alkyne cycloaddition under various conditions.

To alleviate the need for copper, accelerating ligands, reducing agents, and other stabilizing reagents, Bertozzi and coworkers developed the strain-promoted azide-alkyne cycloaddition reaction (SPAAC).<sup>46</sup> The SPAAC reaction proceeds efficiently in the absence of a catalyst due to the high degree of ring strain on the cyclooctyne ring, under mild reaction conditions and times necessary for adaption to biomolecules (Figure 3A). The primary drawbacks of the SPAAC approach is the lack of regioselectivity of the reaction product, forming a mixture of 1,4- and 1,5-substituted products. Initially, the aqueous solubility of the cyclooctyne reagents were of concern, but recent developments have seen the installation of solubilizing moieties such as PEG or sulfate groups in the linker attached to the ring. Furthermore, the cost of the strained cyclooctyne reagents is considerably higher than their terminal alkyne counterparts, but alternate synthetic routes<sup>47</sup> are making SPAAC reagents more accessible and less cost-prohibitive to employ. Alternatively, a number of other strained alkyne moieties have been developed (Figure 3B) and shown to function as a coupling partner in the azide-alkyne click reaction, with varying reaction rates.<sup>48</sup> Photolabile

“caged” cyclooctyne variants (Figure 3B, lower right) present an important added functionality to the reaction, revealing the reactive strained alkyne group under exposure to 350 nm light and enabling spatially-controlled conjugation.<sup>49</sup> This approach is of particular interest in surface functionalization applications where spatiotemporal control of conjugation is critical.<sup>49-50</sup>

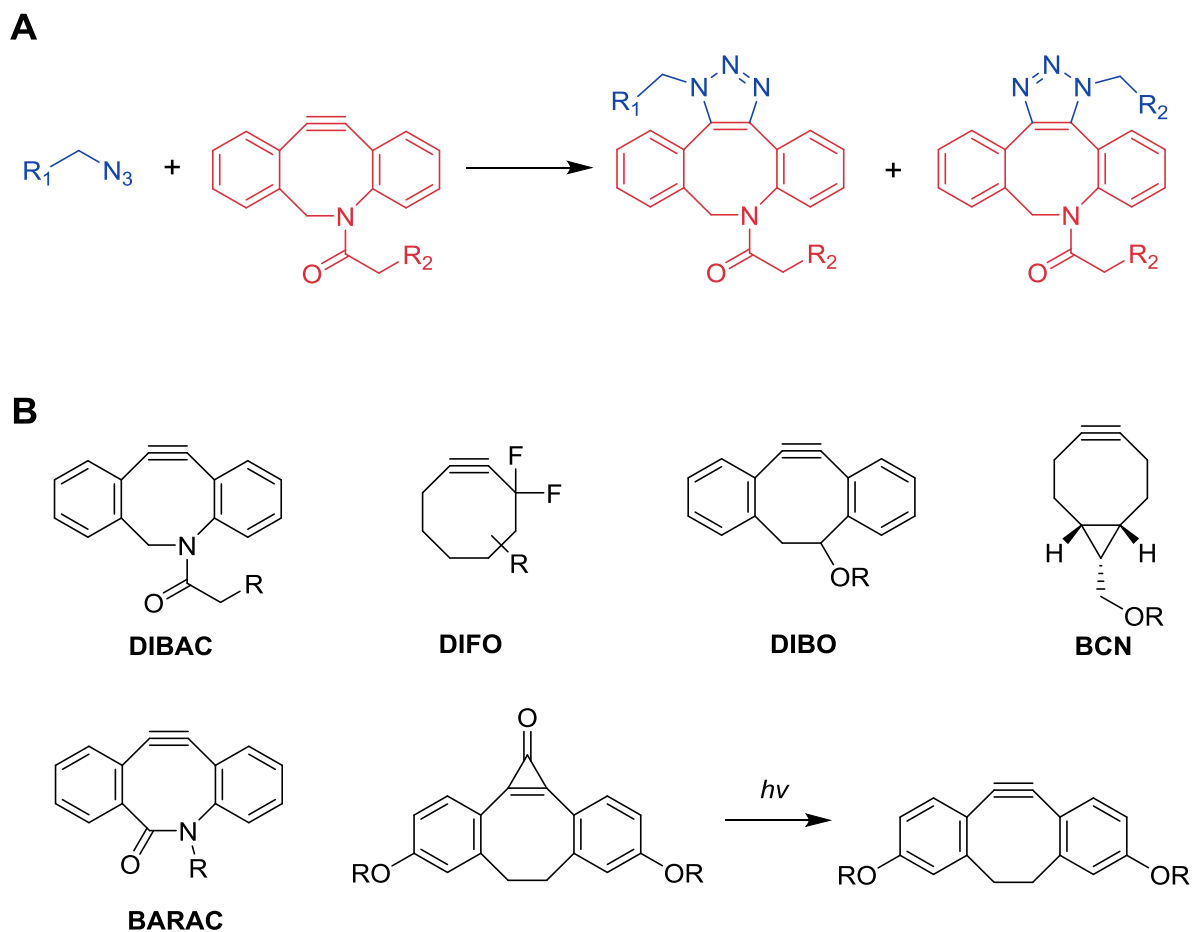


Figure 3: (A) General reaction scheme for the strain-promoted azide-alkyne cycloaddition reaction. (B) Sample strained-alkyne compounds presented in the literature.

### 2.3. Amidation using *N*-Hydroxysuccinimidyl (NHS) Esters

NHS esters are among the most popular compounds used to functionalize biomolecules due to their aqueous compatibility, commercial availability, and selective targeting for primary amines present on lysine residues or the N-terminus (Figure 4). For biomolecules, reaction conditions generally employ aqueous buffers at pH 7-9. At a pH closer to 9, the reaction proceeds at a quicker rate due to a higher degree of amine deprotonation, but more hydrolysis of the activated ester prior to reacting with lysine residues is more problematic. At a pH closer to 7, the reaction proceeds at a slower rate, but favors reactions with primary amines rather than NHS ester hydrolysis by the aqueous environment. Intermediate pH's between 7-9 are commonly employed to balance reaction rate and extent of functionalization while keeping the solubility and stability of the biomolecule in mind. Reactions performed at room temperature are usually complete in 1-2 hours, while reactions involving more sensitive molecules can proceed at 4°C overnight.

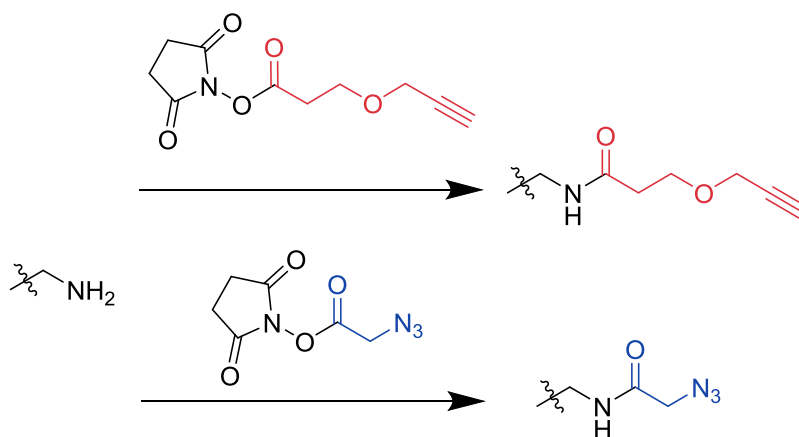


Figure 4: General reaction scheme for azide- or alkyne-labeling of a primary amine using NHS ester chemistry.

Due to the difference in acidity between the  $\alpha$ -amino group of the N-terminus ( $pK_a \sim 8$ ) and the  $\epsilon$ -amino group of lysine residues ( $pK_a \sim 10$ ), selective N-terminal functionalization has been shown at pH values below 7, with pH 6.3 being ideal.<sup>51</sup> Performing the reaction in the absence

of amine-containing buffers such as tris or glycine is essential, however, these can be useful as quenching buffers to ensure no additional reactive NHS ester is available after achieving the desired degree of functionalization. When possible, NHS ester reagent solutions that are prepared in anhydrous organic solvents are preferred to limit hydrolysis prior to initiating the reaction, provided that all reaction components remain compatible. NHS ester reagents are typically not stable for more than a few hours in solution, even when prepared in anhydrous solvents.

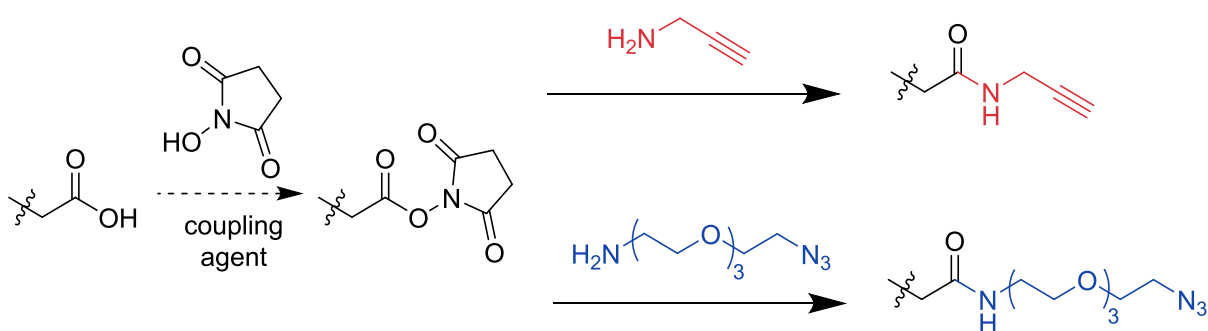


Figure 5: General reaction scheme for azide- or alkyne-labeling of a carboxylic acid using NHS ester chemistry, where the coupling agent could be EDC or DCC depending on the reaction environment.

For small molecules which do not necessitate an aqueous reaction environment, NHS ester reactions in anhydrous organic solvents such as *N,N*-dimethylformamide (DMF), dimethylsulfoxide (DMSO), acetonitrile (MeCN), and dichloromethane (CH<sub>2</sub>Cl<sub>2</sub>) are ideal. This generally results in higher yields and better selectivity for amino functional groups due to a reduction in aqueous hydrolysis. In the absence of amine functionality, NHS esters can also modify other nucleophilic groups in a molecule such as deprotonated hydroxyl or thiol moieties. Alternatively, NHS esters can functionalize carboxylic acids through *in situ* formation of the activated ester using NHS and an appropriate coupling reagent such as 1-ethyl-3-(3-dimethylaminopropyl)carbodiimide (EDC) or *N,N'*-dicyclohexylcarbodiimide (DCC) (Figure 5).



## 2.4. Thioether Formation to Install Azide and Alkyne Groups

The thiol group on cysteine residues is commonly targeted using maleimide reagents, yielding a stable thioether bond and is an effective Michael addition reaction (Figure 6). Similar to the NHS ester, maleimide reactions are pH controlled in aqueous media, generally in the pH range of 6-8. At lower pH values, the reaction proceeds at a slower rate, but favors the thiol-functionalization over hydrolysis. At higher pH values, the reaction proceeds at a faster rate, but hydrolysis of the maleimide is of greater concern. As with NHS esters, reaction buffers should avoid the use of thiols such as dithiothreitol (DTT) or  $\beta$ -mercaptoethanol (BME), but are useful post-reaction to quench any remaining maleimide after achieving the desired conjugation levels.

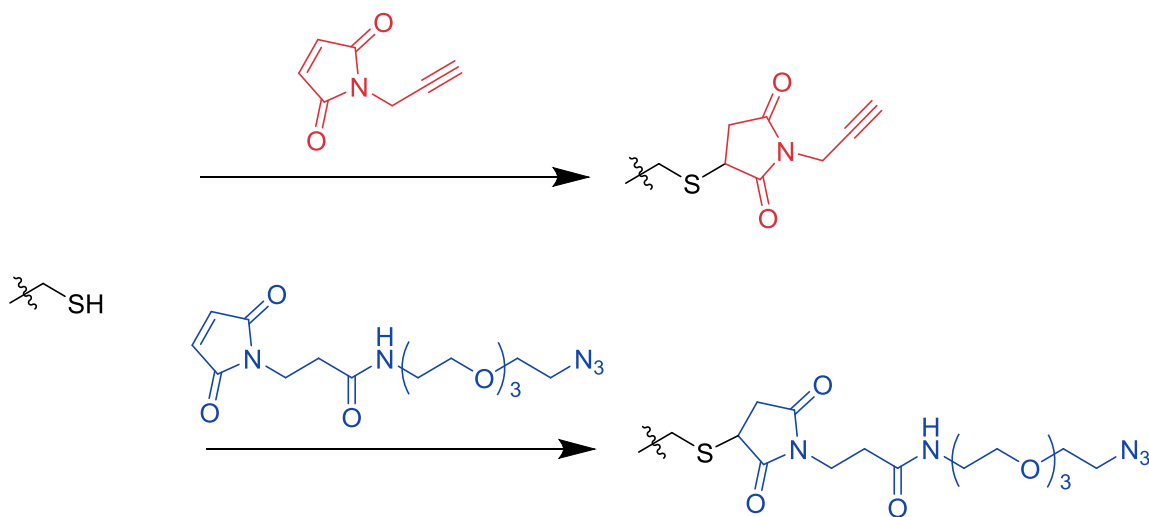


Figure 6: General reaction scheme for azide- and alkyne-functionalization using maleimide chemistry.

Mechanistic investigations of the thiol-maleimide reaction have shown a significant dependence on the solvent, initiator (base), and thiol used, and the reaction mechanism is dependent on these three factors.<sup>52</sup>

## 2.5. Solid-phase peptide synthesis

Solid-phase peptide synthesis (SPPS) is a semi-automated technique commonly employed to synthesize peptides, typically less than 30 amino acids in length. Site-specific functionalization of a reactive handle occurs in one of two different ways, either using an amino acid mimic (Section 2.5.1) within the peptide sequence or by installing a heterobifunctional linker (Section 2.5.2) bearing the reactive functional group of interest.

### 2.5.1. Amino acid mimics

A wide range of amino acid mimics are available with both azide and alkyne functional groups, and protected versions of these compounds (Figure 7) can be used to enable selective incorporation of the desired handle during SPPS.<sup>53</sup> Peptides bearing both azide and terminal alkyne handles also present an attractive way to make cyclic peptides, and have literature precedence.<sup>54</sup> This affords an ideal replacement for the disulfide bond commonly used for cyclization reactions, which is susceptible to oxidizing/reducing environments and disulfide exchange, as the triazole ring adds enhanced stability. Additionally, exploiting the Cu- and Ru-catalyzed variants of the cycloaddition reaction can have a dramatic effect on activity by making small geometric alterations in the binding pocket.<sup>55</sup>

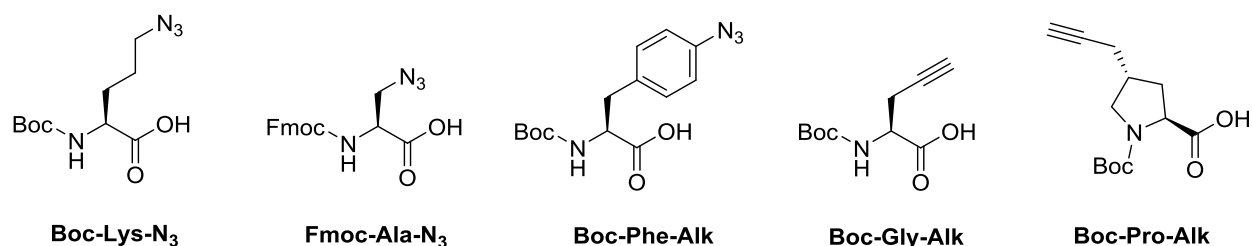


Figure 7: Sample protected amino acids available for incorporation of azide- or alkyne-reactive handles during SPPS.

### 2.5.2. Heterobifunctional linkers

In the event that preservation of side chain binding interactions is required to maintain activity, heterobifunctional reagents can also be useful to install N-terminal linkers as the final step of SPPS. Since these linkers do not contain a primary amine functionality, the need for protection and deprotection is eliminated. The heterobifunctional linker reacts as an amino acid during the peptide synthesis process, which would require a carboxylic acid functionality, in addition to the azide or alkyne functional group of interest (Figure 8). PEGylated forms of the heterobifunctional linkers are available in various lengths, which permits precise spacing of the reactive handle. Successful click conjugation using this approach has been used with a variety of different molecules,<sup>31, 56-57</sup> and enables the selective orientation and spacing to the molecule of interest by varying the length of the linker.

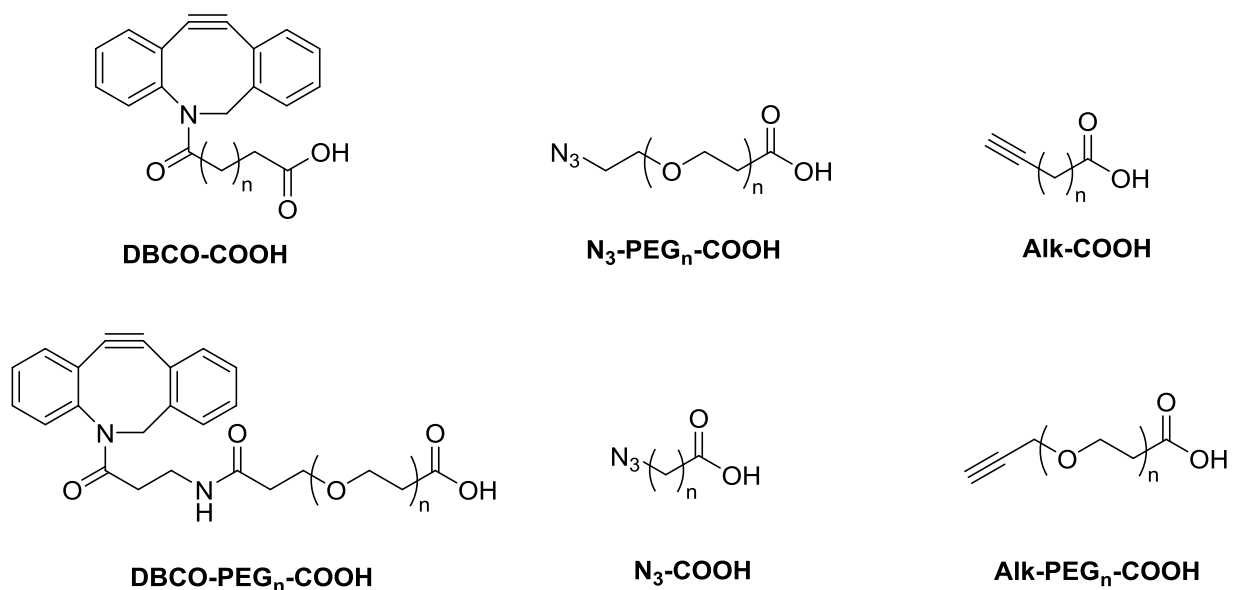


Figure 8: Sample heterobifunctional linkers employed for the installation of a reactive handle.

## 2.6. Metabolic labeling methods

Installation of a reactive handle through metabolic labeling is becoming increasingly popular to provide a measure of metabolic activity, as modified biomolecules incorporate into biosynthetic pathways in the same manner as their unmodified counterparts. However, for biomolecules expressed in cell systems prior to isolation, this provides an attractive method for site-specific incorporation of a reactive handle while still maintaining activity.

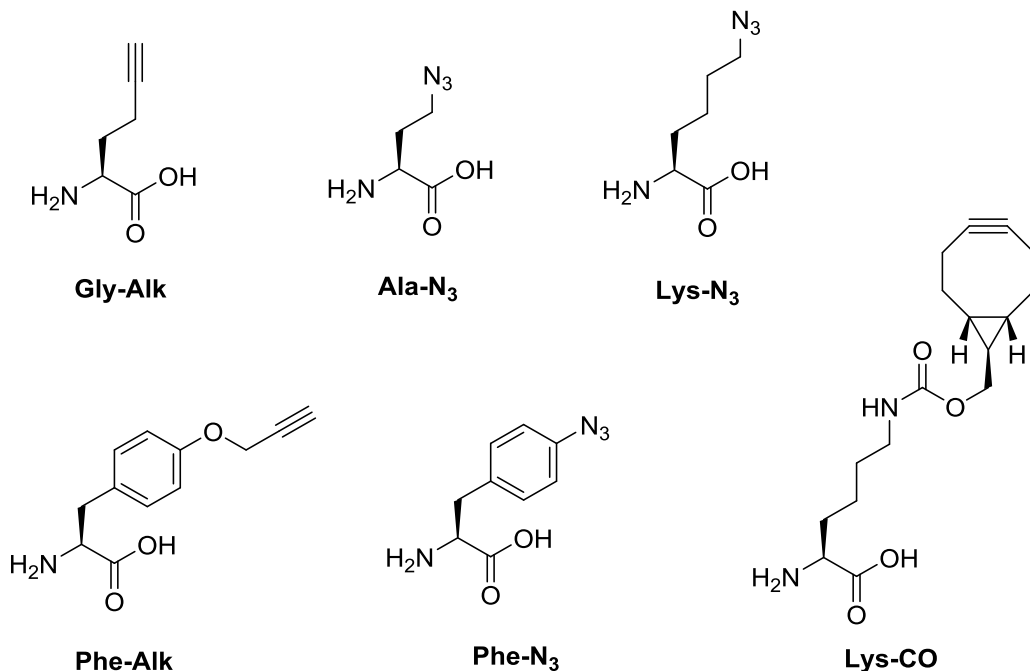


Figure 9: Sample functionalized amino acids for site specific incorporation of a reactive handle.

### 2.6.1. Amino acid mimics

Selective and reproducible modification of larger protein molecules has proved to be challenging with NHS ester or maleimide chemistries, since the surface-exposed lysine and cysteine residues targeted can be abundant on larger proteins. To circumnavigate this challenge, unnatural amino acids (UAAs) bearing reactive functionalities have literature precedence<sup>58-60</sup> (Figure 9) and are successfully incorporated into active protein synthesis with the addition of an engineered tRNA specific for the UAA. Not only does this permit selective incorporation of a reactive handle into the protein, it can also be used in conjunction with an azide- or alkyne-labeled fluorophore to provide a real-time measure of metabolic activity in the cell.

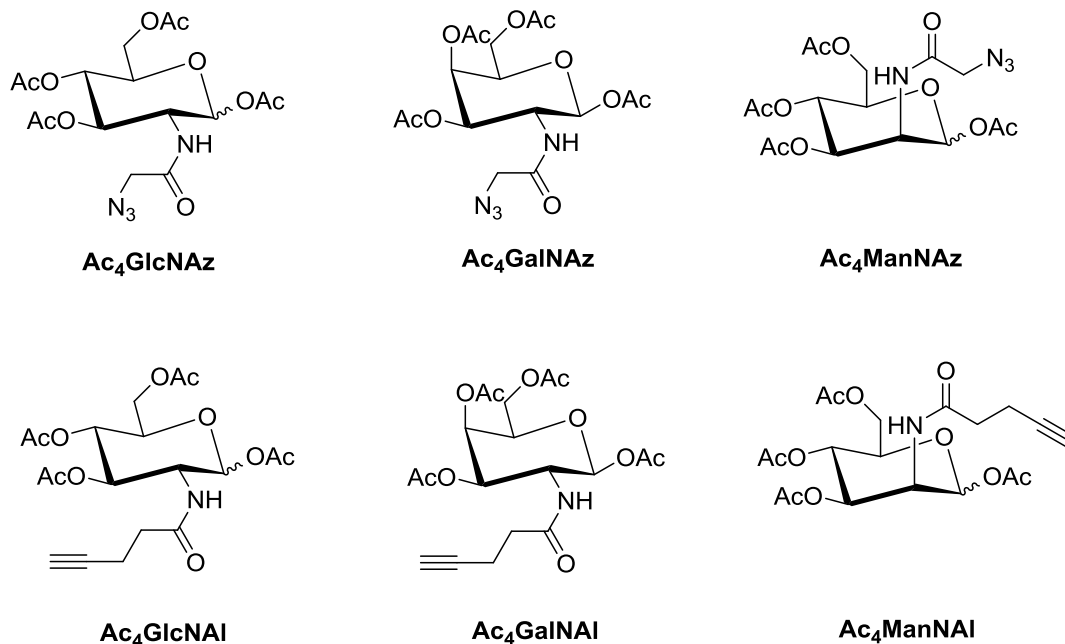


Figure 10: Azide- and alkyne-modified sugars used for metabolic labeling of proteins which undergo post-translational glycosylation.

### 2.6.2. Post-translation modifications

For proteins expressed in cell systems, exploiting post-translational glycosylation becomes another attractive approach for site-specific conjugation. Acetylated versions of modified sugars (Figure 10) added to the growth medium, and following internalization, non-specific proteases hydrolyze the acetate groups and release the sugar mimic bearing an azide or alkyne functional group. These sugars incorporate into glycosylated proteins, permitting subsequent conjugation either *in vitro*, or following protein isolation. For proteins which undergo post-translational lipidation or prenylation, alkyne-modified variants of fatty acids (Figure 11A) or isoprenoid precursors<sup>61</sup> (Figure 11B) can incorporate into biosynthetic pathways in the same manner as their unmodified counterparts, enabling a method of site-specific incorporation of a reactive handle, or

to directly measure metabolic activity when combined with an azide- or alkyne- modified fluorophore.

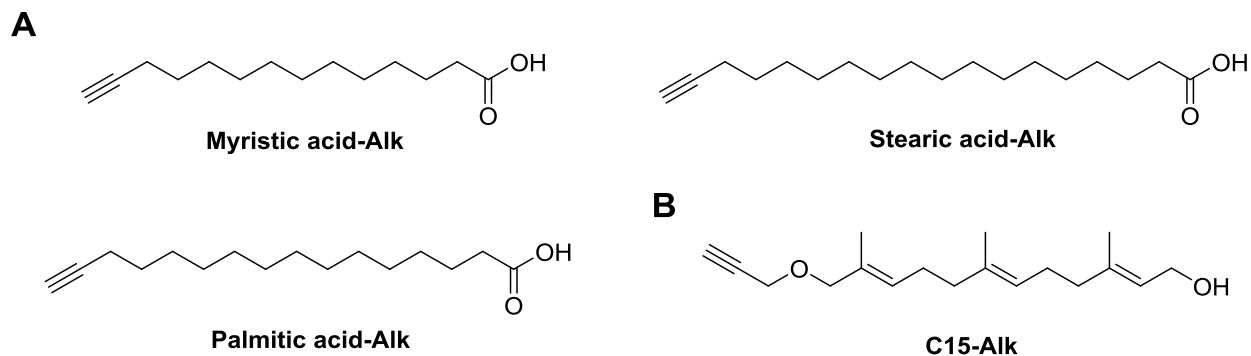


Figure 11: Alkyne-modified fatty acids and isoprenoids used for metabolic labeling of post-translational lipidation or prenylation.

### 2.6.3. Nucleic acids and other anchors for live cell bioconjugation

While primarily used for imaging applications, azide- and alkyne-modified nucleic acids (Figure 12A and B) and other membrane components (Figure 12C and D) have been used to install a reactive handle in actively synthesized DNA,<sup>62</sup> RNA,<sup>63</sup> or cell membrane components. Following installation of the reactive handle, conjugating molecules that enhance targeting, alter binding<sup>64</sup> or expression, provide significant potential for therapeutic use. Additionally, when used in conjunction with a fluorescent probe bearing an azide or alkyne moiety, these molecules are useful as a probe of cellular metabolic activity.

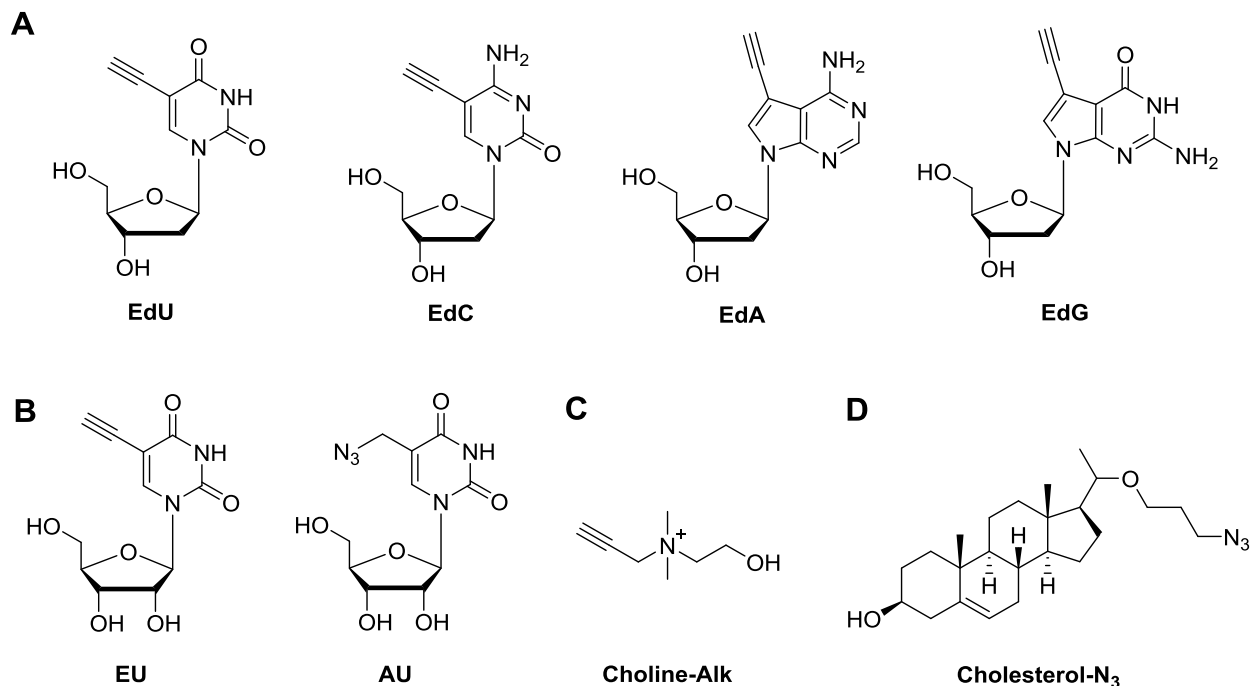


Figure 12: Azide- and alkyne-modified chemical probes used for labeling. (A) DNA probes used for live cell labeling, (B) RNA probe used for live cell labeling, (C) phospholipid precursor used for labeling cell membranes, (D) cholesterol probe used for membrane incorporation.

## 2.7. Payload molecules for modulating biomolecule function

With the significant interest and development surrounding the azide-alkyne click reaction since its inception, a number of molecules have emerged in the literature which enable facile access to key functionalities (Figure 13). Most commonly, fluorescent tags installed on biomolecules permits visualization of a molecule of interest inside a cell, or for quantitation using techniques such as flow cytometry. Sivakumar *et al.* developed a pro-fluorescent coumarin molecule (Coumarin-N<sub>3</sub>, Figure 13A), having negligible fluorescence in the unconjugated form, and becoming fluorescent after the click reaction extends the conjugated system.<sup>65</sup> This molecule has been useful in optimizing reaction conditions and for studying kinetics of the click reaction.<sup>44-45</sup>



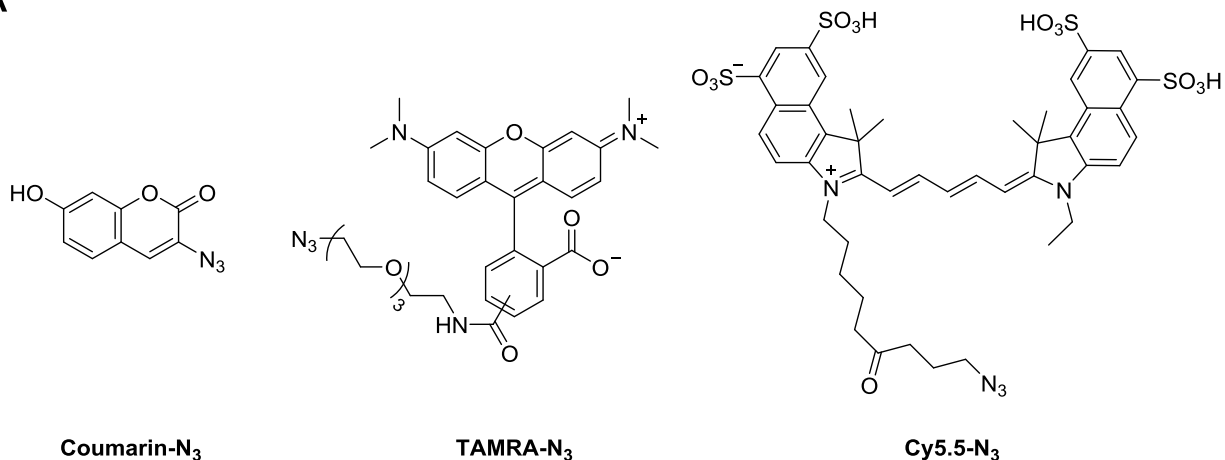
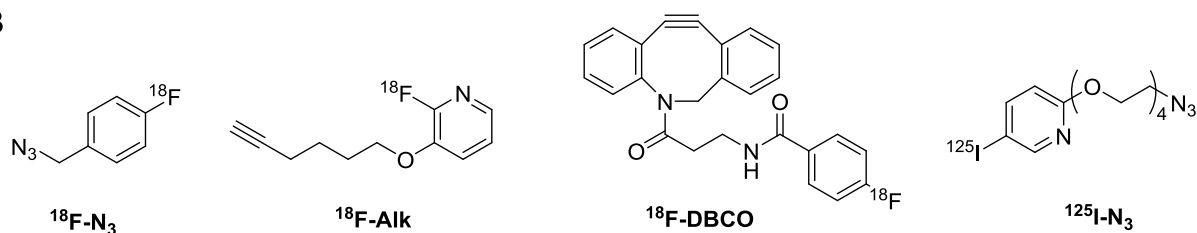
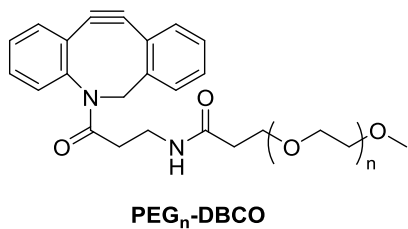
**A****B****C**

Figure 13: Sample payload molecules enabling facile access to added functionality. (A) Fluorophores spanning the spectral range, (B) radiolabels for incorporating a non-fluorescent tracer, (C) PEGylating reagents.

A significant number of radiolabels (Figure 13B) have been described in the literature, enabling access to both targeted radiotherapy and *in vivo* visualization and quantitation techniques not possible with fluorescence labels, such as positron emission tomography (PET) and single photon emission computed tomography (SPECT).<sup>66</sup> PEGylation reagents (Figure 13C) are also available

as a method to modify clearance or other pharmacokinetic parameters of a biomolecule, or to alter the biodistribution of a molecule by making significant changes to its molecular weight.

## **2.8. Challenges associated with bioconjugates**

### ***2.8.1. Synthetic and analytical considerations***

Bioconjugates are an exciting area that can exploit the benefits of multiple molecules with different properties, but their complexity often brings new challenges with respect to the synthesis and analysis of these constructs. Synthetic complications typically center on solubility or stability of the parent molecules or resulting conjugate, since proteins and other biomolecules are generally more sensitive than the payload to temperature and other environmental factors such as organic solvents, thereby limiting the approaches available to the traditional synthetic chemist. Analytical hurdles reside around heterogeneity, deconvolution of data and limited sample quantities due to high costs of proteins, which has led to the adaption of methods and techniques to comply with these demands.

Solubility of the biomolecule and payload are required for the success of the conjugation reaction. However, payload molecules with minimal aqueous solubility will require assistance from an organic solvent to ensure the conjugation reaction can proceed. Dimethylsulfoxide (DMSO), *N,N*-dimethylformamide (DMF), and acetonitrile (MeCN) have seen use in these situations, removed effectively by dialysis or other size exclusion method after the completion of the reaction. Biomolecules with higher order structure can be conformationally altered in the presence of organic solvents, or have limited solubility as the organic concentration increases. Therefore, minimizing the overall organic solvent concentrations used in the reaction is often essential. NHS ester (Section 2.3) and related chemistries which target surface-exposed lysines or

other charged amino acids will have a greater impact on the overall solubility of the conjugate, since these amino acids assist in solubility of the biomolecule and will not remain charged following conjugation. To negate some of the deleterious effects of conjugation on solubility, linkers which have solubilizing moieties can either counteract or enhance solubility as desired in the conjugate.

Importantly, a thorough understanding of the stability and degradation mechanisms of the parent molecules will guide the chemist in selecting appropriate reaction conditions while maintaining the integrity of the functional entities involved. These studies must assess both the physical and chemical stability of the molecules, since mechanisms leading to instabilities in small molecules are different than those seen for larger biomolecules. Proteins have a frequent propensity to aggregate in solution, a phenomenon which can be either reversible or irreversible. Aggregation can be especially problematic during synthesis, leading to precipitation and lower yields if not properly controlled. Aggregation during a chemical reaction can be limited by excipient addition, modifying the reaction environment (pH or ionic strength), decreasing reaction temperature, and limiting the amount of time the biomolecule is in solution. Any aggregates that form during the reaction should be separated from the product prior to final isolation, typically by filtration, centrifugation, or other size exclusion methods. Analytical techniques employed for studying aggregation in biomolecules include size exclusion chromatography (SEC), gel electrophoresis, or various spectrophotometric and light scattering particle sizing methods appropriate for the aggregate size involved. Liquid chromatography coupled with tandem mass spectrometry (LC/MS/MS), often preceded by enzymatic digestion, is a powerful technique for understanding chemical degradation products in biomolecules. Small molecules are generally

more robust than biomolecules and the degradation products can be more easily understood using LC/MS and NMR techniques.

Purification of bioconjugates constructed via the azide-alkyne cycloaddition reaction often require additional considerations. When employing the CuAAC variant, residual copper is undesirable in final products due to toxic and oxidative effects in living systems, but removal through common techniques appropriate for the compounds involved is generally adequate. For small molecules, copper binding resins such as Cuprisorb or chelators such as ethylenediaminetetraacetic acid (EDTA) are added following the reaction, which can also serve to quench the reaction.<sup>34</sup> Peptides and proteins can be purified by chromatographic techniques like reverse phase high pressure liquid chromatography (HPLC), or through size exclusion methods such as dialysis where appropriate. Avoiding metal binding resins such as Cuprisorb due to a tendency to bind biomolecules is ideal. Following purification, inductively coupled plasma mass spectrometry (ICP-MS) is a useful technique for assessing the residual copper levels in the sample.

Limiting side reactions with amino acid residues of biomolecules is a necessity to maintain activity in the final conjugate. CuAAC reactions employing the common  $\text{Cu}^{2+}$  and sodium ascorbate catalyst system (forming the corresponding dehydroascorbate byproduct) are known to lead to the formation of reactive oxygen species, which can degrade certain amino acids including histidine, arginine, cysteine and methionine.<sup>67</sup> Cu-chelating ligands such as THPTA or TBTA can assist in limiting degradation, and the addition of reagents such as aminoguanidine, which act as a side chain surrogate for aminoguanidine, can also limit chemical degradation of the biomolecule. Cyclooctyne compounds are known to react with reduced cysteine residues through a thiol-yne mechanism, although this has been shown to be mitigated through pre-incubation with iodoacetamide, which is compatible with the subsequent SPAAC conjugation reaction.<sup>68</sup>

The AAC reaction carries significant precedence in the polymers field with respect to hydrogels.<sup>69-72</sup> An added complication of bioconjugation to polymers is the tendency for intra- or inter-molecular entanglement, limiting the accessibility to reactive sites. Reduction of this phenomenon can occur through the addition of organic solvents known to denature the polymer,<sup>34</sup> addition of heat to induce thermal unfolding, or altering pH or ionic environment to disrupt specific interactions causing entanglement.<sup>73</sup> In other cases, limited reactive site availability is due to the viscosity of high MW polymers, requiring more dilute reaction conditions. In general, conjugation efficiency will decrease as molecular weight increases due to reduced collisions with appropriate geometry and sufficient energy to react, especially in polymers such as hyaluronic acid which are self-associating or have secondary structure.<sup>74</sup>

### ***2.8.2. Biological consequences of solubility***

Solubility plays an important role in many physiological processes from biodistribution and clearance to immune recognition and response. Insoluble antigens are often processed by macrophages, while dendritic cells tend to process soluble materials.<sup>1</sup> Therefore, modification of the native biomolecule's solubility through conjugation can perturb native function, altering recognition, trafficking or uptake events. An understanding of aggregation propensity, with the associated decrease in solubility, is of critical importance in protein therapeutics, since aggregated proteins have the potential to induce an undesired immune response and lead to potentially serious adverse events for the patient.<sup>75</sup> In 2014, the FDA issued guidance on immunogenicity assessment as a key parameter in the development of therapeutic protein products. Recent studies have also shown the impact of immunogenicity through the formation of anti-drug antibodies upon repeat administration of biologic treatments such as rituximab.<sup>76-77</sup>

In the context of antibody-drug conjugates (ADCs), most drugs conjugated to the antibody are relatively hydrophobic and have minimal aqueous solubility, while the antibody has sufficient aqueous solubility. Therefore, the resulting conjugate generally has intermediate solubility, often proportional to the molecular weight contribution of the parent compounds to the overall conjugate. This can be of significant benefit for the drug molecule, since hydrophobic drug molecules which typically enter cells via passive diffusion can exploit the active transport mechanisms used to internalize the antibody, but can also be detrimental to the pharmacokinetic properties of the antibody. Additionally, studies have shown high drug-to-antibody ratios (DAR) impact both potency and clearance, although modulated through varying the hydrophilic or hydrophobic nature of the linker.<sup>78-79</sup>

Efflux pumps such as the multidrug resistance (MDR) proteins target molecules for export, and are more effective at transporting hydrophobic molecules than hydrophilic molecules. A correlation between MDR expression and poor clinical response has been documented,<sup>80</sup> which is an important observation and should be taken into consideration in bioconjugate design. Studies have shown that trastuzumab linked to the maytansinoid DM1 via a hydrophilic PEGylated linker were more potent towards MDR<sup>+</sup> cells than those containing the more hydrophobic *N*-succinimidyl-4-(maleimidomethyl)cyclohexane-1-carboxylate (SMCC) linker,<sup>81</sup> highlighting the important impact of solubility on therapeutic function.

### ***2.8.3. Linker stability***

Another critical component to a bioconjugate is the design of the linker, since this can also have a dramatic impact on the efficacy of the bioconjugate. Both cleavable and non-cleavable linker strategies have been used in the ADC field as well as in other bioconjugates. Cleavable

linkers typically exploit environmental factors present in the cellular location where payload release is desired, involving either pH, oxidizing/reducing conditions, or the presence of a relevant enzyme. While this approach may be attractive in theory, and may be necessary for successful action of the payload, the mechanisms that release the payload may not be specific to only the desired target location. For example, pH sensitive linkers present in the bioconjugate can encounter acidic microenvironments during trafficking to the target location, and could release the payload in unintended locations throughout the body, yielding adverse side effects for the patient.

The ‘bystander effect’ in ADCs that specifically target solid tumors is documented, and is known to express surface antigens in a heterogeneous manner. In these cases, an understanding of the drug release mechanism is essential, since treatment with an ADC may not be sufficient to eliminate all of the solid tumor, given that cell populations with limited surface antigen expression will see limited targeting by the ADC. Brentuximab vedotin utilizes a cathepsin cleavable linker to conjugate the toxin monomethyl auristatin E (MMAE) to the antibody, releasing the toxin in a neutral form capable of crossing biological membranes of adjacent tumor cells not initially targeted by the ADC. When the structural analogue, monomethyl auristatin F (MMAF), is conjugated to an antibody and released in active form as a charged species, diffusion across membranes is limited, and the bystander effect is reduced. Cleavable linkers, present in trastuzumab duocarmazine,<sup>82</sup> are more prone to the bystander effect<sup>83</sup> than those containing non-cleavable thioether linkages, such as trastuzumab emtansine. This underlines the importance of a thorough understanding of the stability of the linker and payload release, since the bystander effect provides an added mechanism to tune therapeutic specificity.

#### 2.8.4. Conjugation site and loading

Inactivation of the small molecule can occur through structural modifications that impart improper active site geometry. When available, crystal structures or models of drug molecules bound to their target can assist in selection of potential linkage sites on the active compound.<sup>84-85</sup> Similarly, the site of conjugation to the biomolecule is critical to maintain activity of the conjugate. Modern ADCs employ site specific approaches to conjugate drugs in the Fc region of antibodies to prevent inhibition of binding between the antibody Fab region and the cell surface antigen, thereby increasing therapeutic activity.<sup>86</sup> The construction of reproducible and homogeneous bioconjugates has improved in recent years with the advent of unnatural amino acids (Figure 9) and engineered cysteines.<sup>19</sup>

Multiple groups have demonstrated the impact of DAR on efficacy, and commercially-approved ADCs are present as mixtures of regioisomers, each having different safety and efficacy profiles.<sup>78</sup> DAR 0 species are particularly unfavorable due to competitive binding with antigenic receptors without delivering the warhead, leading to an overall decreased potency of the therapeutic. Most ADCs target a DAR of 3-4, with higher values altering clearance and biodistribution without a continued increase in activity,<sup>78</sup> resulting in a higher toxicity and lower therapeutic index.<sup>87</sup> Supporting these findings is the observation of increased liver accumulation with high DAR species, leading to faster clearance rates.<sup>78</sup> Physical instabilities with high DAR species is also noted, leading to increased aggregation with elevated DAR.<sup>88</sup>

Bioconjugates involving two larger molecules such as polymers and proteins have to consider the impact of the size of the resulting conjugate, including hydrodynamic radius and structure. While two independent molecules may localize specifically *in vivo*, the modification in size can have implications on trafficking,<sup>89</sup> clearance, immune response,<sup>29</sup> and cellular uptake.<sup>90</sup>



This effect of size on biodistribution is a phenomenon also seen in the nanoparticle field,<sup>91</sup> and is an important characteristic to consider when designing bioconjugates and must be adequately characterized using size-appropriate analytical methods.

## **2.9. Conclusions and Future Directions**

Bioconjugates represent a rapidly growing field by creating hybrid molecules that exploit the advantages of multiple molecular entities. As the field continues to emerge, an increased understanding of the impact of key parameters such as solubility, stability, and size have on the pharmacokinetics, pharmacodynamics, and safety profile are of paramount importance. Efforts to limit therapeutic heterogeneity and increase the specificity of these complex molecules have seen improvements in patient outcomes and will only continue to increase as development progresses.

Given the significant clinical advancement of ADCs, a broad expansion of the toolbox of available linkers, antibodies and warheads will further the applicability of this approach. Applying the AAC reaction to a large set of functionalized molecules has enabled a combinatorial approach to high-throughput conjugate generation,<sup>92-93</sup> which could be optimized over time once lead candidate have been identified. An additional benefit of toolbox development is the ability to overcome resistance by altering one of the components which may be targeted by mechanisms such as efflux pumps, altered expression of pro-apoptotic proteins, or downregulation of cell-surface antigens.<sup>19</sup> Studies have shown that overcoming resistance to a warhead present on an ADC is possible by altering the payload molecule,<sup>94</sup> highlighting the critical need for a wide array of drug molecules available to combat resistance.

**CHAPTER 3:**  
**ANTIGEN-DRUG CONJUGATES AS A NOVEL**  
**THERAPEUTIC CLASS FOR ANTIGEN-SPECIFIC**  
**AUTOIMMUNE DISORDERS**

## **CHAPTER 3: ANTIGEN-DRUG CONJUGATES AS A NOVEL THERAPEUTIC CLASS FOR ANTIGEN-SPECIFIC AUTOIMMUNE DISORDERS**

### **3.1. Introduction**

The adaptive immune response is dependent on recognition of target antigens, and autoimmune diseases occur when the body fails to maintain tolerance toward self-antigens.<sup>1</sup> These self-antigens can be present in a number of host tissues in various organs, leading to diseases such as multiple sclerosis (MS).<sup>2</sup> MS is the most common cause of neurological disability in young adults, affecting approximately 2.5 million patients worldwide,<sup>3</sup> and is highly variable in terms of clinical manifestation.<sup>4</sup> While the mechanism has not been fully elucidated, the prevailing theory is that proteins composing the myelin sheath coating neurons of the central nervous system (CNS), such as proteolipid protein (PLP) and myelin basic protein (MBP), trigger recruitment of myelin-specific CD4<sup>+</sup> T cells, resulting in inflammation leading to demyelination.<sup>95</sup>

The treatment landscape for MS is expanding as our understanding of pathogenesis continues to evolve. Corticosteroids have been a cornerstone for MS therapy,<sup>12</sup> acting through downregulation of pro-inflammatory cytokine production, inhibiting antibody production, or reducing BBB permeability.<sup>96</sup> IFN- $\beta$  reduces T-cell activation and proliferation, in addition to downregulating the cell surface receptors involved in antigen presentation.<sup>96</sup> Glatiramer acetate is thought to function by blocking lymphocyte sensitization to MBP via competitive inhibition of antigen presentation.<sup>13</sup> Newer monoclonal antibody therapies alleviate inflammation in the CNS through a variety of mechanisms, including altered immune cell trafficking (natalizumab), B-cell depletion (rituximab and alemtuzumab), or T-cell expansion (daclizumab).<sup>96</sup> Importantly, all of these treatments lead to undesired side effects, can be minimally efficacious, and modify normal immune system functions. Typically, these effects are a result of a lack of therapeutic specificity,

and here, we present antigen-drug conjugates (AgDCs) as an alternative to these approaches with the potential to mitigate the detriments of these treatments to increase both safety and efficacy.

AgDCs are a combination of the two general approaches to combat autoimmunity – immunomodulatory agents and hyposensitization therapy. While hyposensitization therapies have shown minimal efficacy in clinical studies for autoimmune diseases, they provide the specificity necessary to reverse an immune response toward a particular antigen, and have been effective at inducing tolerance towards allergens. Immunomodulatory agents show greater efficacy in autoimmune diseases, but suffer from systemic action and subsequent global immunosuppression, which can be problematic in immunocompromised patient populations by increasing the vulnerability to opportunistic infections. Through conjugation of the antigen and immunomodulator, the antigen is able to function as a directing agent to target the immunomodulator to offending immune cell populations and limit off target effects seen with treatment by the immunomodulator alone. An analogous approach has seen significant clinical success in recent years in the field of immunooncology with the development of antibody-drug conjugates (ADCs). The inverse concept of AgDCs has yet to be attempted for autoimmune indications.

MS is a neurodegenerative disease unique to humans, but can be effectively mimicked in the murine model of experimental autoimmune encephalomyelitis (EAE).<sup>8</sup> The relapsing-remitting EAE model exhibits CD4<sup>+</sup> T cell-mediated disease, leading to primary demyelination of the axonal tracks in the CNS and subsequent progressive paralysis of the limbs.<sup>7</sup> Disease induction occurs through an adjuvanted ‘vaccine’ containing the antigenic epitope, PLP<sub>139-151</sub>, injected subcutaneously, and mimics the clinical and histopathological similarities seen with relapsing-

remitting multiple sclerosis (RRMS) in humans.<sup>2</sup> EAE is considered to be the best defined preclinical model for organ-specific autoimmunity mediated by a Th1/Th17-driven response.<sup>2</sup>

### **3.2. Materials and Methods**

Dexamethasone, tris(3-hydroxypropyltriazolylmethyl)amine (THPTA), and sodium ascorbate (NaAsc) were purchased from Sigma-Aldrich (St. Louis, MO). Copper(II) sulfate pentahydrate ( $\text{CuSO}_4 \cdot 5\text{H}_2\text{O}$ ) was purchased from Acros Organics (Geel, Belgium). 2,5-dioxopyrrolidin-1-yl 2-azidoacetate, DBCO-PEG<sub>4</sub>-Maleimide, DBCO-NH<sub>2</sub>, and MMAE-DBCO were purchased from Clickchemistrytools, LLC (Scottsdale, AZ). Doxorubicin hydrochloride was purchased from LC Laboratories (Woburn, MA). Mertansine (DM1) was purchased from Carbosynth Limited (Berkshire, UK). All other chemicals and reagents were analytical grade and were used as received without further purification.

The peptides PLP<sub>139-151</sub>-Alk and PLP<sub>139-151</sub>-N<sub>3</sub> have been synthesized in our laboratory via solid phase peptide synthesis on a Wang resin, but larger quantities of each peptide were obtained from Biomatik Corporation (Wilmington, DE). In each case, the linker 3-(2-(2-(2-azidoethoxy)ethoxy)ethoxy)propanoic acid was purchased from PurePEG, LLC (San Diego, CA) and 4-pentynoic acid was purchased from Sigma-Aldrich (St. Louis, MO).

### 3.2.1. Synthetic procedures

#### 3.2.1.1. Synthesis of DBCO-functionalized Rhodamine B (Rhod-DBCO)

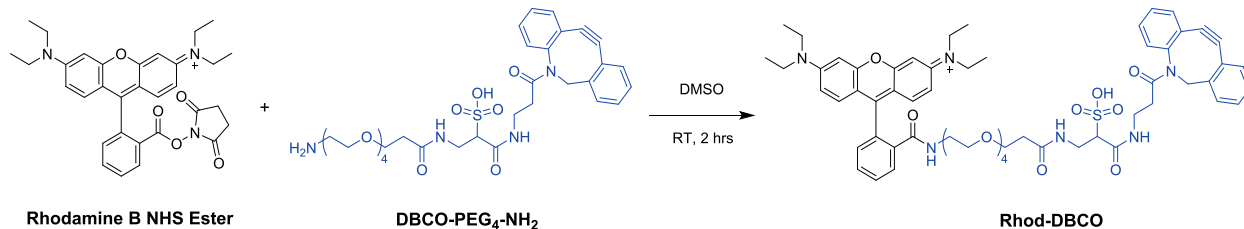


Figure 14: Reaction scheme for the synthesis of Rhod-DBCO.

The starting Rhodamine B NHS Ester was synthesized from the parent Rhodamine B dye, according to a literature procedure.<sup>97</sup> DBCO-PEG<sub>4</sub>-NH<sub>2</sub> (29.6  $\mu\text{mol}$ ) in 2 mL of DMSO was added to a solution of Rhodamine B NHS Ester (37.0  $\mu\text{mol}$ , 1.2 eq.) in 2 mL of DMSO. The solution was allowed to stir at room temperature while protected from light, while periodically removing an aliquot to monitor reaction progress by analytical HPLC. After 2 hours, the solution was purified by preparative HPLC on a Waters XBridge BEH C<sub>18</sub>, 5  $\mu\text{m}$ , 130  $\text{\AA}$ , 19x250 mm column using a gradient of MeCN in H<sub>2</sub>O (constant 0.05% TFA). The isolated fractions were evaporated under reduced pressure to remove residual MeCN, then frozen at -20°C and lyophilized to yield a purple powder. Expected  $[M]^+ = 1099.4845$  Da,  $[M+H]^{2+} = 550.2459$  Da; Observed  $[M]^+ = 1099.4762$  Da,  $[M+H]^{2+} = 550.2509$  Da.

### 3.2.1.2. Synthesis of azide-functionalized dexamethasone (Dex-N<sub>3</sub>)

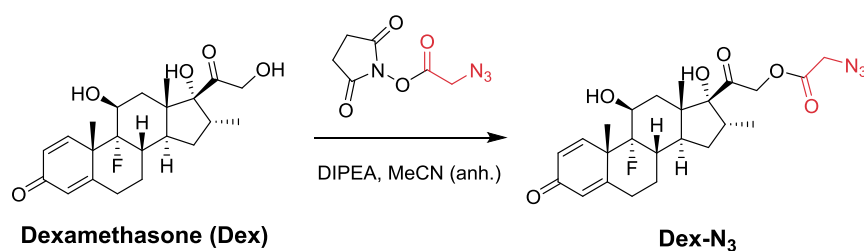


Figure 15: Reaction scheme for the synthesis of Dex-N<sub>3</sub>.

Dexamethasone was added to a flame dried 250mL round bottom flask with a stir bar and septa. Anhydrous MeCN was added under nitrogen, then DIPEA via glass syringe. The flask was stirred for 10 min before azidoacetic acid NHS ester was added as a powder. The reaction mixture was stirred overnight at room temperature before being analyzed by HPLC. Additional equimolar aliquots of azidoacetic acid NHS ester were added, followed by stirring for 2 hours at room temperature and analyzing by HPLC, until no additional benefit was observed. The crude reaction mixture was evaporated under reduced pressure, then dissolved in 4:6 MeCN:H<sub>2</sub>O and purified by prep HPLC. The resulting column fractions were evaporated under reduced pressure to yield the final product as a white powder. <sup>1</sup>H NMR (500 MHz, DMSO-*d*<sub>6</sub>) δ 7.30 (d, J = 10.2 Hz, 1H), 6.23 (dd, J = 10.1, 1.9 Hz, 1H), 6.01 (t, J = 1.7 Hz, 1H), 5.45 (dd, J = 5.0, 1.4 Hz, 1H), 5.23 (s, 1H), 5.17 (d, J = 17.5 Hz, 1H), 4.90 (d, J = 17.6 Hz, 1H), 4.32 – 4.19 (m, 2H), 4.19 – 4.11 (m, 1H), 2.88 (dq, J = 11.5, 7.2, 4.1 Hz, 1H), 2.62 (tdd, J = 13.6, 6.0, 1.7 Hz, 1H), 2.44 – 2.32 (m, 1H), 2.35 – 2.28 (m, 1H), 2.22 – 2.05 (m, 3H), 1.77 (dt, J = 11.2, 5.2 Hz, 1H), 1.70 – 1.58 (m, 1H), 1.56 (dd, J = 13.8, 2.0 Hz, 1H), 1.49 (s, 3H), 1.35 (qd, J = 12.9, 5.0 Hz, 1H), 1.08 (ddd, J = 12.1, 8.2, 4.1 Hz, 1H), 0.89 (s, 3H), 0.80 (d, J = 7.2 Hz, 3H). <sup>13</sup>C NMR (126 MHz, DMSO-*d*<sub>6</sub>) δ 204.36, 185.30, 168.28, 167.10, 152.77, 129.03, 124.12, 102.00, 100.61, 90.52, 70.63, 70.34, 69.00, 49.34, 48.09,

48.05, 47.87, 43.33, 35.69, 35.53, 33.67, 33.51, 31.92, 30.28, 27.32, 23.03, 22.98, 16.31, 15.15, 1.19. Expected  $[M+H]^+ = 476.2191$  Da; Observed  $[M+H]^+ = 476.2067$  Da.

### 3.2.1.3. Synthesis of azide-functionalized doxorubicin (Dox-N<sub>3</sub>)

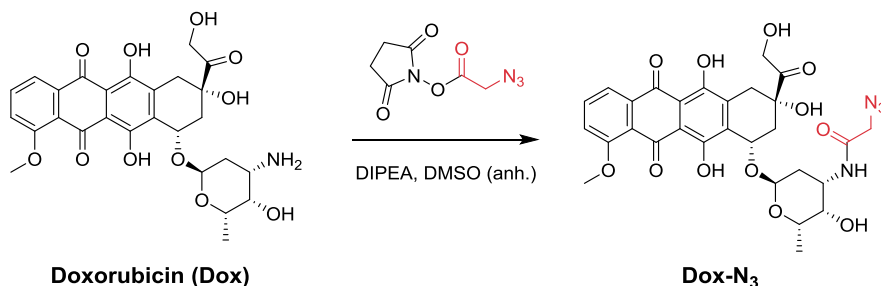


Figure 16: Reaction scheme for the synthesis of Dox-N<sub>3</sub>.

To a flame dried 20 mL scintillation vial (protected from light) with stir bar was added doxorubicin hydrochloride, followed by anhydrous DMSO. Once dissolved, DIPEA was added via syringe, then stirred for 5 min, followed by azidoacetic acid NHS ester as a powder. The solution was stirred overnight at room temperature, then analyzed by analytical HPLC to determine the extent of reaction. The crude mixture was purified by prep HPLC, and the column fractions were evaporated under reduced pressure to yield a red powder. <sup>1</sup>H NMR (500 MHz, DMSO-*d*<sub>6</sub>)  $\delta$  14.02 (s, 1H), 13.26 (s, 1H), 7.94 – 7.85 (m, 3H), 7.67 – 7.60 (m, 1H), 5.23 (d, *J* = 3.5 Hz, 1H), 4.93 (dd, *J* = 5.6, 3.3 Hz, 1H), 4.58 (s, 2H), 4.19 (dt, *J* = 7.3, 6.0 Hz, 2H), 4.01 (ddd, *J* = 9.7, 4.6, 2.3 Hz, 1H), 3.97 (s, 4H), 3.76 (d, *J* = 4.8 Hz, 2H), 3.48 – 3.39 (m, 2H), 3.03 – 2.88 (m, 2H), 2.24 – 2.16 (m, 1H), 2.10 (dd, *J* = 14.3, 5.7 Hz, 1H), 1.84 (td, *J* = 12.9, 3.8 Hz, 1H), 1.45 (dd, *J* = 12.5, 4.6 Hz, 1H), 1.13 (d, *J* = 6.5 Hz, 3H), 1.05 (t, *J* = 7.0 Hz, 1H). <sup>13</sup>C NMR (126 MHz, DMSO-*d*<sub>6</sub>)  $\delta$  213.91, 186.57, 186.48, 166.61, 160.79, 156.12, 154.51, 136.24, 135.52, 134.69, 134.10, 120.01, 119.75, 119.01, 110.80, 110.67, 100.31, 100.25, 74.94, 70.02, 69.98, 67.85, 66.63, 66.58, 63.71,



56.63, 56.57, 50.58, 50.53, 50.48, 45.37, 45.32, 36.65, 32.06, 29.65, 17.02, 17.00. Expected  $[M+Na]^+ = 649.1752$  Da; Observed  $[M+Na]^+ = 649.1498$  Da.

#### 3.2.1.4. Synthesis of DBCO-functionalized DM1 (DM1-DBCO)

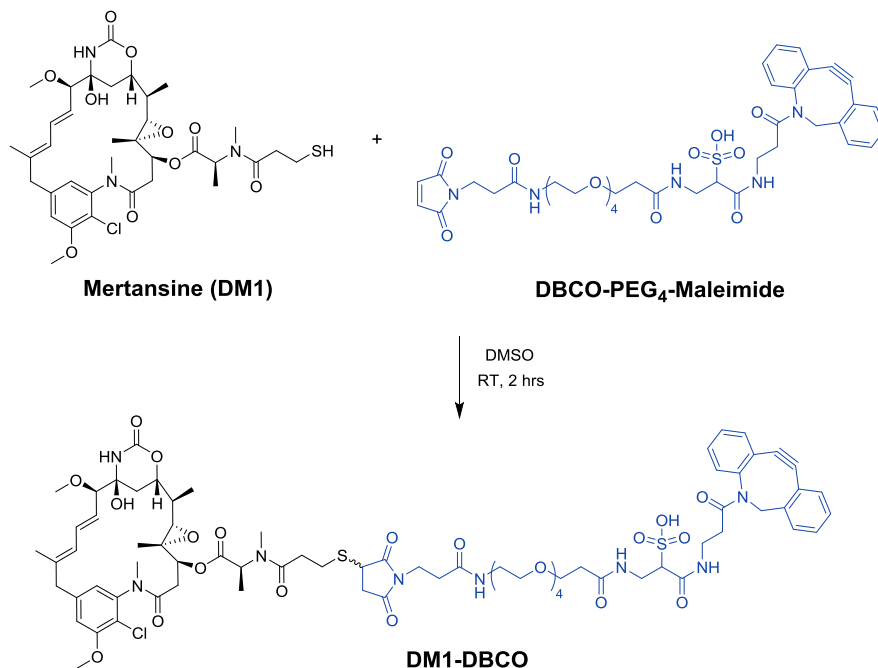


Figure 17: Reaction scheme for the synthesis of DM1-DBCO.

DM1 (33.9  $\mu\text{mol}$ ) in 2.5 mL of DMSO was added to DBCO-PEG<sub>4</sub>-Maleimide (36.35  $\mu\text{mol}$ , 1.07 eq.) in 2.5 mL of DMSO. The solution was stirred at room temperature for 1 hour before an aliquot was removed for reaction monitoring by analytical HPLC. After 2 hours, the reaction was purified by preparative HPLC on a Waters XBridge BEH C<sub>18</sub>, 5  $\mu\text{m}$ , 130  $\text{\AA}$ , 19x250 mm column using a gradient of MeCN in H<sub>2</sub>O (constant 0.05% TFA). The isolated fractions were evaporated under reduced pressure to remove residual MeCN, then frozen at  $-20^\circ\text{C}$  and lyophilized to yield a white powder. Expected  $[M+H]^+ = 1563.5713$  Da; Observed  $[M+H]^+ = 1563.5530$  Da.

### 3.2.1.5. Synthesis of PLP<sub>139-151</sub>-Rhodamine B (PLP<sub>139-151</sub>-Rhod)

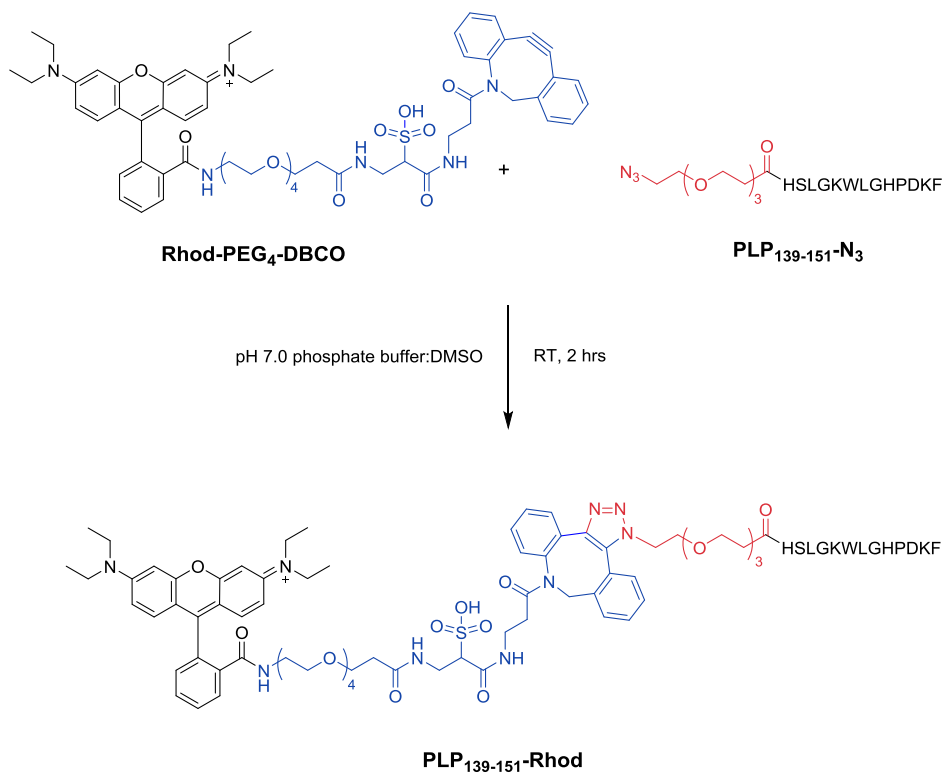


Figure 18: Reaction scheme for the synthesis of PLP<sub>139-151</sub>-Rhod.

PLP<sub>139-151</sub>-N<sub>3</sub> (18.3  $\mu\text{mol}$ ) in 3.0 mL of 20 mM phosphate buffer (pH 7.0) was added to Rhod-DBCO (18.2  $\mu\text{mol}$ , 1.0 eq.) in 3.0 mL of DMSO. The solution was allowed to stir at room temperature for 1 hour before an aliquot was removed for reaction monitoring by analytical HPLC. After 2 hours, the reaction was purified by preparative HPLC on a Waters XBridge BEH C<sub>18</sub>, 5  $\mu\text{m}$ , 130  $\text{\AA}$ , 19x250 mm column using a gradient of MeCN in H<sub>2</sub>O (constant 0.05% TFA). The isolated fractions were evaporated under reduced pressure to remove residual MeCN, then frozen at -20°C and lyophilized to yield a purple powder. Expected  $[\text{M}+2\text{H}]^{3+} = 950.7992 \text{ Da}$ ,  $[\text{M}+3\text{H}]^{4+} = 713.3512 \text{ Da}$ ; Observed,  $[\text{M}+2\text{H}]^{3+} = 950.8094 \text{ Da}$ ,  $[\text{M}+3\text{H}]^{4+} = 713.3638 \text{ Da}$ .

### 3.2.1.6. Synthesis of PLP<sub>139-151</sub>-Doxorubicin (PLP<sub>139-151</sub>-Dox)

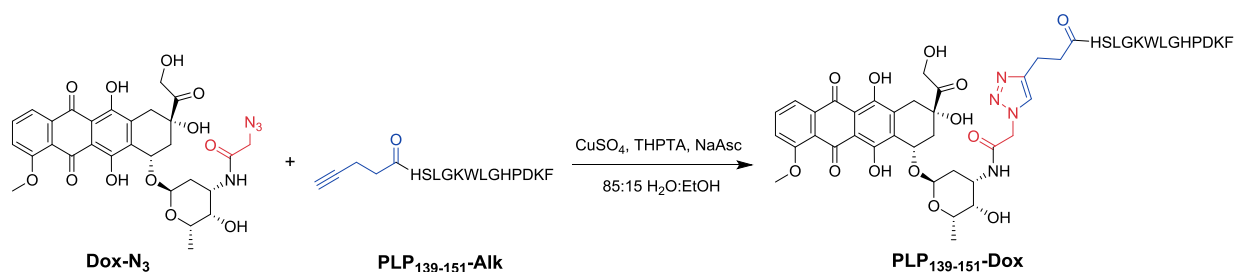


Figure 19: Reaction scheme for the synthesis of PLP<sub>139-151</sub>-Dox.

To a solution of PLP<sub>139-151</sub>-Alk (12.5  $\mu$ mol) in 5 mL deionized H<sub>2</sub>O was added Dox-N<sub>3</sub> (19.2  $\mu$ mol, 1.53 eq.) in 1 mL EtOH, while protecting the reaction from light. 225  $\mu$ L of a premixed solution of CuSO<sub>4</sub>•5H<sub>2</sub>O (1.5  $\mu$ mol) and THPTA (7.5  $\mu$ mol) in deionized H<sub>2</sub>O was added to the reaction mixture, followed by 320  $\mu$ L of NaAsc (32.3  $\mu$ mol) in deionized H<sub>2</sub>O. The reaction was allowed to stir at room temperature for 1 hour before an aliquot was removed for analytical HPLC to monitor reaction progress. After 2 hours, the reaction mixture was purified by preparative HPLC on a Waters XBridge BEH C<sub>18</sub>, 5  $\mu$ m, 130  $\text{\AA}$ , 19x250 mm column using a gradient of MeCN in H<sub>2</sub>O (constant 0.05% TFA). The isolated fractions were evaporated under reduced pressure to remove residual MeCN, then frozen at -20°C and lyophilized to yield a red powder. Expected  $[M+2H]^{2+} = 1115.0095$  Da,  $[M+3H]^{3+} = 743.6754$  Da; Observed  $[M+2H]^{2+} = 1115.0045$  Da,  $[M+3H]^{3+} = 743.6735$  Da.

### 3.2.1.7. Synthesis of PLP<sub>139-151</sub>-Dexamethasone (PLP<sub>139-151</sub>-Dex)

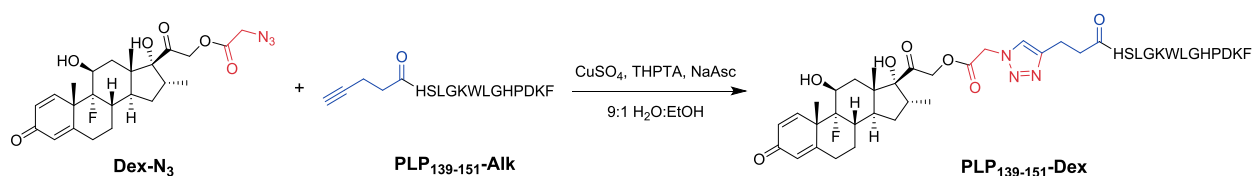


Figure 20: Reaction scheme for the synthesis of PLP<sub>139-151</sub>-Dex.

To a solution of PLP<sub>139-151</sub>-Alk (93.6  $\mu$ mol) in 120 mL deionized H<sub>2</sub>O was added Dex-N<sub>3</sub> (189.4  $\mu$ mol, 2.02 eq.) in 12 mL EtOH. 5.7 mL of a premixed solution of CuSO<sub>4</sub>•5H<sub>2</sub>O (38.1  $\mu$ mol) and THPTA (189.8  $\mu$ mol) in deionized H<sub>2</sub>O was added to the reaction mixture, followed by 7.2 mL of NaAsc (726.9  $\mu$ mol) in deionized H<sub>2</sub>O. The reaction was allowed to stir at room temperature for 1 hour before an aliquot was removed for analytical HPLC to monitor reaction progress. After 3 hours, the reaction mixture was concentrated under reduced pressure, and purified by preparative HPLC on a Waters XBridge BEH C<sub>18</sub>, 5  $\mu$ m, 130  $\text{\AA}$ , 19x250 mm column using a gradient of MeCN in H<sub>2</sub>O (constant 0.05% TFA). The isolated fractions were evaporated under reduced pressure to remove residual MeCN, then frozen at -20°C and lyophilized to yield a white powder. Expected  $[M+2H]^{2+} = 1039.5224$  Da,  $[M+3H]^{3+} = 693.3507$  Da; Observed  $[M+2H]^{2+} = 1039.5145$  Da,  $[M+3H]^{3+} = 693.3478$  Da.

### 3.2.1.8. Synthesis of PLP<sub>139-151</sub>-Mertansine (PLP<sub>139-151</sub>-DM1)

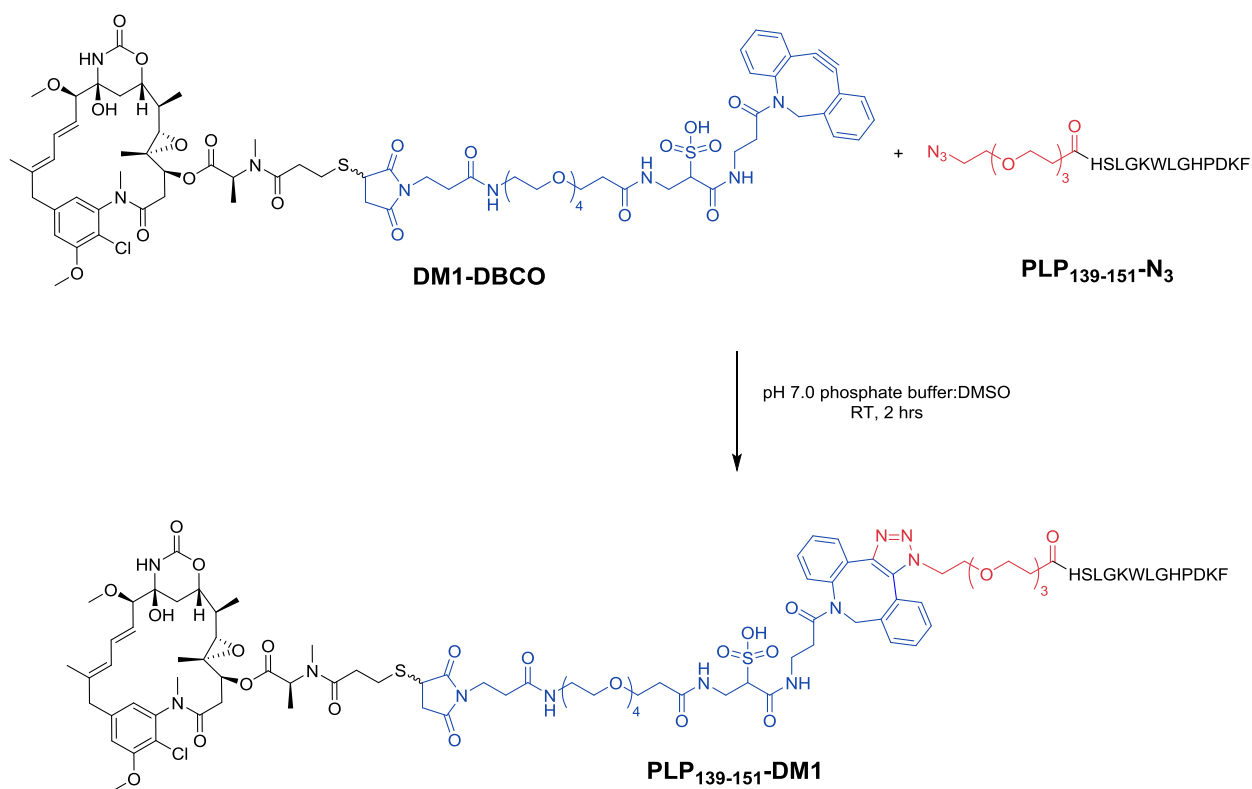


Figure 21: Reaction scheme for the synthesis of PLP<sub>139-151</sub>-DM1.

DM1-DBCO (6.4  $\mu\text{mol}$ ) in 2 mL of DMSO was added to PLP<sub>139-151</sub>-N<sub>3</sub> (6.9  $\mu\text{mol}$ , 1.07 eq.) in 2 mL of 20 mM phosphate buffer (pH 7.0). The solution was stirred at room temperature for 1 hour before an aliquot was removed for reaction monitoring by analytical HPLC. After 2 hours, the reaction was purified by preparative HPLC on a Waters XBridge BEH C<sub>18</sub>, 5  $\mu\text{m}$ , 130  $\text{\AA}$ , 19x250 mm column using a gradient of MeCN in H<sub>2</sub>O (constant 0.05% TFA). The isolated fractions were evaporated under reduced pressure to remove residual MeCN, then frozen at  $-20^\circ\text{C}$  and lyophilized to yield a white powder. Expected  $[\text{M}+3\text{H}]^{3+} = 1105.4948 \text{ Da}$ ; Observed  $[\text{M}+3\text{H}]^{3+} = 1105.4955 \text{ Da}$ .

### 3.2.1.9. Synthesis of *PLP*<sub>139-151</sub>-Monomethyl auristatin E (*PLP*<sub>139-151</sub>-MMAE)

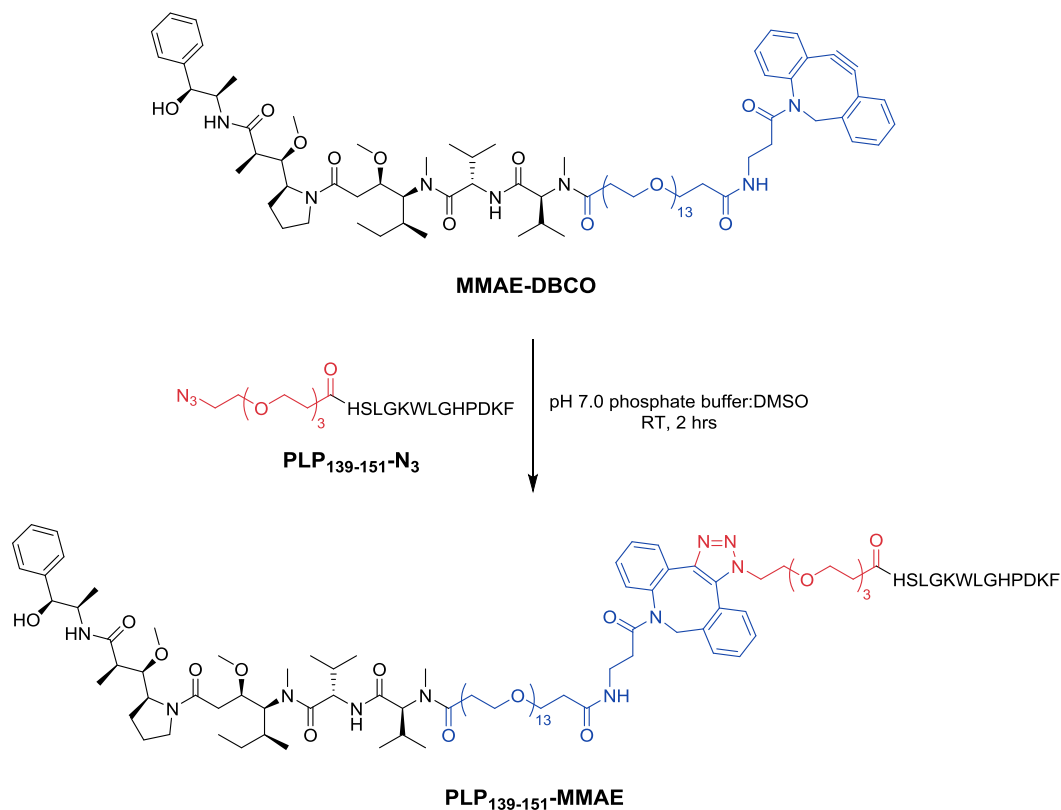


Figure 22: Reaction scheme for the synthesis of *PLP*<sub>139-151</sub>-MMAE.

MMAE-DBCO (3.0  $\mu\text{mol}$ ) in 1 mL of DMSO was added to *PLP*<sub>139-151</sub>-N<sub>3</sub> (3.0  $\mu\text{mol}$ , 1.0 eq.) in 1 mL of 20 mM phosphate buffer (pH 7.0). The solution was stirred at room temperature for 1 hour before an aliquot was removed for reaction monitoring by analytical HPLC. After 2 hours, the reaction was purified by preparative HPLC on a Waters XBridge BEH C<sub>18</sub>, 5  $\mu\text{m}$ , 130  $\text{\AA}$ , 19x250 mm column using a gradient of MeCN in H<sub>2</sub>O (constant 0.05% TFA). The isolated fractions were evaporated under reduced pressure to remove residual MeCN, then frozen at -20°C and lyophilized to yield a white powder. Expected  $[\text{M}+3\text{H}]^{3+} = 1133.9656 \text{ Da}$ ,  $[\text{M}+4\text{H}]^{4+} = 850.7260 \text{ Da}$ ; Observed  $[\text{M}+3\text{H}]^{3+} = 1133.9634 \text{ Da}$ ,  $[\text{M}+3\text{H}]^{3+} = 850.7256 \text{ Da}$ .

### **3.2.2. Analytical characterization**

All HPLC chromatographic analysis was conducted with a Waters Alliance HPLC system equipped with either a diode array detector or dual wavelength UV/Vis detector. For RP-HPLC, general chromatographic conditions employed a linear elution gradient from 5-95% acetonitrile in water (constant 0.05% trifluoroacetic acid) over 50 min, on a Waters XBridge BEH C<sub>18</sub>, 3.5 μm, 130 Å stationary phase (4.6 x 150 mm), with a 1.0 mL/min flow rate and a 35°C column temperature. For semi-preparative HPLC, a linear elution gradient of acetonitrile in water (constant 0.05% trifluoroacetic acid) over 20 min, on a Waters XBridge BEH C<sub>18</sub>, 5 μm, 130 Å stationary phase (19 x 250 mm), with a 14.0 mL/min flow rate. Gradients were optimized for each run using the identical stationary phase in a 4.6 x 250 mm configuration.

LC/MS sample analysis was performed with a Waters Xevo G2, employing linear elution gradients of 15-100% acetonitrile in water (constant 0.1% formic acid) over 45 min, on a Waters XBridge BEH C<sub>18</sub>, 1.7 μm, 130 Å stationary phase (0.075 x 250 mm), with a 0.5 μL/min flow rate and 50°C column temperature. Electrospray ionization, operating in the positive mode (ESI+), was used as the ionization source with a QToF mass analyzer used for detection.

NMR spectra were collected on a Bruker Avance AVIII 500 MHz spectrometer equipped with a dual carbon/proton cryoprobe. All samples were dissolved in 650 μL of D<sub>2</sub>O or DMSO-*d*<sub>6</sub>. Data processing was performed using MestReNova 11.0 (Santiago de Compostela, Spain).

### **3.2.3. Drug release and stability studies**

Release and stability studies were conducted via HPLC with UV detection by dissolving the compound of interest in buffers relevant for *in vivo* administration of analytical sample analysis, typically deionized H<sub>2</sub>O, saline, phosphate buffered saline (pH 7.4), 10 mM phosphate

(pH 7.4) or 10 mM acetate (pH 5.5) and evaluating the release at temperatures and times relevant to the particular study. For compounds such as PLP<sub>139-151</sub>-Dex where the released drug has a significantly different extinction coefficient at the detection wavelength, drug release was measured using a linear calibration curve.

#### **3.2.4. Determination of IC<sub>50</sub> in EAE splenocytes**

Splenocytes were harvested from EAE mice on day 12 (peak of disease), which received no previous treatment, and cultured in the specified treatment at the designated concentrations for 120 hrs before being subjected to resazurin (N = 6 spleens/group). All data points were normalized to the mean resazurin response generated from untreated splenocytes.

#### **3.2.5. In vivo studies in EAE mice**

*In vivo* studies were carried out with 4-6 week old SJL/J (H-2) female mice. Mice were housed under specified, pathogen-free conditions and all experiments were approved by the University of Kansas Institutional Animal Care and Use Committee. On day 0, all mice were induced with EAE to mimic the effects of multiple sclerosis, by 4 subcutaneous injections of an emulsion containing PLP and complete Freund's adjuvant (CFA) which contains killed *Mycobacterium tuberculosis* capsid. Four subcutaneous injections were administered (N = 5 mice/group) above each shoulder blade (200 µL total). Pertussis toxin (100 ng in 100 µL) was injected intraperitoneally on day 0 and day 2 post-immunization. 100 µL treatments were administered subcutaneously on days 4, 7, and 10, with 400 nmol (Dex basis), with the control group receiving PBS. All mice were weighed and scored daily on a scale of 0-5, with 5 indicating highest disease severity. All mice were euthanized on day 25.



### 3.3. Results and Discussion

#### 3.3.1. *Therapeutic design, rationale, and drug selection*

AgDCs were designed to utilize antigen as a guide molecule for delivering a drug to cells contributing to autoimmunity. Active drug molecules were selected based on mechanism of action, potency, appropriate target location, and the presence of an available synthetic handle. Whenever possible, available crystal structures or other structural data were included in synthetic design to avoid inactivating the drug molecule due to inappropriate active site geometry or pharmacophore availability following conjugation. Two primary drug classes were selected in these studies, depending on the desired therapeutic outcome. Upon uptake into diseased cell populations, Dex is expected to mitigate inflammation by suppressing the normal immune response induced by PLP. Alternatively, potent cytotoxins such as mertansine (DM1), monomethyl auristatin E (MMAE), or doxorubicin (Dox) targeting the same cell populations would induce apoptosis and prevent further immune cell activation. All three of the cytotoxic compounds have been used clinically as ADC payloads,<sup>19</sup> and DM1 and MMAE are conjugated to directing antibodies in the commercially-approved therapeutics trastuzumab emtansine (T-DM1) and brentuximab vedotin (B-MMAE), respectively. All of these compounds, either in their parent form or commercially available derivative, contain reactive functionalities suitable for conjugation. Additionally, a fluorescently labeled conjugate based on the fluorophore rhodamine B was synthesized to elucidate antigen binding kinetics and specificity in future studies.

The encephalitogenic peptide selected as the targeting moiety is a portion of the intracellular loop<sup>98</sup> of the full-length proteolipid protein, PLP<sub>139-151</sub>. Previous studies have shown the impact of PLP<sub>139-151</sub> sequence variability on binding affinity,<sup>99</sup> highlighting the necessity to maintain the native sequence unchanged. Therefore, employing traditional synthetic methods

targeting side chain residues of the native sequence will likely alter conjugate binding and/or uptake. To circumnavigate these potential deleterious effects, all modifications to the targeting antigen occurred through the N-terminal amino acid, functionalized with heterobifunctional linkers as the final step of solid-phase peptide synthesis prior to cleavage from the resin.

Linker length, flexibility, and stability were key AgDC design considerations. Short linkers could potentially alter binding, while long linkers could affect mechanisms of internalization. For hydrophobic drug molecules, PEGylated or sulfonated linkers were used to increase aqueous solubility and compatibility with downstream reactions. In T-DM1, the payload is linked via a non-cleavable thioether bond, and preclinical studies employing disulfide linkages showed similar efficacy. To decrease the possibility of off target effects from cleavage of the drug following administration but prior to internalization, a thioether linker was selected. B-MMAE employs a valine-citrulline linker, which is cleaved by cathepsin B post-internalization, but previous studies have shown conjugates formed using non-cleavable maleimidocaproyl linkers also maintain activity following lysosomal catabolism.<sup>100</sup> Doxorubicin immunoconjugates have typically been constructed with acid labile hydrazone linkages<sup>101</sup> or through carbamate formation or amidation of the daunosamine ring,<sup>102-103</sup> and a stable amide bond was selected here to limit off-target toxicity.

### ***3.3.2. Synthetic strategy and optimization***

The overarching strategy was the development of a modular antigen and payload library that would enable the rapid and efficient synthesis of therapeutic or diagnostic conjugates (Figure 23). For this reason, two primary variants of the 1,3-dipolar cycloaddition reaction were employed,

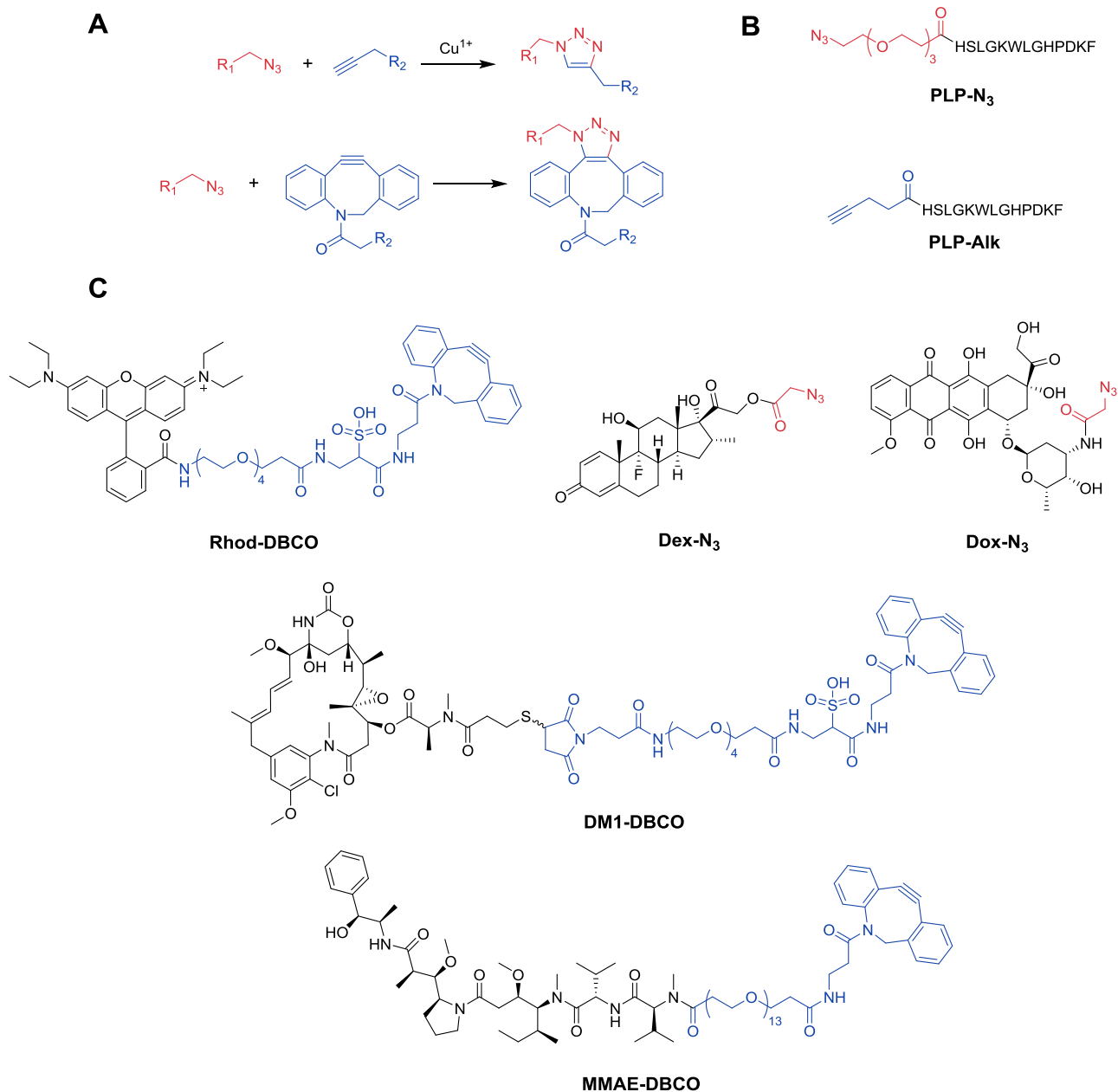


Figure 23: Compound library employed for AgDCs. A) General reaction schemes for the copper-catalyzed azide-alkyne cycloaddition (CuAAC) and strain-promoted azide-alkyne cycloaddition (SPAAC) reactions used for conjugation. B) Functionalized antigenic carrier peptides. C) Functionalized 'payload' molecules.

the copper-catalyzed azide-alkyne cycloaddition (CuAAC), and the strain-promoted azide-alkyne cycloaddition (SPAAC). Both reactions carry significant precedence, with a wealth of development and optimization studies available in the primary literature.<sup>32-34, 44</sup> There is also

significant precedence with respect to application of these chemistries in the field of bioconjugation,<sup>18, 33, 92, 104</sup> making construction of the payload library a less difficult endeavor.

Azide- and alkyne-functionalization of payload molecules generally involved *N*-hydroxysuccinimidyl activated esters (NHS esters) with a corresponding nucleophilic group on the payload, or Michael additions to electrophilic centers via maleimide chemistry. Both types of chemistry are routinely employed in bioconjugation applications, targeting side chains of lysine or cysteine residues, respectively. Due to the biocompatibility of this approach, minimal side reactions are observed, making the synthesis and purification more favorable. Similarly, peptide antigens employed the compounds 4-pentynoic acid and COOH-PEG<sub>3</sub>-N<sub>3</sub> for alkyne- and azide-functionalization, respectively.

One additional strength to the CuAAC and SPAAC conjugation chemistries is the relatively high yields, fast reaction times, and mild reaction conditions. Optimization of conjugation conditions generally began in aqueous media, with the exception of those conjugates involving less soluble payloads which required the assistance of organic solvents such as DMSO, DMF, or EtOH. Evaluation of reaction conditions occurred on the sub-milligram scale with the simultaneous development of HPLC methods employed for the downstream purification and analysis. In general, higher initial success was observed with SPAAC conjugates, yielding suitable reaction conditions with minimal development due to the lack of necessary catalyst, ligand, and reducing agent. As the initial molecular weights of the antigen and payloads were on the same order of magnitude, a 1:1 stoichiometric ratio was sufficient to produce high yields of the conjugate (>80%), which could be easily isolated from residual starting materials by preparative HPLC. Conjugates constructed with CuAAC chemistry typically involved more development with respect to reactant and catalyst concentrations, in addition to stoichiometric excess of the payload relative

to the antigen. In all cases, the amphiphilic nature of the conjugates made HPLC method development relatively straightforward, with significant retention differences between the hydrophilic peptide and hydrophobic drug often leaving the conjugate with an intermediate retention time compared to the parent compounds.

### ***3.3.3. Characterization of conjugates and intermediates***

The payload molecules and conjugates described were characterized by traditional chemical methods, including NMR, HPLC, LC/MS, and other spectroscopic means to confirm the structure of the entity. As opposed to ADCs which present additional analytical challenges due to molecular heterogeneity, AgDCs synthesized here were a more defined molecular species with high purity. HPLC analysis of the conjugates with UV/Vis detection provides typical purity values in excess of 93-95% following purification (Figure 24, Figure 25, and Figure 26), with impurities generally having retention times close to the parent conjugate. A similar analysis by UPLC with detection by mass spectrometry corroborated these results, showing multiple charge states of the compound indicative of attachment of the peptide antigen. Analysis of NMR proved to be more suitable for structural confirmation of small molecule payloads. However, one added benefit to the CuAAC chemistry when installing alkyne linkers on the peptide was the presence of a distinct resonance in  $^1\text{H}/^{13}\text{C}$  heteronuclear single quantum coherence (HSQC) NMR, corresponding to the terminal alkyne correlation ( $\delta(^1\text{H}) \approx 2.3$  ppm,  $\delta(^{13}\text{C}) \approx 70$  ppm), which is present in a unique chemical environment and well separated from other signals. After conjugation, this resonance undergoes a significant downfield shift upon incorporation as part of the conjugated triazole ring system (Figure 27).

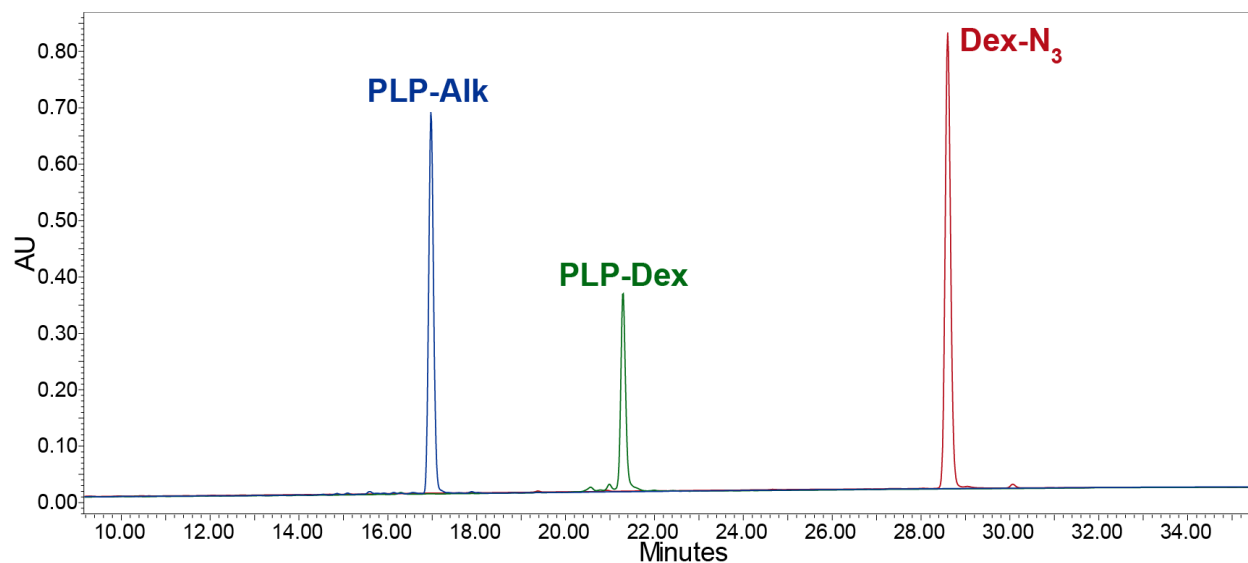


Figure 24: Representative analytical HPLC chromatogram showing the starting materials, PLP-Alk, and Dex-N<sub>3</sub>, along with the purified reaction product, PLP-Dex.

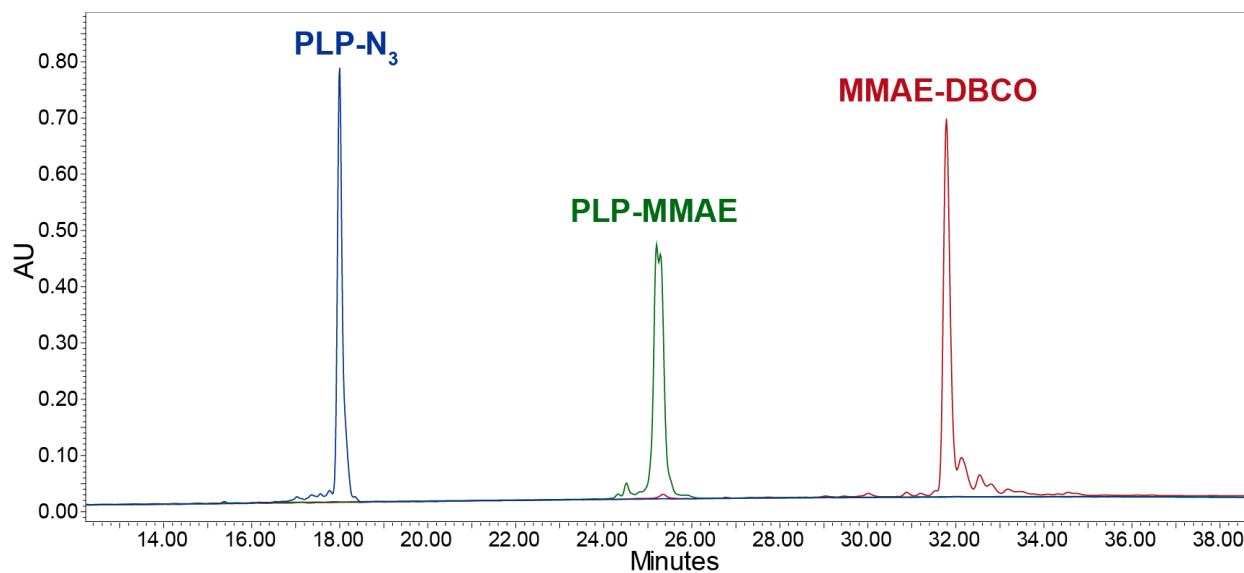


Figure 25: Analytical HPLC chromatograms of the starting materials and the purified reaction product, PLP<sub>139-151</sub>-MMAE. The presence of a split peak in the reaction product is indicative of the formation of regioisomers during the reaction.

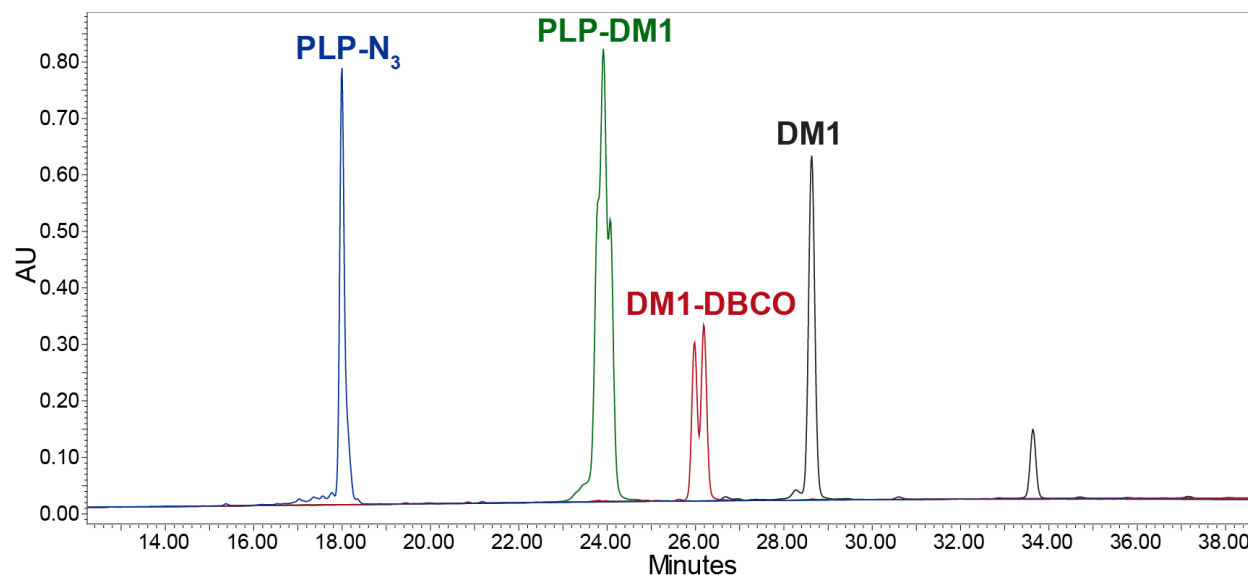


Figure 26: Analytical HPLC chromatograms of the starting materials and the purified reaction product, PLP<sub>139-151</sub>-DM1. The presence of a split peak in the DM1-DBCO reaction product suggests the presence of a chiral center, and the heterogeneity of the PLP<sub>139-151</sub>-DM1 peak indicates the formation of regioisomers produced from each of the starting stereoisomers.

One additional advantage of conjugating hydrophobic drug molecules to hydrophilic peptides was the impact on aqueous solubility. The PLP<sub>139-151</sub> peptide is soluble in excess of 60 mg/mL, providing a significant enhancement in drug solubility of the resulting amphiphilic conjugates. A noteworthy observation from HPLC analysis of conjugates synthesized using SPAAC chemistry was the formation of regioisomers with no apparent preference for a single isomer, potentially attributed to flexibility of the linker systems installed on each component. While semi-preparative HPLC is unable to resolve the regioisomers, they can be observed as a split peak by analytical HPLC when utilizing high peak capacity methods, but show consistent mass across the entire analyte peak by LC/MS. We do not anticipate any binding preference for either form due to linker flexibility. Importantly, for conjugates employing sulfonate functional groups in the linker region, the formation of isomers is possible and would yield an identical mass, but is not expected here due to known selectivity of the reactions. Additional NMR characterization data with larger batches is expected to confirm the proposed structures.

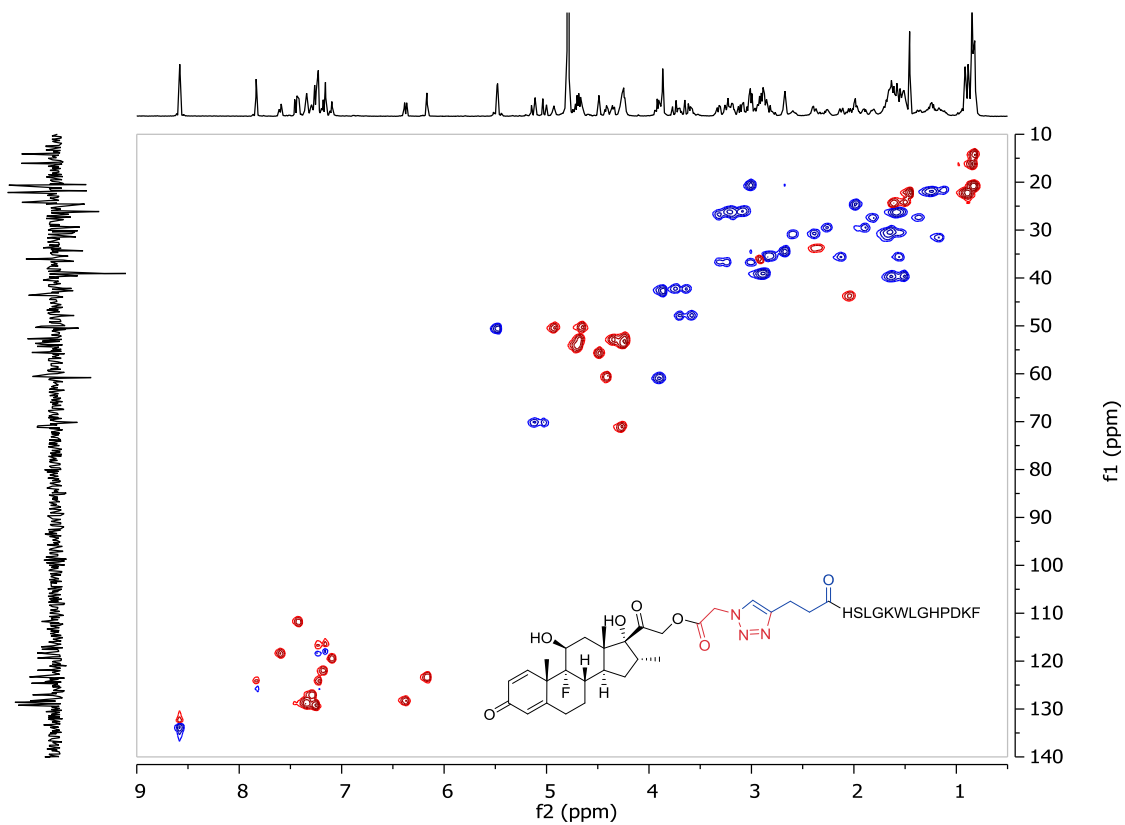
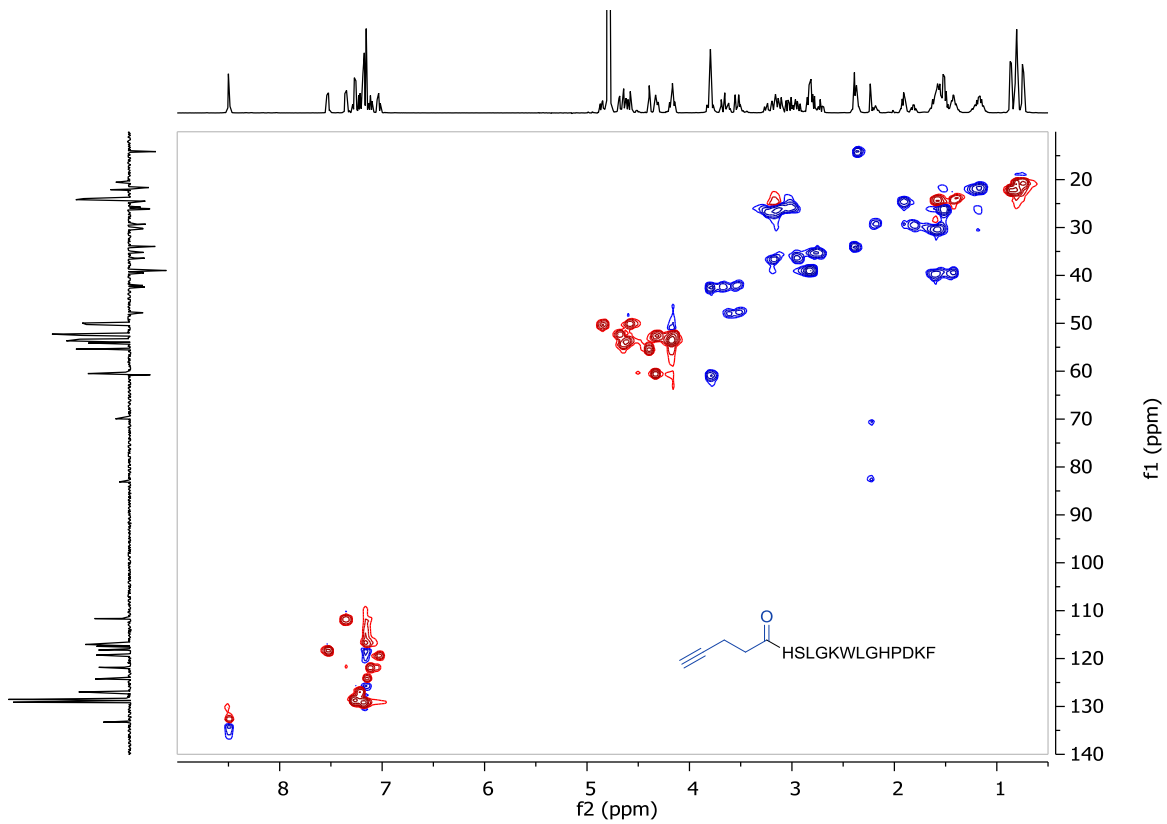


Figure 27:  $^1\text{H}/^{13}\text{C}$  HSQC NMR data for PLP<sub>139-151</sub>-Alk (top) and PLP<sub>139-151</sub>-Dex (bottom).



### 3.3.4. Stability and release kinetics

Throughout development, the starting peptides were stable in solution for time periods relevant to synthesis and analysis of the conjugates (at least a day). Of the therapeutic conjugates presented, only PLP<sub>139-151</sub>-Dex contains an acid-labile ester linkage capable of releasing the unadulterated parent drug in acidic microenvironments. Interestingly, the initial hypothesis was that Dex release would increase with decreasing pH, however, release of Dex was actually greater at pH 7.4 than at pH 5.5 (Figure 28). To better understand this observation, further studies focused

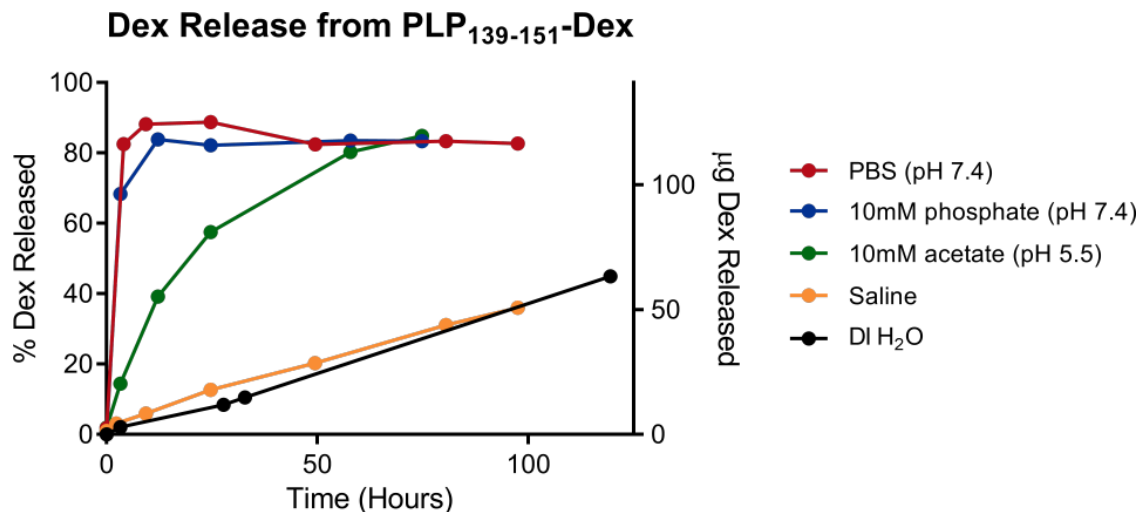


Figure 28: Release of Dex from PLP<sub>139-151</sub>-Dex as a function of time and buffer, at 37°C. Starting peptide concentration was 1 mg/mL, corrected for potency, and quantified via linear calibration curve.

on the parent Dex-N<sub>3</sub> in conditions that varied the concentration of phosphate buffer, showing quicker release as the concentration of phosphate increases (Figure 29). Taken together, it is thought that the phosphate anion plays a role in catalyzing the release of Dex from the peptide, probably through nucleophilic attack. Therefore, the dosing vehicle for subsequent *in vivo* studies was saline, adjusted to pH 6, to ensure complete solubility of the treatment and prevent premature release of Dex. Control experiments with both functionalized and unfunctionalized PLP<sub>139-151</sub> did

not show any significant degradation in the presence of phosphate buffer under the same conditions.

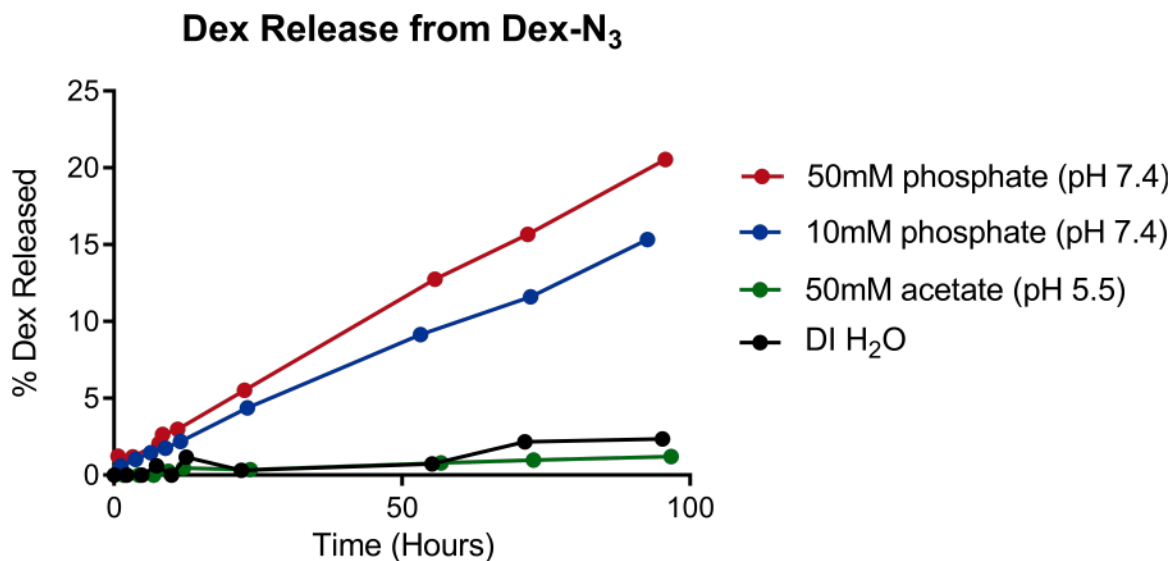


Figure 29: Release of Dex from Dex-N<sub>3</sub> as a function of time and buffer, at 25°C. To maintain Dex solubility for the duration of the analysis, the study was completed in 1:1 buffer:MeCN.

### 3.3.5. Efficacy studies

Splenocytes harvested from EAE mice at peak of disease provided a model cell system to evaluate drug activity, in terms of half-maximal inhibitory concentration (IC<sub>50</sub>). PLP<sub>139-151</sub>-Dex showed a similar IC<sub>50</sub> value when compared to Dex alone (Figure 30), indicating that the drug still remained active following conjugation, potentially due to the site selected for conjugation. When administered as a treatment regimen in EAE mice, PLP<sub>139-151</sub>-Dex showed complete suppression of disease symptoms, with all mice (N = 5 mice/group) showing no sign of disease throughout the duration of the study (Figure 31). Additionally, the mean weight of the PLP<sub>139-151</sub>-Dex treatment group increased over the course of the study, when compared to the PBS control group, which showed a decrease in weight correlating to an increase in clinical score (Figure 32).

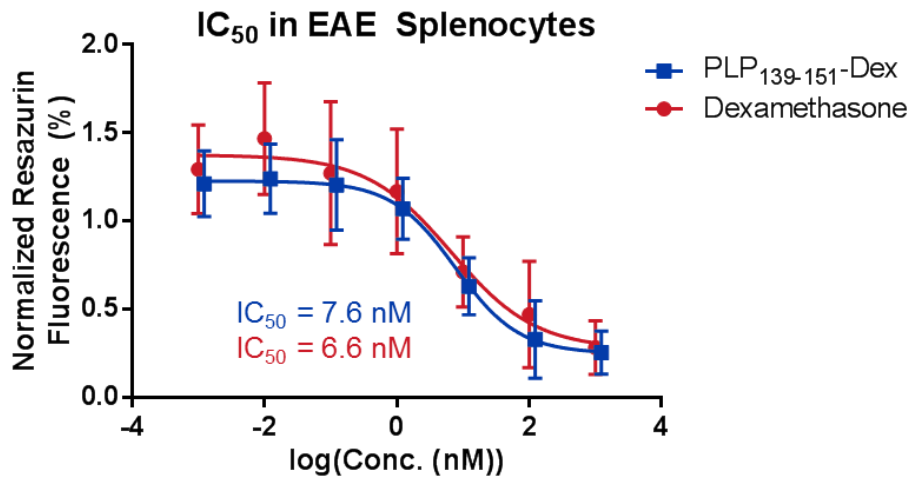


Figure 30: Determination of IC<sub>50</sub> for Dex and PLP<sub>139-151</sub>-Dex in EAE splenocytes.

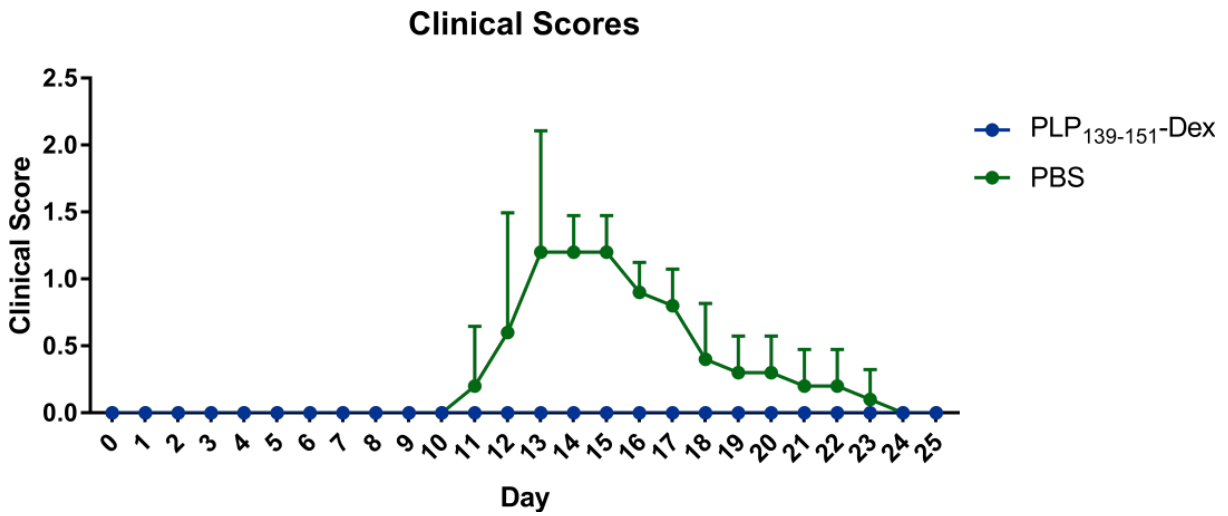


Figure 31: In vivo study in EAE mice, comparing clinical scores of a PLP<sub>139-151</sub>-Dex treatment group to a PBS control group. N=5 mice/group.

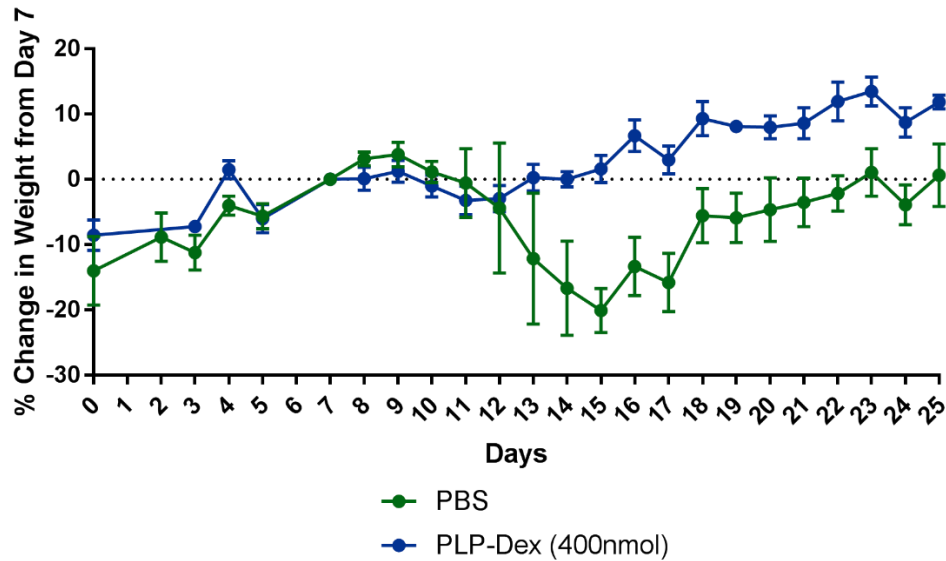


Figure 32: *In vivo* study in EAE mice, comparing normalized weights of a PLP<sub>139-151</sub>-Dex treatment group to a PBS control group. N=5 mice/group.

### 3.3.6. AgDCs uniquely combine two therapeutic approaches

AgDCs present a novel combination of two current treatment strategies, exploiting the specificity of the disease-causing autoantigen and potency of an immunomodulatory drug. As opposed to current treatments aimed at symptom suppression and reduction of disease progression, AgDCs have the potential to reverse autoimmune disease by targeting offending immune cells and deleting these cells or inducing tolerance to a specified autoantigen. *In vivo* studies have shown complete suppression of symptoms in the EAE model using PLP as a directing peptide, however, a different effect may be observed when the drug is conjugated to full length protein. The BCR is thought to be the target of AgDCs, since the BCR is a high affinity receptor. Studies employing BCR antibodies to block antigen binding, used in conjugation with fluorescently labeled peptide autoantigen may help to elucidate this mechanism. Other less likely mechanisms, such as direct binding to MHC II, could be probed in a similar manner. If our hypothesis is correct, conjugating

drug directly to full length protein autoantigens would target a wide repertoire of BCRs on B cells contributing to autoimmunity.

### **3.4. Conclusion**

Antigen-drug conjugates (AgDCs) represent a novel class of therapeutics with broad applicability to a variety of antigen-specific autoimmune disorders. By harnessing the benefits of two traditional therapeutic approaches, hyposensitization and immunomodulatory therapy, AgDCs employ a synergistic approach by conjugating the antigen to the immunomodulatory agent. PLP<sub>139-151</sub>-Dex showed promising *in vivo* results that warrant further screening and mechanistic evaluation of the AgDC strategy. Experiments to improve understanding of cellular localization and uptake will utilize compounds such as PLP<sub>139-151</sub>-Rhod, which provides a fluorescent probe on the antigenic peptide.

Ongoing efforts to expand the AgDC platform in our laboratory are multi-faceted, from expanding the antigen and payload library within the MS indication, to adaption across the landscape of antigen-specific autoimmune disorders. The modular nature of this AgDC approach, coupled with the consistency and specificity of the chemistries employed, make AgDCs a promising therapeutic class for the treatment of autoimmune disorders. Additional AgDCs presented in this chapter, including PLP<sub>139-151</sub>-MMAE, PLP<sub>139-151</sub>-DM1, and PLP<sub>139-151</sub>-Dox will undergo further evaluation in *in vivo* or *in vitro* systems as a continued effort to identify improved treatments for MS.

**CHAPTER 4:**  
**MULTIVALENT SOLUBLE ANTIGEN ARRAYS EXHIBIT  
HIGH AVIDITY BINDING AND MODULATION OF B CELL  
RECEPTOR-MEDIATED SIGNALING TO DRIVE EFFICACY  
AGAINST EXPERIMENTAL AUTOIMMUNE  
ENCEPHALOMYELITIS**

## **CHAPTER 4: MULTIVALENT SOLUBLE ANTIGEN ARRAYS EXHIBIT HIGH AVIDITY BINDING AND MODULATION OF B CELL RECEPTOR-MEDIATED SIGNALING TO DRIVE EFFICACY AGAINST EXPERIMENTAL AUTOIMMUNE ENCEPHALOMYELITIS**

### **4.1. Introduction**

Autoimmune diseases such as multiple sclerosis (MS) are typified by a breakdown of healthy immune regulation and subsequent misrecognition of self for non-self.<sup>105-106</sup> The autoimmune breakdown in MS is largely propagated by autoreactive T and/or B cell clonal expansion and attack against myelin sheath autoantigens, leading to demyelination and neurodegeneration.<sup>107-110</sup> Activation of naïve T cells against autoantigen requires two signals from an antigen presenting cell (APC): (1) primary antigenic signal delivered through the major histocompatibility complex (MHC) on the APC to the T cell receptor (TCR) on the T cell, and (2) secondary costimulatory signal (i.e., CD80/CD86) delivered to the cognate receptor (i.e., CD28) on the T cell.<sup>111-119</sup> B cells, as professional APCs that possess antigen specificity and immunological memory, play a particularly pivotal role in immune regulation.<sup>120-122</sup> Indeed, loss of B cell tolerance has been implicated in numerous autoimmune diseases.<sup>123-125</sup> Autoimmune therapies targeting B cells have been successful in treating MS (i.e., rituximab), but general B cell depletion or inactivation may induce global immunosuppression, trigger adverse side effects, and suffer from limited efficacy.<sup>126-128</sup> Development of an antigen-specific immunotherapy (ASIT) that targets and silences autoreactive B cells in a selective manner would address an important need for safer and more effective treatment.<sup>129-131</sup>

Modulation of B cells in a direct, antigen-specific manner requires targeting of the B cell receptor (BCR).<sup>122</sup> Antigen binding to the BCR can trigger receptor clustering and antigen-specific B cell activation.<sup>132-136</sup> However, continuous antigen binding and occupation of the BCR in the absence of secondary costimulatory signals results in B cell anergy, or a state of antigen

unresponsiveness, that is marked by reduced calcium signaling.<sup>131, 137-139</sup> Induction of B cell anergy can have a two-fold therapeutic effect by inducing (1) an effector B cell population that is not responsive to autoantigen and (2) B cells with reduced APC capacity due to downregulation of costimulatory signals CD80 and CD86.<sup>119, 129-130, 140</sup> Thus, a promising avenue for modulating the immune response in an antigen-specific manner is to induce these B cell phenotypes through BCR engagement.

Multivalent linear polymers are especially adept at engaging cell surface receptors such as the BCR, where high avidity multivalent antigen is aided by the molecule's conformational flexibility to permit greater interaction with the cell surface to bind and cluster receptors.<sup>132, 134, 141-147</sup> For example, the spacing and orientation of ligands on a linear polymer may adapt to the contour and dynamic receptor spacing of the cell surface, whereas spherical or globular particles (i.e., dendrimers, nanoparticles, liposomes) are inherently more rigid with relatively fixed spacing and orientation of ligands. As such, multivalent linear polymers may be particularly suited for B cell and BCR targeted therapies. We previously reported on multivalent soluble antigen arrays (SAgA<sub>PLP:LABL</sub>) consisting of a linear hyaluronic acid (HA) polymer co-grafted with myelin autoantigen peptide (proteolipid protein peptide, PLP<sub>139-151</sub>) and intercellular adhesion molecule-1 (ICAM-1) inhibitor peptide (LABL) derived from leukocyte function associated antigen-1 (LFA-1).<sup>148-154</sup> In this molecule, PLP acts as the primary antigenic signal to drive antigen-specific B cell binding, while LABL enhances cellular engagement by targeting ICAM-1, exploiting the ICAM-1/LFA-1 interaction that promotes and sustains intercellular adhesion.<sup>148, 155-158</sup> Our previous studies established that *in vivo* treatment with SAgA<sub>PLP:LABL</sub> significantly alleviated experimental autoimmune encephalomyelitis (EAE), a murine model of relapsing-remitting multiple sclerosis.<sup>150-154</sup> Importantly, multivalent presentation of *both* PLP and LABL on a polymer carrier



was necessary for therapeutic efficacy,<sup>149, 151, 153</sup> and presentation on soluble linear HA was more effective than presentation on insoluble PLGA nanoparticles.<sup>152</sup>

The SAg<sub>PLP:LABL</sub> molecule studied up to this point employed a degradable linker to codeliver PLP and LABL. ‘Hydrolyzable SAg<sub>PLP:LABL</sub>’ exhibited antigen-specific binding with B cells by targeting the BCR, remained on the cell surface for an extended period of time, and dampened BCR-mediated signaling *in vitro*.<sup>148</sup> Our results pointed to sustained BCR engagement as the molecule’s therapeutic mechanism, so we hypothesized that using non-hydrolyzable conjugation chemistry to develop a non-degradable SAgA would enhance and maintain the molecule’s action at the cell surface to improve efficacy. Here, we have developed a new version of the SAgA molecule, termed ‘click SAgA’ (cSAg<sub>PLP:LABL</sub>), using a hydrolytically stable covalent conjugation chemistry rather than hydrolyzable grafting of multivalent PLP<sub>139-151</sub> and LABL peptides to HA using a hydrolyzable oxime bond. We explored whether this non-hydrolyzable conjugation chemistry improved B cell engagement and modulation of BCR-mediated signaling, and if *in vivo* efficacy was correspondingly improved.

B cell binding, signaling, and therapeutic efficacy in EAE were compared between SAg<sub>PLP:LABL</sub> (oxime conjugation chemistry) and cSAg<sub>PLP:LABL</sub> (‘click’ conjugation chemistry) through a combination of *in vitro* and *in vivo* studies. Binding avidity was evaluated in immortalized human Raji B cells as a model APC system using flow cytometry binding assays developed previously.<sup>148</sup> Modulation of BCR-mediated signaling was assessed using flow cytometry calcium flux assays. Engagement and organization of BCR on the cell surface was observed through real-time fluorescence microscopy. Lastly, *in vivo* efficacy was compared across various doses in the EAE model.

## 4.2. Materials and Methods

Hyaluronic acid (HA) sodium salt (MW 16 kDa) was purchased from Lifecore Biomedical (Chaska, MN). 11-azido-3,6,9-trioxaundecan-1-amine (NH<sub>2</sub>-PEG<sub>3</sub>-N<sub>3</sub>), *N*-hydroxysuccinimide, *N*-(3-dimethylaminopropyl)-*N'*-ethylcarbodiimide hydrochloride (EDC), 2-(*N*-morpholino)ethane-sulfonic acid sodium salt (MES), tris(3-hydroxypropyltriazolylmethyl)amine, and sodium ascorbate (NaAsc) were purchased from Sigma-Aldrich (St. Louis, MO) and used as received without further purification. Copper(II) sulfate pentahydrate (CuSO<sub>4</sub> • 5H<sub>2</sub>O) was purchased from Acros Organics (Geel, Belgium). Alkyne-functionalized peptides bearing an *N*-terminal 4-pentynoic acid (homopropargyl, hp) modification, hpPLP<sub>139-151</sub> (hp-HSLGKWLGHDPKF-OH) and hpLABL (hp-ITDGEATDSG-OH), were originally synthesized in our laboratory via solid phase peptide synthesis. Larger quantities of both hpPLP<sub>139-151</sub> and hpLABL peptides were obtained from Biomatik USA, LLC (Wilmington, DE). Unmodified PLP (NH<sub>2</sub>-HSLGKWLGHDPKF-OH) peptide was purchased from PolyPeptide Laboratories (San Diego, CA). Incomplete Freund's adjuvant (IFA) and killed *Mycobacterium tuberculosis* strain H37RA were purchased from Difco (Sparks, MD). Pertussis toxin was purchased from List Biological Laboratories (Campbell, CA). Fluo-4 AM calcium indicator was purchased from Thermo Fisher Scientific (Waltham, MA). Immortalized human Raji B cells were purchased from American Type Culture Collection (ATCC, Manassas, VA). AffiniPure F(ab')<sub>2</sub> fragment goat anti-human IgM and AlexaFluor® 647 AffiniPure F(ab')<sub>2</sub> fragment goat anti-human IgM were purchased from Jackson ImmunoResearch Laboratories (West Grove, PA). All other chemicals and reagents were analytical grade and used as received.

#### 4.2.1. Synthesis of alkyne-modified Pennsylvania Green (Penn Green-Alk)

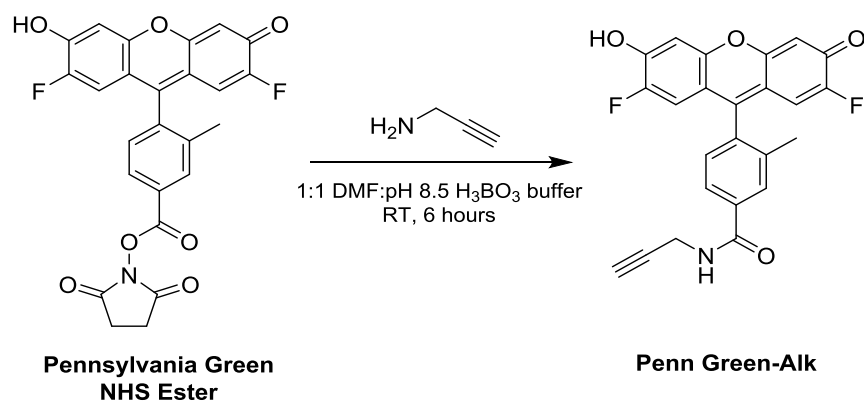


Figure 33: Scheme for the synthesis of Pennsylvania Green alkyne.

Synthesis of 4-(2,7-difluoro-6-hydroxy-3-oxo-3H-xanthen-9-yl)-3-methyl-N-(prop-2-yn-1-yl)benzamide (Penn Green-Alk) was adapted from Meng *et al.*<sup>97</sup> To a mixture of 2,5-dioxopyrrolidin-1-yl 4-(2,7-difluoro-6-hydroxy-3-oxo-3H-xanthen-9-yl)-3-methylbenzoate (55.3  $\mu$ mol) in DMF (0.5 mL), propargylamine (61.2  $\mu$ mol) in 0.5 mL H<sub>3</sub>BO<sub>3</sub> buffer (pH = 8.5, 50 mM) was added and stirred at room temperature for 6 hours. The reaction mixture was frozen and lyophilized to give the crude product as an orange liquid. The crude product was dissolved in DMSO and purified by preparative RP-HPLC (Waters XBridge C<sub>18</sub>, 5  $\mu$ m, 10x250 mm, linear gradient from 5-95% MeCN (+ 0.05% TFA) in H<sub>2</sub>O (+ 0.05% TFA) over 30 min, detection at 280 nm) to give the final product (22.5 mg, 84.7%) as an orange-yellow solid; <sup>1</sup>H NMR (400 MHz, DMSO-*d*<sub>6</sub>)  $\delta$  7.99 (s, 1H), 7.93-7.87 (m, 1H), 7.40 (d, J = 7.9 Hz, 1H), 6.85 (br s, 2H), 6.63 (d, J = 11.2 Hz, 2H), 4.11 (dd, J = 5.6, 2.5 Hz, 2H), 3.17 (t, J = 2.5 Hz, 1H), 2.08 (s, 3H); HRMS (TOF ESI+) expected [M+Na]<sup>+</sup>: 442.0867, found: 442.0870.

#### 4.2.2. Synthesis of azide-functionalized hyaluronic acid (HA-N<sub>3</sub>)

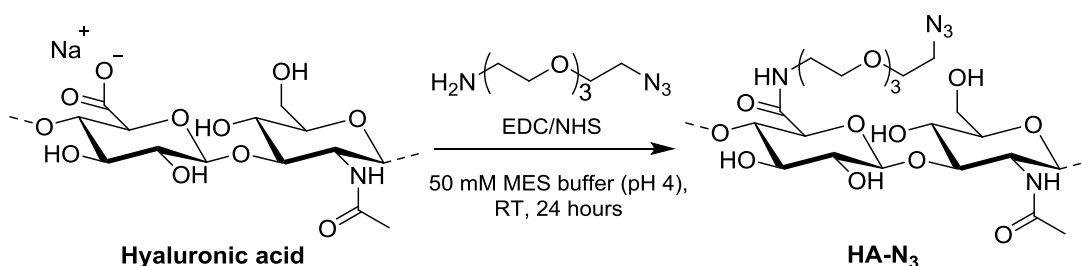


Figure 34: Scheme for the synthesis of HA-N<sub>3</sub>.

Synthesis of HA-N<sub>3</sub> was adapted from Hu *et al* and Di Meo *et al*.<sup>159-160</sup> Sodium hyaluronate (93.9 μmol, 16 kDa average MW) was added to a 250 mL round bottom flask with stir bar, followed by 100 mL of 50 mM MES buffer (pH = 4.0). The mixture was stirred until in solution (~15 min) before EDC (23.1 mmol) was added neat, then *N*-hydroxysuccinimide (18.8 mmol) added neat. The mixture was stirred for 5 min before H<sub>2</sub>N-PEG<sub>3</sub>-N<sub>3</sub> (4.51 mmol) in 20 mL MES buffer was added. The solution was then stirred for 24 hours at room temperature before being dialyzed in 6-8 kDa cutoff dialysis tubing against 4.5 L of 1.0 M NaCl solution for 24 hours, then 4.5 L of deionized water (4 x 12 hours). The volume in the bag was then transferred to vials, frozen, and lyophilized to yield a white powder (1.61 g, 95.0%).

### 4.2.3. Synthesis of Soluble Antigen Arrays

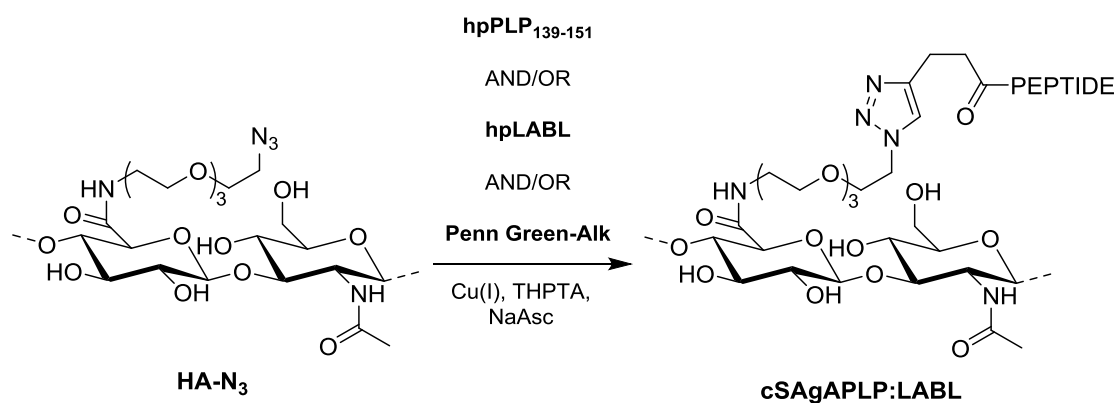


Figure 35: General scheme for the synthesis of cSAgAs.

HA-N<sub>3</sub> (2 μmol) was added as a 50 μM solution in deionized H<sub>2</sub>O to a 250 mL round bottom flask with stir bar. Each component peptide (40 μmol) was then added as a ~3 mM solution in deionized H<sub>2</sub>O, followed by a premixed solution of THPTA (70 μmol) and CuSO<sub>4</sub> • 5H<sub>2</sub>O (14 μmol) in deionized H<sub>2</sub>O. In the case with fluorescently-labeled variants, a 2.4 mM Penn Green-Alk solution in DMF (2.0 equivalents relative to HA-N<sub>3</sub>) was also added. The solution was allowed to stir for 1-2 min before a 100 μL aliquot was removed for HPLC analysis. NaAsc (300 μmol) was then added to the reaction mixture as a 100 mM solution in deionized H<sub>2</sub>O. The reaction was allowed to proceed under varying conditions depending on the starting components and desired valency (cHA<sub>PLP</sub>: 18 hours at 37°C; cHA<sub>LABEL</sub> and cSAgA<sub>PLP:LABEL</sub>: 18 hours at 50°C; fcHA and fcHA<sub>PLP</sub>: 24 hours at 37°C; fcHA<sub>LABEL</sub> and fcSAgA<sub>PLP:LABEL</sub>: 24 hours at 50°C). Additional 100 μL aliquots were removed throughout the course of the reaction to determine the extent of conjugation. Once the target conjugation values were achieved, the reaction solution was transferred to 6-8 kDa dialysis tubing and dialyzed against 4.5 L of 1.0 M NaCl (3 x 8 hours), then 4.5 L of deionized H<sub>2</sub>O (5 x 8 hours). The volume in the bag was then transferred to vials, frozen, and lyophilized.

#### 4.2.4. Analytical Characterization of Soluble Antigen Arrays

FTIR spectra were collected on a Bruker Tensor 27 FTIR spectrometer equipped with an Attenuated Total Reflectance (ATR) cell. Purified samples were analyzed at ambient temperature in the solid state by collecting a total of 32 scans per sample. NMR spectra were collected on a Bruker Avance AVIII 500 MHz spectrometer equipped with a dual carbon/proton cryoprobe (unless otherwise noted), and all samples were dissolved in 650  $\mu\text{L}$  of  $\text{D}_2\text{O}$  for analysis. MestReNova 11.0 was used for NMR data analysis. The amide methyl resonance ( $\delta \sim 1.90\text{-}2.05$  ppm) of all  $^1\text{H}$  NMR spectra was normalized to an integration of 3.0, and the sum of all other signals in the range of  $\delta \sim 1.0\text{-}4.0$  ppm was used to ratiometrically determine the number of azide functionalization sites during HA- $\text{N}_3$  synthesis.

RP-HPLC and SEC analysis were conducted using a Waters Alliance HPLC system equipped with either a diode array detector or dual wavelength UV/Vis detector. For the quantitative determination of peptide conjugation by RP-HPLC, the following equation was used:

$$N_{\text{con}} = \left[ \left( \frac{n_{\text{pep}}}{n_{\text{HA}}} \right) \left( \frac{V_{\text{pre}} - V_{\text{sam}}}{V_{\text{pre}}} \right) \right] \left( 1 - \frac{PA_t}{PA_{\text{start}}} \right) \quad \text{Equation 1}$$

where  $N_{\text{con}}$  = number of conjugated peptides per backbone,  $n_{\text{pep}}$  = moles of peptide used in the reaction,  $n_{\text{HA}}$  = moles of HA- $\text{N}_3$  used in the reaction,  $V_{\text{pre}}$  = total reaction volume before NaAsc is added,  $V_{\text{sam}}$  = volume of “pre-NaAsc” sample removed from reaction mixture,  $PA_t$  = measured peak area of peptide at time  $t$ ,  $PA_{\text{start}}$  = measured peak area of free peptide before NaAsc is added to the reaction. General chromatographic conditions employed a Waters XBridge C<sub>4</sub>, 3.5  $\mu\text{m}$ , 300  $\text{\AA}$  stationary phase under ion pairing (0.05% TFA in  $\text{H}_2\text{O}$  and MeCN) mobile phase conditions, utilizing a linear elution gradient (5-60%) with detection at 214 nm.

#### **4.2.5. Cell Culture**

Raji B cells (human B lymphocytes, ATCC) were cultured in RPMI-1640 supplemented with L-glutamine, 10% fetal bovine serum (FBS), and 1% penicillin/streptomycin (P/S) at 37°C and 5% CO<sub>2</sub>. Cell assays were consistently performed after cells reached confluency (~2 weeks) and following no more than 8-10 passages, per ATCC guidelines.

#### **4.2.6. Flow Cytometry Binding Assay**

Association binding studies were performed by flow cytometry (MoFlo XDP Cell Sorter, Beckman Coulter Inc., Brea, CA), as previously reported.<sup>148</sup> Cell nuclei were stained with Hoechst and propidium iodide (PI) was used as a dead cell indicator; data acquisition was triggered off the Hoechst signal. Cell samples were warmed to 37°C for 2 min prior to the flow cytometry run. Fluorescence was excited using 488, 405, and 640 nm lasers and was collected using 529/28, 457/40, and 670/30 nm bandpass emission filters.

To observe maximum steady state binding, cells were mixed with the treatment to achieve a final concentration of  $1 \times 10^6$  cells/mL immediately before injecting on the flow cytometer. Sample concentration was determined from preliminary saturation studies.<sup>148</sup> Samples were added at an equimolar PLP dose (353  $\mu$ M PLP for fHA<sub>PLP</sub> and fSAg<sub>PLP:LABEL</sub>, or 353  $\mu$ M LABEL for fHA<sub>LABEL</sub>) and fHA was dosed at 39  $\mu$ M (the HA molar equivalent to a 353  $\mu$ M PLP dose of fSAg<sub>PLP:LABEL</sub>) to mimic the dosing scheme from *in vivo* studies. The sample was allowed to run for 5 min to ensure that maximum steady state was established, which occurs after approximately 3-4 min.

Flow cytometry binding data was first gated to remove doublets, dead cells, and debris using Kaluza Flow Analysis software (Beckman Coulter, Inc., Brea, CA). Additional data

processing was performed using KNIME software (Konstanz Information Miner, KNIME, Zurich, Switzerland). Nonlinear regression and additional statistical analysis was performed using GraphPad Prism (GraphPad Software, Inc., La Jolla, CA).

#### ***4.2.7. Calcium Flux Signaling Assay***

Raji B cells were loaded with 5  $\mu\text{M}$  Fluo-4 AM for 30 min at room temperature in PBS, then kept on ice in HBSS (Hanks Balanced Salt Solution) containing 1.3 mM  $\text{Ca}^{2+}$  and 0.9 mM  $\text{Mg}^{2+}$  before analysis. Cells were run through a BD FACSFusion cytometer and fluorescence was monitored in the 530/30 nm channel. After baseline quantification for ~30 sec, crosslinking goat anti-human IgM (Jackson ImmunoResearch) was added at a final concentration of 20  $\mu\text{g}/\text{mL}$  to stimulate the cells. This concentration was determined from a preliminary study where a range of anti-human IgM concentrations (5-40  $\mu\text{g}/\text{mL}$ ) was evaluated and 20  $\mu\text{g}/\text{mL}$  achieved greatest stimulation of Raji B cells. Changes in Fluo-4 fluorescence were measured for 1 min to establish an anti-IgM stimulated baseline, followed by addition of (c)SAgA treatment (dosed at 353  $\mu\text{M}$  PLP, same concentration used in binding studies) to determine the effect on IgM-stimulated signaling. Data was acquired for an additional 3 min until steady state was established. To measure inhibition of anti-IgM stimulation, (c)SAgA<sub>PLP:LABEL</sub> was added to cells prior to anti-IgM stimulation. KNIME was used to process and plot the kinetic data, while Kaluza and GraphPad Prism were used for the remaining analysis.

#### ***4.2.8. Fluorescence Microscopy***

Live cell imaging of fcSAgA binding and surface IgM clustering was observed under fluorescence microscopy (Olympus IX81 Inverted Epifluorescence Microscope) using the same



concentrations from flow cytometry association binding experiments. CellASIC ONIX M04S Microfluidics Switching Plates and Microfluidics Platform (EMD Millipore, Billerica, MA) were utilized for controlled perfusion of fluorescent samples and media with cells during real-time imaging. Raji B cells were stained with Hoechst and mixed with AlexaFluor® 647 goat anti-human IgM (Jackson ImmunoResearch) at 20 µg/mL to stimulate the cells and label surface IgM, then loaded into the imaging chamber. fcSAgA was perfused into the chamber for 10 minutes (3 psi for 5 minutes, 0.25 psi for 5 minutes) to allow binding with cells, followed by gentle media perfusion (0.25 psi for 5 minutes) to rinse unbound fcSAgA, followed by immediate image capture. Images were processed using Slidebook 5.5 (Intelligent Imaging Innovations, Inc., Denver, CO) and quantitative BCR clustering analysis was performed using ImageJ. Otsu thresholding was applied to the IgM channel to identify IgM capping, where cells with a single localized area of IgM fluorescence above a brightness threshold of 65 were considered positive for capping. This method was applied to 100-250 IgM-positive stained cells per sample to determine % IgM capping. IgM pixel intensity was plotted for individual cells (N = 10 per sample) as a function of diameter to generate profile plots relative to normalized diameter (d/D) and to determine the maximum IgM pixel intensity per cell.

#### ***4.2.9. Preclinical EAE Study in Mice***

*In vivo* studies were carried out with 4-6 week old SJL/J (H-2) female mice purchased from Envigo Laboratories (Indianapolis, IN). Mice were housed under specified, pathogen-free conditions at the University of Kansas and all experiments were approved by the University's Institutional Animal Care and Use Committee. Complete Freund's adjuvant (CFA) was made by combining IFA and killed *M. tuberculosis* strain H37RA at a final concentration of 4 mg/mL.

Animals were induced with experimental autoimmune encephalomyelitis (EAE), the PLP-specific mouse model of relapsing-remitting MS, on day 0 of the study. Immunization was accomplished using a 0.2 mL emulsion containing 200 µg PLP<sub>139-151</sub> peptide, plus equal volumes of PBS and CFA. The emulsion was administered subcutaneously (s.c.) as a total of four 50 µL injections, located above each shoulder and each hind flank. Pertussis toxin (100 ng in 100 µL) was injected intraperitoneally on day 0 and day 2 post-immunization.

Treatments were administered on days 4, 7, and 10 as 100 µL subcutaneous injections at the nape of the neck (N = 3-6 mice per treatment group), with the exception of one group in the dosing study that received treatments on days 4 and 7 only. Samples were administered at a dose equivalent to 50, 133, or 200 nmol PLP per 100 µL (0.5, 1.33, or 2 mM PLP, respectively). This three-day dosing schedule and dose of 200 nmol PLP were found to be efficacious in a previous SAg<sub>APLP:LABL</sub> study.<sup>153</sup> Disease progression was evaluated by a single observer using the following clinical score system: 0, no clinical disease symptoms; 1, weakness or limpness of the tail; 2, weakness or partial paralysis of one or two hind limbs (paraparesis); 3, full paralysis of both hind limbs (paraplegia); 4, paraplegia plus weakness or paralysis of forelimbs; 5, moribund (at which point mice were euthanized). In addition to animal scoring, body weight measurements were performed daily for the 26-day duration of the EAE study.

#### ***4.2.10. Statistical Analysis***

GraphPad Prism was used to perform statistical analysis including sigmoidal nonlinear regression, ordinary one-way or two-way analysis of variance (ANOVA), and unpaired t-test. ANOVA was followed by Tukey's or Sidak's post-hoc test, where appropriate. The threshold for statistical significance was set to  $p < 0.05$ .

## 4.3. Results and Discussion

### 4.3.1. Structural design of click soluble antigen arrays

Multivalent soluble antigen arrays (SAgA<sub>PLP:LABL</sub>) consist of a 16 kDa HA linear polymer conjugated with approximately 10 PLP and 10 LABL peptides. The molecule was rationally designed based on studies by Dintzis *et al.* that suggested multivalent linear polymers with a valency of 10-20 antigens and MW < 100 kDa could induce a tolerogenic immune response,<sup>146, 161-162</sup> combined with studies by Siahaan *et al.* that showed linking PLP and LABL peptides in a bifunctional molecule was therapeutic in EAE.<sup>157-158, 163-167</sup> Previous SAgA<sub>PLP:LABL</sub> molecules studied in our research group employed a hydrolyzable linker chemistry to conjugate both PLP<sub>139-151</sub> and LABL peptides to HA, and have been shown to significantly suppress disease severity in EAE.<sup>148-154</sup> This approach was built upon our earlier two-signal hypothesis that SAgA<sub>PLP:LABL</sub> inhibited autoimmune activation via the immunological synapse by promoting antigen processing without the necessary secondary signal, a mechanism that would necessitate antigen uptake, processing, and presentation. However, our recent *in vitro* studies instead pointed to a therapeutic mechanism in which SAgA<sub>PLP:LABL</sub> acted through sustained BCR engagement, targeting BCR signaling while exhibiting prolonged residence on the cell surface.<sup>148</sup> Whereas our early hypothesis motivated a degradable SAgA molecule to permit antigen uptake and processing, these results motivated the development of a non-degradable SAgA molecule to enhance and maintain the molecule's surface activity. Thus, we synthesized 'click' cSAgA variants that exploit a non-cleavable linker chemistry to evaluate whether possible release of PLP<sub>139-151</sub> and LABL influenced the efficacy of the molecule. cSAgA multivalent arrays utilize the Copper-catalyzed Azide-Alkyne Cycloaddition (CuAAC) reaction as a stable attachment chemistry, which carries significant literature precedence with respect to application<sup>168-169</sup> and optimization<sup>170-171</sup>. The versatility of the

CuAAC reaction was a major consideration in the implementation of an alternative conjugation chemistry, since the wide range of available reaction conditions can enable improved control over valency.

#### 4.3.2. Analytical characterization of click soluble antigen arrays

Characterization was completed using a variety of qualitative and quantitative analytical techniques. Initial azide-functionalization was confirmed by FTIR spectroscopy, showing the presence of a characteristic azide stretching band after synthesis of HA-N<sub>3</sub>, which disappeared following utilization of the azide moiety during conjugation (Figure 36). Quantitation by <sup>1</sup>H NMR proved challenging due to signal broadening of the increasingly heterogeneous polymeric systems, and the high molecular weight of the multivalent arrays led to decreasing sensitivity with increasing conjugation, eventually limited by sample solubility. For an analysis of azide functionalization, integration ranges were used to account for signal overlap between the polymer backbone resonances and those on the linker. To assess the validity of this approach, two additional batches of HA-N<sub>3</sub> were prepared using a reduced number of molar equivalents of linker relative to the starting HA, resulting in a reduced number of azide functionalized sites (Table 1).

Table 1: Azide functionalization of hyaluronic acid, as measured by <sup>1</sup>H NMR.

<b>HA-N<sub>3</sub> Batch</b>	<b>H<sub>2</sub>N-PEG<sub>3</sub>-N<sub>3</sub> Molar Equivalents<sup>a</sup></b>	<b>% Functionalization</b>	<b>Average N<sub>3</sub> Sites per Polymer</b>
<b>Batch #1</b>	48	50	21
<b>Batch #2</b>	25	45	19
<b>Batch #3</b>	12	31	13

<sup>a</sup> Relative to the starting 16 kDa HA

It should be noted, however, that manual integration was required to perform this analysis, and coupled with the broad resonances observed from the polymeric system, this technique is considered to be a semi-quantitative approach to justify subsequent peptide conjugation. Additional NMR studies in the solid-state or observation of alternative nuclei may aid in the quantitative nature of the analytical methodology.  $^1\text{H}/^{13}\text{C}$  Heteronuclear Single Quantum Coherence (HSQC) NMR spectroscopy was used qualitatively to confirm the existence of resonances present in both peptide samples, which carried over to the final dialyzed products (Figure 37). Importantly, these experiments also showed the disappearance of the terminal alkyne resonance from the linker on each peptide along with the concomitant appearance of a broadened aromatic resonance not present in any individual component, corresponding to the new triazole ring.

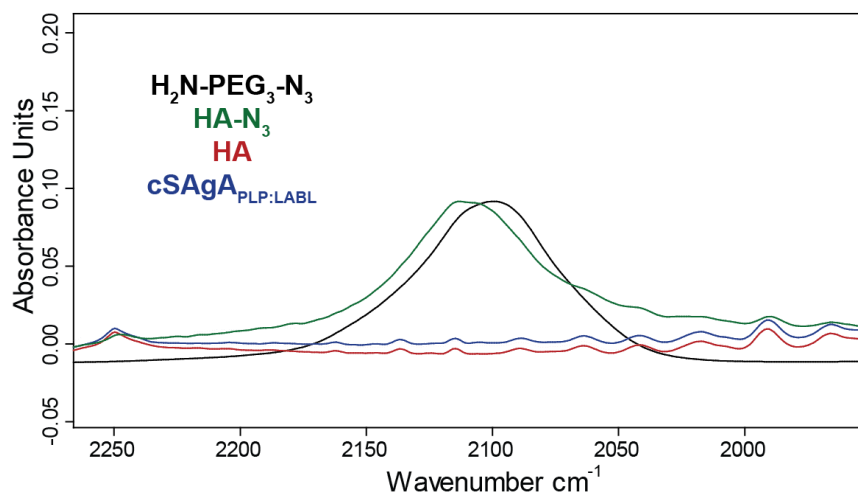


Figure 36: FTIR spectra collected after functionalization and conjugation of HA.

Quantitative analysis of peptide conjugation efficiency was conducted via RP-HPLC by measuring the decrease in peak area of the free alkyne-containing peptide(s) throughout the course of the reaction. The CuAAC conjugation chemistry requires an active  $\text{Cu}^{1+}$  catalyst for the reaction

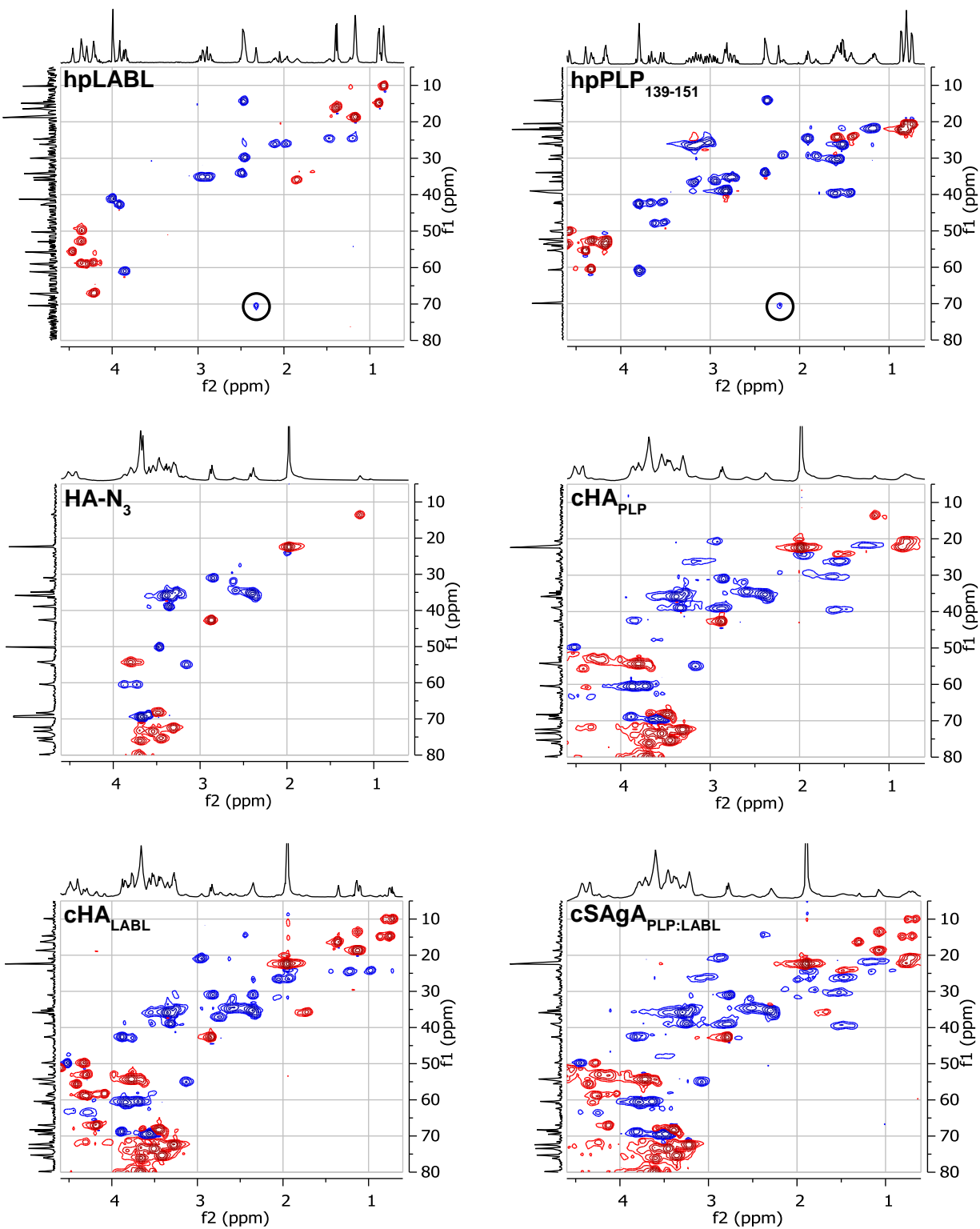


Figure 37: Qualitative confirmation of conjugation by 2D HSQC NMR where a  $^1\text{H}$  spectrum is shown on the x-axis and a  $^1\text{H}$ -decoupled  $^{13}\text{C}$  spectrum is shown on the y-axis.

to proceed, which is generated *in situ* through addition of the reducing agent NaAsc to an inactive  $\text{Cu}^{2+}$  in solution. Prior to this final NaAsc addition step, an aliquot of the reaction mixture was removed for HPLC analysis to establish a baseline response correlating to the molar excess of peptide used in the reaction. Subsequent to the addition of NaAsc, any decrease in peak area of free alkyne-containing peptide was attributed to conjugation (Figure 38). Standard curves for both peptides were linear to 110% of the nominal concentrations used in the reaction mixture (0.81 mM for hpPLP<sub>139-151</sub> and 0.71 mM for hpLABL), exhibiting  $R^2$  values  $>0.99$  upon linear regression analysis. Additional control experiments showed both hpPLP and hpLABL displayed  $<5\%$  degradation (0.8% and 4.5%, respectively) at  $37^\circ\text{C}$  in  $\text{H}_2\text{O}$  over 20 hours in the absence of all other reaction components, indicating a minimal impact of peptide degradation on the accuracy of the analytical methodology.

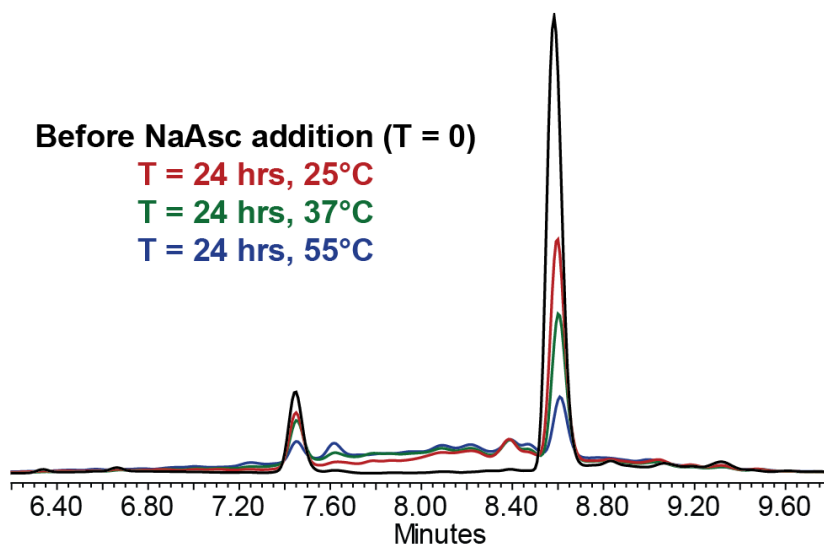


Figure 38: Representative HPLC chromatograms used to quantify the number of conjugated peptides as a function of reaction temperature.

Further, the final dialyzed products showed no evidence of peptide release after 18 hours at room temperature in either pH  $\sim 2.4$ , 5.0, or 7.0 buffers, confirming the basis behind the non-

hydrolyzable linker design of the cSAgA molecular platform (Figure 39). An abbreviated reaction optimization study showed that conjugation ratios could be significantly influenced by buffer, temperature, reactant concentrations, and molar excess of free peptide. From these observations, reaction conditions were identified that achieved a desired peptide valency. Quantitative peptide conjugation of representative test articles is provided in Table 2, showing that target conjugation efficiencies of approximately 25% per peptide (relative to theoretically available disaccharide monomers) were achieved in cHA<sub>PLP</sub> (10 PLP<sub>139-151</sub>), cHA<sub>LABL</sub> (12 LABL), and cSAgA<sub>PLP:LABL</sub> (11 PLP<sub>139-151</sub>, 9 LABL). Size exclusion chromatography (SEC) was primarily used to verify the success of dialysis, showing no evidence of free peptide or other reaction components in any purified cSAgA samples (Figure 40). HA samples of varying molecular weight were used as standards to compare against purified reaction products. HA-N<sub>3</sub> exhibited a slight decrease in retention time compared to 16 kDa HA, indicating an increase in molecular weight following azide

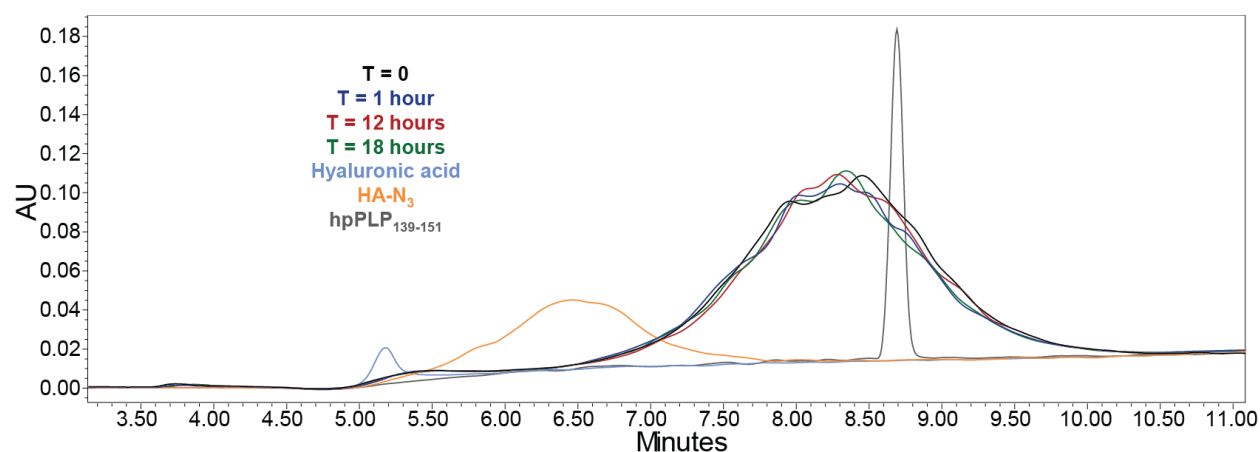


Figure 39: Reverse-phase analytical high-performance liquid chromatography (RP-HPLC) from a room temperature solution stability study of cHA<sub>PLP</sub> at pH 2.4 (measured pH of aqueous component of mobile phase, 0.05% TFA in H<sub>2</sub>O), showing negligible degradation and release of PLP. This study was also conducted at pH 5.0 (100 mM acetate buffer) and pH 7.0 (100 mM phosphate buffer) with cHA<sub>PLP</sub> and other conjugates, all showing similar results.



functionalization. Retention time increased following peptide conjugation; however, this was likely a reflection of the molecule's altered physicochemical properties and increased secondary interactions with the stationary phase rather than a reflection of molecular size. Given that hpPLP<sub>139-151</sub> eluted after the retention time observed for salts, the increased retention of peptide-conjugated samples was likely due to secondary interactions between peptide in solution and the stationary phase overcoming the primary interactions that drive SEC separation. This secondary interaction was evident throughout method development regardless of mobile phase pH, salt concentration, and stationary phase composition.

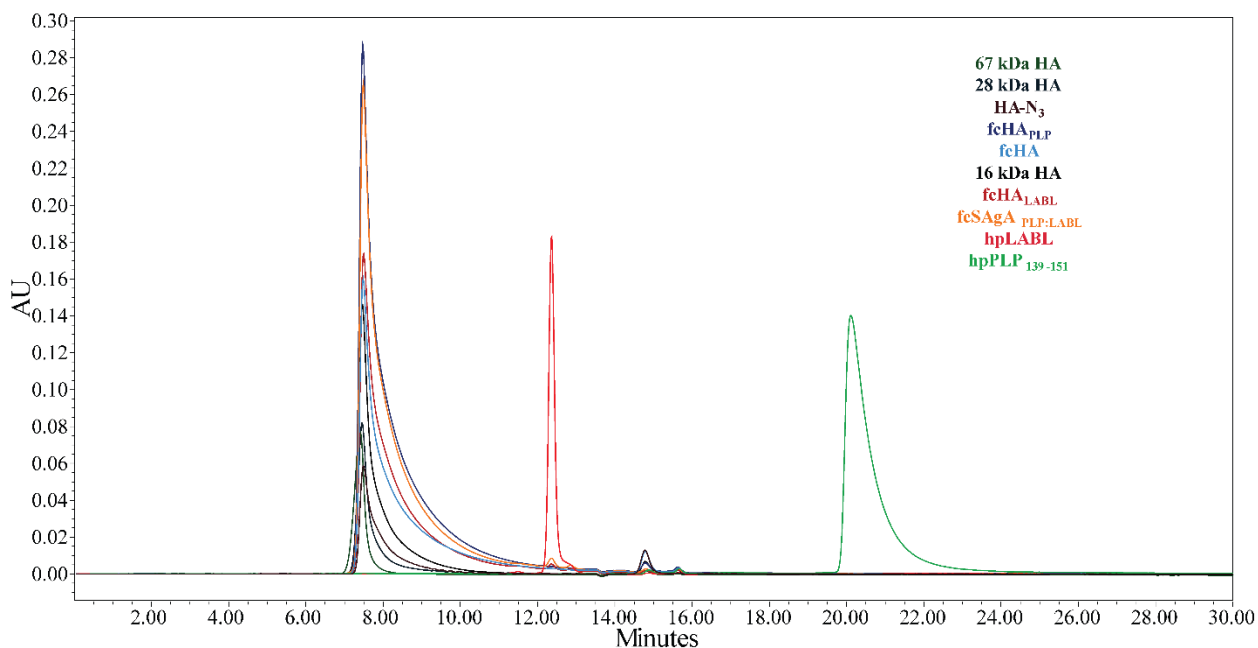
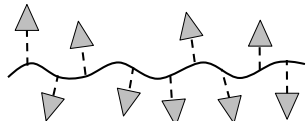
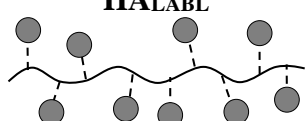

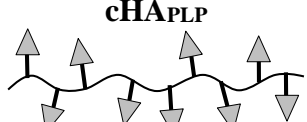
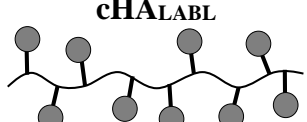
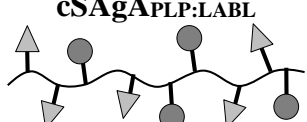


Figure 40: Size exclusion chromatography (SEC) for fluorescently-labeled multivalent arrays. The top overlay shows the full length chromatogram, and the bottom overlay shows normalized expansion of the HA-containing species. Chromatographic conditions – column: Waters XBridge SEC, 125 Å, 3.5 µm, 7.8x300 mm; Mobile phase: 50mM phosphate (pH 7.0) with 0.2M NaCl; Flow rate: 0.8 mL/min; Detection: UV at 214 nm. Samples were prepared in mobile phase at 2 mg/mL, with the exception of hpPLP<sub>139-151</sub> and hpLABEL, which were prepared at 1 mg/mL.

### 4.3.3. Flow Cytometry Binding Assay

A flow cytometry binding assay was used to compare the relative binding avidities of hydrolyzable fSAgA and click-conjugated fcSAgA with Raji B cells. Binding kinetics were observed during association between the fluorescently labeled polymer arrays and Raji B cells

Table 2: Peptide molar conjugation of hydrolyzable and click conjugates, as determined by RP- HPLC.<sup>a</sup>

Sample	Approx. MW (kDa) <sup>b</sup>	Average Molar Ratio per Polymer <sup>c</sup>		% Molar Conjugation	
		PLP:HA	LABL:HA	PLP	LABL
 <p><b>HAPLP</b></p>	30.4	9	0	21	0
 <p><b>HALABL</b></p>	26.0	0	10	0	24
 <p><b>SAgAPLP:LABL</b></p>	46.3	10	13	24	31
 <p><b>cHAPLP</b></p>	41.2	10	0	24	0
 <p><b>cHALABL</b></p>	37.2	0	12	0	28
 <p><b>cSAgAPLP:LABL</b></p>	52.1	11	9	26	21

<sup>a</sup> Results are an average of triplicate injections from a single batch preparation. In the molecule schematics, dotted lines represent hydrolyzable oxime linker chemistry while solid lines represent non-hydrolyzable 'click' linker chemistry.

<sup>b</sup> Calculated from RP-HPLC data. MW, molecular weight.

<sup>c</sup> HA, hyaluronic acid; PLP, proteolipid protein peptide; LABL, inhibitor peptide derived from leukocyte function associated antigen-1.

until maximum steady state (max. SS) was reached (illustrated in Figure 41A). It was previously observed that fSAg<sub>PLP:LABL</sub>, co-grafted with both PLP<sub>139-151</sub> and LABL, exhibited greater binding with Raji B cells than the polymer alone (fHA) or the homopolymers grafted with only one signal (fHA<sub>PLP</sub> or fHA<sub>LABL</sub>).<sup>148</sup> A similar trend was observed with click-conjugated arrays: fcSAg<sub>PLP:LABL</sub> exhibited the highest amount of binding, followed by fcHA<sub>PLP</sub>, while fcHA exhibited the lowest amount of binding (Figure 42A). Comparison of the maximum SS indicated that fcSAg<sub>PLP:LABL</sub> binding was significantly greater than that of fcHA<sub>PLP</sub>, fcHA<sub>LABL</sub>, and fcHA, while fcHA<sub>PLP</sub> binding was significantly greater than that of fcHA<sub>LABL</sub> and fcHA (Figure 42B). Thus, multivalent PLP<sub>139-151</sub> and LABL appear to have a cooperative effect on avidity. We previously reported that SAg<sub>PLP:LABL</sub> exhibited PLP-specific binding and BCR targeting, implying that PLP may enhance B cell avidity by providing specific affinity for the BCR.<sup>148</sup> Meanwhile, LABL, derived from LFA-1 and specific for ICAM-1, may enhance B cell avidity by promoting cell adhesion through the LFA-1/ICAM-1 interaction.<sup>111, 115-117, 155-158, 172</sup> ICAM-1 and LFA-1 expression are upregulated on B cells during surface BCR engagement to promote intercellular adhesion, since the ICAM-1/LFA-1 interaction is critical for B cell:T cell conjugate formation during signaling.<sup>173</sup> This may explain why multivalent LABL exerted a cooperative effect on binding avidity when presented alongside PLP in fcSAg<sub>PLP:LABL</sub>, but a minimal effect when presented alone in fcHA<sub>LABL</sub>.

Comparison of click-conjugated versus hydrolyzable compound binding revealed that both fcSAg<sub>PLP:LABL</sub> and fcHA<sub>PLP</sub> exhibited significantly enhanced binding compared to their hydrolyzable counterparts, fSAg<sub>PLP:LABL</sub> and fHA<sub>PLP</sub>, respectively (Figure 42C). Differences in kinetics and maximum SS binding between fcSAg<sub>PLP:LABL</sub>, fSAg<sub>PLP:LABL</sub>, and fHA illustrate how avidity was altered when multivalent peptide was conjugated to HA in a hydrolyzable versus

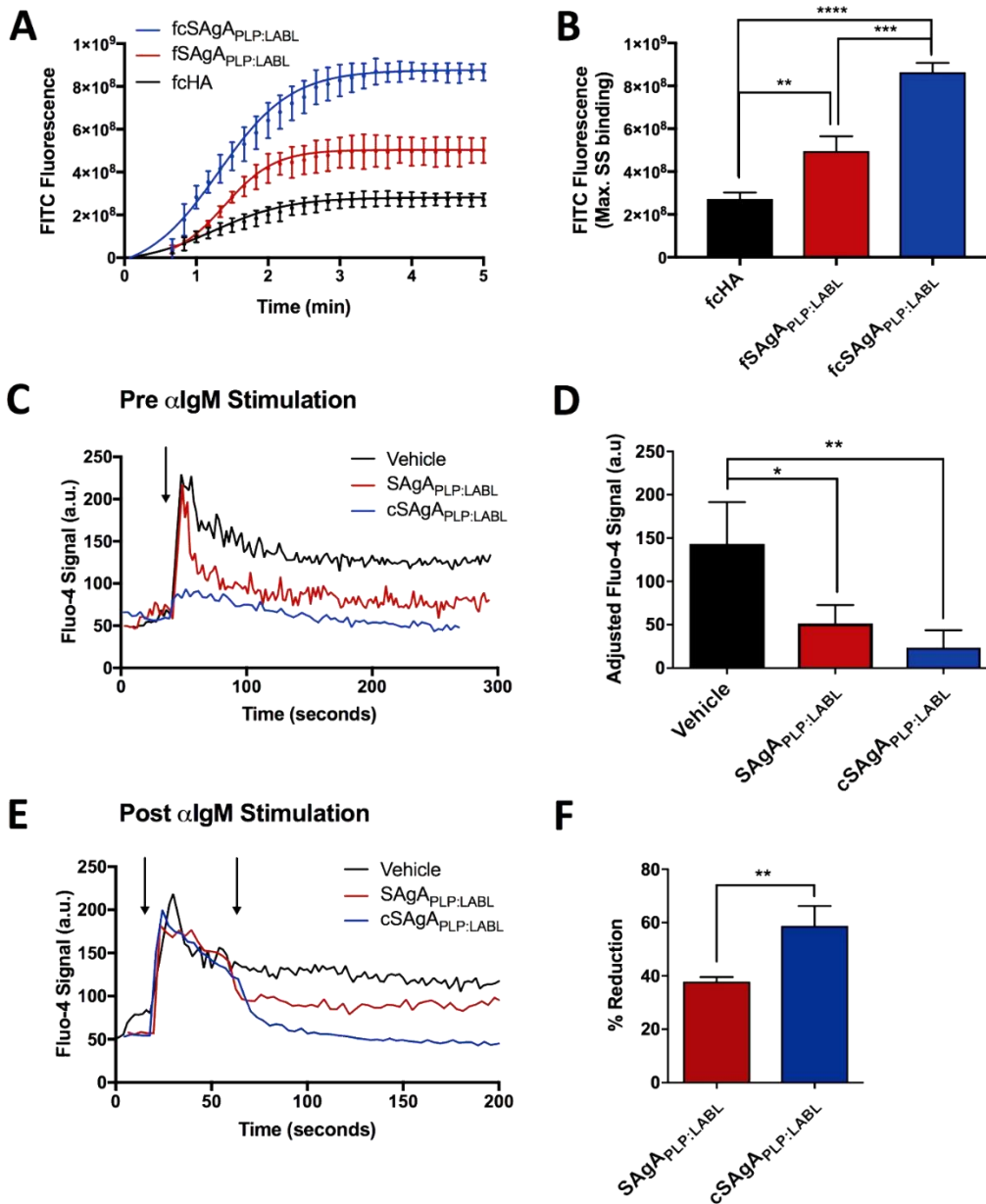


Figure 41: Comparing SAgA<sub>PLP:LABEL</sub> and cSAgA<sub>PLP:LABEL</sub> binding and IgM-stimulated (BCR-mediated) calcium flux signaling in Raji B cells through flow cytometry assays: (A) Binding kinetics and (B) maximum steady state (max. SS) binding with fSAgA<sub>PLP:LABEL</sub>, fcSAgA<sub>PLP:LABEL</sub>, and fcHA. (C) Calcium flux inhibition: Fluo-4 loaded cells were first pretreated with vehicle (HBSS), SAgA<sub>PLP:LABEL</sub>, or cSAgA<sub>PLP:LABEL</sub>, then stimulated with anti-IgM (αIgM, black arrow) to evaluate signaling inhibition. (D) Relative IgM signaling stimulation following pretreatment; baseline-adjusted values determined from mean steady state values. (E) Calcium flux reduction: Fluo-4 loaded cells were first stimulated with αIgM at ~30 s (black arrow), then treated with vehicle (HBSS), SAgA<sub>PLP:LABEL</sub>, or cSAgA<sub>PLP:LABEL</sub> after ~60 s (black arrow) to evaluate signaling reduction. (F) Percent reduction from IgM-stimulated baseline following sample addition, determined from mean steady state values. Statistical significance was determined by ANOVA followed by Tukey's post hoc test with  $p < 0.05$  and  $n = 3$  (\* $p < 0.05$ , \*\* $p < 0.01$ , \*\*\* $p < 0.001$ , \*\*\*\* $p < 0.0001$ ). Calcium flux kinetics in (C) and (D) show median Fluo-4 fluorescence values. Robust curve fitting in (A) was performed using sigmoidal nonlinear regression. Calcium flux data was pooled from three independent experiments.

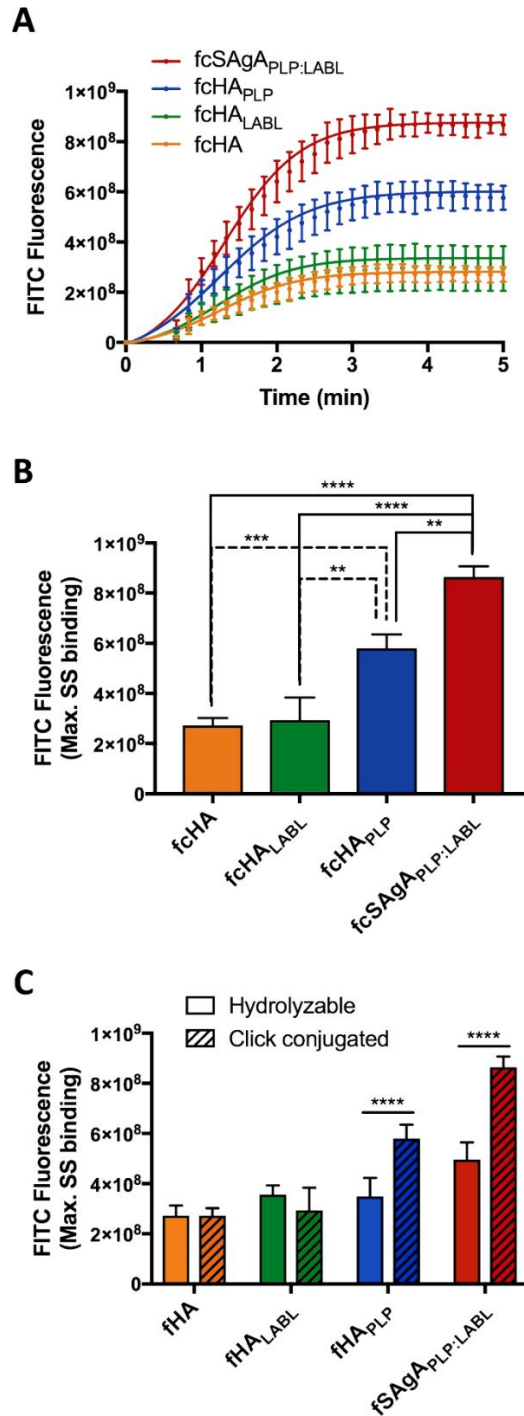


Figure 42: Binding of  $fcHA$ ,  $fcHA_{LABL}$ ,  $fcHA_{PLP}$ , and  $fcSAG_{A_{PLP:LABL}}$  with Raji B cells determined by flow cytometry: (A) Binding kinetics showing association through steady state. (B) Relative binding at maximum steady state (max. SS). (C) Comparison of max. SS binding with hydrolyzable versus click-conjugated arrays. Statistical significance determined by ANOVA followed by Tukey's (B) or Sidak's (C) post hoc test with  $p < 0.05$  and  $n = 3$  (\* $p < 0.05$ , \*\* $p < 0.01$ , \*\*\* $p < 0.001$ , \*\*\*\* $p < 0.0001$ ). Robust curve fitting in (A) was performed using sigmoidal nonlinear regression.

non-hydrolyzable manner (Figure 41AB). While both methods of multivalent modification resulted in significantly increased binding compared to the polymer alone, click-conjugated fcSAgA<sub>PLP:LABL</sub> exhibited significantly greater maximum SS binding ( $p < 0.001$ ) than hydrolyzable SAgA<sub>PLP:LABL</sub>. Thus, multivalent co-presentation of PLP and LABL through non-hydrolyzable modification increased the avidity of the polymer array more than hydrolyzable modification. This result is supportive of literature stating that multivalent antigens exhibit superior binding avidity, higher ‘effective concentration’, and an enhanced ability to engage cell receptors compared to monovalent (or in this case, hydrolyzable) antigen.<sup>131, 142-143, 145, 174</sup>

#### ***4.3.4. Calcium Flux Signaling Flow Cytometry Assay***

Flow cytometry calcium flux assays were used to compare the ability of SAgA and cSAgA molecules to modulate BCR-mediated signaling in Raji B cells. Signaling modulation was evaluated in Fluo-4 loaded Raji B cells prior to stimulation (Figure 41CD) and after stimulation (Figure 41EF) with crosslinking  $\alpha$ IgM. The relative signal increase from resting baseline (Figure 41D) or reduction from stimulated baseline (Figure 41F) was determined using mean Fluo-4 fluorescence values at steady state.

We reported previously that SAgA<sub>PLP:LABL</sub> was capable of both inhibiting and reducing IgM-stimulated signaling.<sup>148</sup> Here, pre-treatment with SAgA<sub>PLP:LABL</sub> prior to addition of  $\alpha$ IgM significantly inhibited IgM-stimulated calcium signaling compared to the vehicle ( $p < 0.05$ ) (Figure 41CD). However, pre-treatment with cSAgA<sub>PLP:LABL</sub> significantly inhibited IgM-stimulated calcium signaling to a greater extent ( $p < 0.01$ ), largely preventing even the initial spike in calcium flux observed with SAgA<sub>PLP:LABL</sub> after  $\alpha$ IgM addition. Similarly, addition of cSAgA<sub>PLP:LABL</sub> after  $\alpha$ IgM stimulation caused a greater reduction in calcium signaling than SAgA<sub>PLP:LABL</sub> ( $p < 0.01$ )

(Figure 41EF). cSAg<sub>APLP:LABEL</sub> reduced signaling by ~60% while SAg<sub>APLP:LABEL</sub> reduced signaling by ~40% relative to the vehicle control. These results indicated that click-conjugated cSAg<sub>APLP:LABEL</sub> was significantly more effective at dampening BCR-mediated signaling – both through inhibition and reduction – compared to its hydrolyzable counterpart.

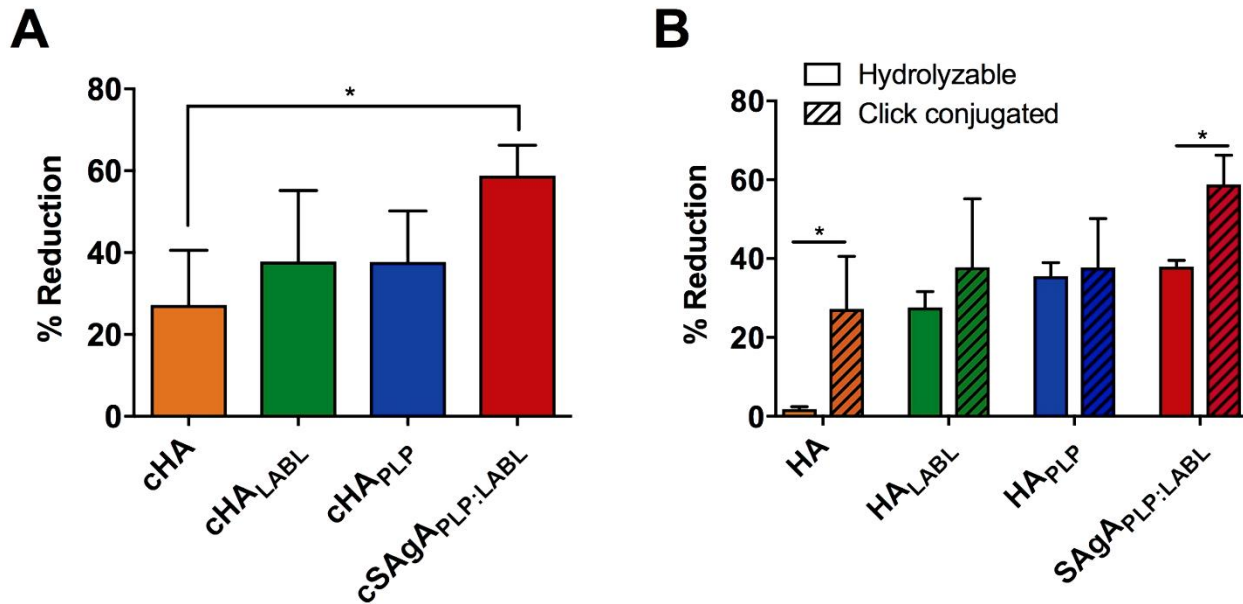


Figure 43: Reduction in IgM-stimulated (BCR-mediated) calcium flux signaling in Fluo-4 loaded Raji B cells determined by flow cytometry: (A) Percent reduction from  $\alpha$ IgM-stimulated baseline following addition of cHA, cHA<sub>LABEL</sub>, cHA<sub>PLP</sub>, or cSAG<sub>APLP:LABEL</sub>, determined from mean steady state values. (B) Comparison of reduction in  $\alpha$ IgM-stimulated signaling from hydrolyzable versus click-conjugated arrays. Data was pooled from three independent experiments. Statistical significance was determined by ANOVA followed by Tukey's post hoc test (A) or unpaired t-test (B) with  $p < 0.05$  and  $n = 3$  (\* $p < 0.05$ , \*\* $p < 0.01$ , \*\*\* $p < 0.001$ , \*\*\*\* $p < 0.0001$ ).

Previously, we reported a significant reduction in signaling from addition of SAg<sub>APLP:LABEL</sub>, HA<sub>PLP</sub>, and HA<sub>LABEL</sub>, but negligible change in signaling from addition of vehicle (HBSS) or HA.<sup>148</sup> The click conjugates exhibited a similar trend: cSAG<sub>APLP:LABEL</sub> caused the greatest reduction in signaling while cHA caused the smallest reduction ( $p < 0.05$ ) (Figure 43A). However, while cSAG<sub>APLP:LABEL</sub> caused a greater reduction than hydrolyzable SAg<sub>APLP:LABEL</sub>, there was not a significant difference between cHA<sub>PLP</sub> vs. HA<sub>PLP</sub> and cHA<sub>LABEL</sub> vs. HA<sub>LABEL</sub> (Figure 43B). It is also interesting to note that cHA (HA-N<sub>3</sub>) caused a greater reduction than unmodified HA, which may

be due to the presence of azide groups on the HA backbone leading to a greater degree of nonspecific binding.

#### ***4.3.5. Fluorescence Microscopy***

Fluorescence microscopy was performed using a microfluidics platform that enabled real time observation of binding and BCR clustering on the cell surface. Previously, we observed that fSAg<sub>PLP:LABL</sub> binding induced mature receptor clustering in Raji B cells while the polymer alone did not, and concluded that LABL may contribute to the SAg<sub>PLP:LABL</sub> molecule's ability to cluster receptors.<sup>148</sup> Here, we observed receptor clustering following binding and also labeled IgM to monitor BCR organization on the cell surface. Negative control cells treated with media exhibited diffuse BCR staining (Figure 44A), while cells treated with fcHA<sub>LABL</sub> (Figure 44C), fcHA<sub>PLP</sub> (Figure 44D), and fcSAg<sub>PLP:LABL</sub> (Figure 44E) exhibited BCR capping. BCR capping occurs when BCR clusters coalesce to form a single aggregate (i.e., one area of high intensity IgM fluorescence).<sup>175</sup> In contrast, cells treated with unmodified fcHA polymer exhibited BCR microclustering, which occurs when BCR clusters fail to coalesce into a single aggregate (i.e., multiple areas of moderate intensity IgM fluorescence) (Figure 44B). BCR capping on individual cells was quantified by plotting IgM pixel intensity relative to normalized cell diameter (Figure 45A), revealing that fcHA<sub>LABL</sub>, fcHA<sub>PLP</sub>, and fcSAg<sub>PLP:LABL</sub> induced clusters with significantly higher IgM intensity than the vehicle or fcHA (Figure 45B). Additionally, fcHA<sub>LABL</sub>, fcHA<sub>PLP</sub>, and fcSAg<sub>PLP:LABL</sub> induced IgM capping in a significantly higher fraction of cells than the vehicle or fcHA (Figure 45C). fcHA<sub>LABL</sub> and fcSAg<sub>PLP:LABL</sub> appeared particularly adept at inducing a high degree of IgM capping in a large fraction of cells. These trends echoed our previous observations that polymer modified with multivalent PLP<sub>139-151</sub> and LABL, but not unmodified



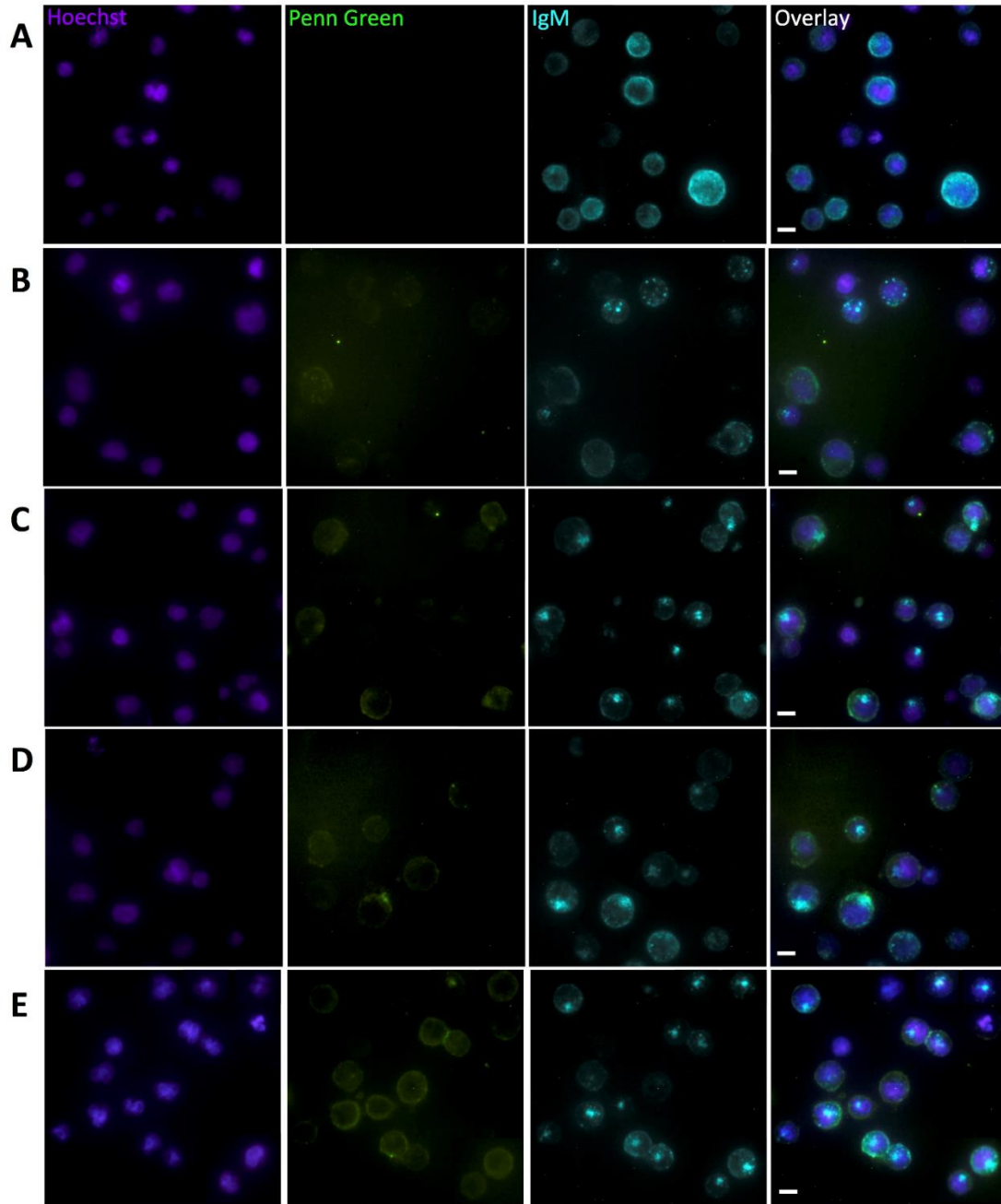


Figure 44: Fluorescence microscopy showing binding and BCR clustering in Raji B cells following perfusion of (A) vehicle, (B)  $fcHA$ , (C)  $fcHA_{LABL}$ , (D)  $fcHA_{PLP}$ , and (E)  $fcSAG_{APLP.LABL}$ . Cell nuclei were stained with Hoechst (violet – Panel 1) and surface IgM was stained with AlexaFluor® 647-conjugated  $\alpha IgM$  (blue – Panel 3). Penn Green-labeled polymer arrays are shown binding to the cell surface (green – Panel 2). In contrast to the diffuse IgM fluorescence in (A), highly localized punctate IgM fluorescence in (C), (D), and (E) indicates BCR clustering and capping in cells treated with  $fcHA_{LABL}$ ,  $fcHA_{PLP}$ , and  $fcSAG_{APLP.LABL}$ . Capping occurs when BCR clusters coalesce to form a single aggregate (i.e., one area of high intensity IgM fluorescence). Captured using the M04S plate and CellASIC Onyx Microfluidics platform on an Olympus IX81 inverted Epifluorescence microscope. Magnification: 60X air. Scale bar equals 10  $\mu m$ .

HA, induced mature receptor clustering.<sup>148</sup> PLP may promote clustering due to its antigen-specific affinity for BCR. LABL may promote clustering due to its affinity for ICAM-1, which (along with LFA-1) plays an integral role in the organization of supramolecular activation clusters (SMACs) during BCR signaling by forming a peripheral ring (pSMAC) around the central BCR cluster (cSMAC).<sup>111, 156, 176-177</sup>

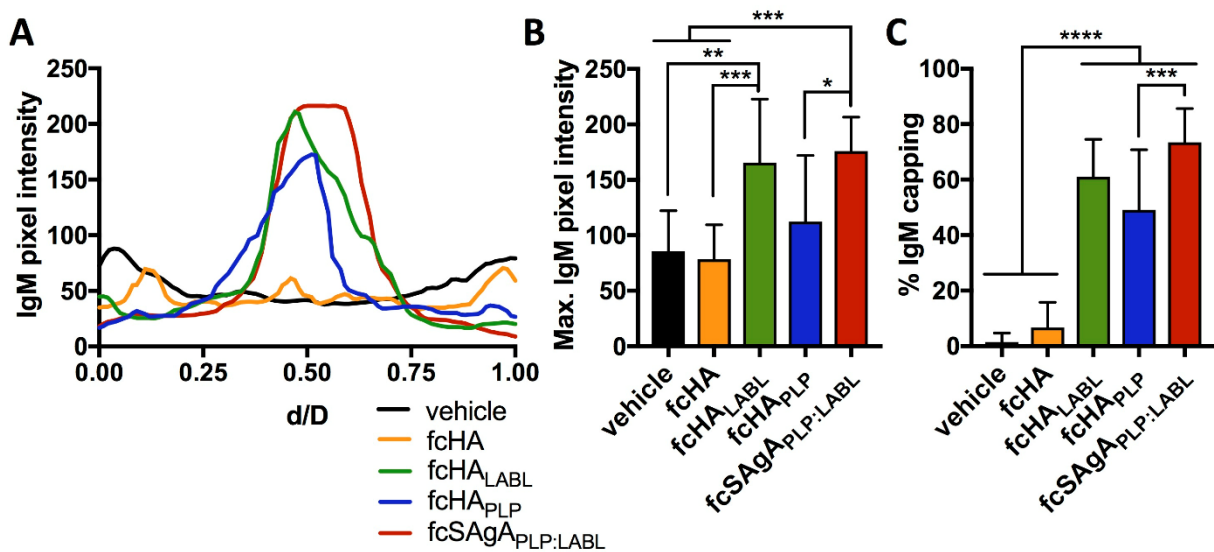


Figure 45: Quantification of BCR clustering in Raji B cells following perfusion of vehicle, fcHA, fcHA<sub>LABL</sub>, fcHA<sub>PLP</sub>, or fcSAgA<sub>PLP:LABL</sub> in the microfluidics plate. (A) Representative cell profile plots of IgM pixel intensity relative to normalized cell diameter, d/D. (B) Maximum IgM pixel intensity per cell determined from profile plots of individual cells (n=10). (C) Percent of cells positive for IgM capping (fully coalesced IgM clustering) determined using otsu thresholding (n=100-250 cells per sample). Statistical significance was determined by ANOVA followed by Tukey's post hoc test with p<0.05 (\*p<0.05, \*\*p<0.01, \*\*\*p<0.001, \*\*\*\*p<0.0001). Mean + SD shown. Images were captured using the M04S plate and CellASIC Onyx Microfluidics platform on an Olympus IX81 inverted Epifluorescence microscope and analyzed in ImageJ.

It has been suggested that quantitative differences in the degree of BCR clustering and crosslinking may drive qualitative differences in BCR signaling.<sup>178</sup> In general, our observations of BCR clustering corroborated our calcium flux results, since cHA<sub>PLP</sub>, cHA<sub>LABL</sub>, and in particular cSAgA<sub>PLP:LABL</sub> reduced BCR-mediated signaling to a greater extent than cHA. Combined with previous evidence supporting BCR as a target for SAgA<sub>PLP:LABL</sub> binding,<sup>148</sup> these results suggested

that cS<sub>Ag</sub>A<sub>PLP:LABL</sub> engagement and subsequent clustering of the BCR may dampen signaling. Our observations are consistent with reports that continuous BCR engagement and clustering are a mechanism for inducing B cell anergy that is accompanied by reduced calcium flux signaling.<sup>138-</sup>

139

#### **4.3.6. Preclinical EAE Studies**

Therapeutic efficacy of S<sub>Ag</sub>A<sub>PLP:LABL</sub> and cS<sub>Ag</sub>A<sub>PLP:LABL</sub> was evaluated in EAE mice induced with PLP<sub>139-151</sub> to model the relapsing-remitting form of MS. Disease symptoms emerged on day 10-12 with peak of disease occurring on day 13-15 before progressing to remission around day 20-25. Efficacy was measured by clinical score, weight change, and clinical score area under the curve (AUC) relative to the PBS control. AUC representation of clinical data has been reported as an informative secondary measure for overall extent of disease because it provides a cumulative measure not weighted by the scaling or time course of disease.<sup>179</sup> Disease incidence and mortality rate are provided as supplemental information (Figure 46). Statistical differences were determined by comparing treated groups with the negative PBS control.

A three-day dosing schedule with a dose equivalent to 200 nmol PLP<sub>139-151</sub> administered on days 4, 7, and 10 was found to be efficacious in previous S<sub>Ag</sub>A<sub>PLP:LABL</sub> studies.<sup>149-154</sup> This dose and schedule were mirrored in a preliminary *in vivo* study with cS<sub>Ag</sub>A<sub>PLP:LABL</sub>. It is important to note that shortly after the third administration on day 10, five out of six mice that received cS<sub>Ag</sub>A<sub>PLP:LABL</sub> died from apparent anaphylaxis. This result may be due to a greater effective concentration of PLP antigen being delivered to immune cells with the click-conjugated platform over the acid-labile platform. As is the case with allergen tolerization therapy, where an offending allergen is administered in gradually increasing doses over time to desensitize the allergic immune

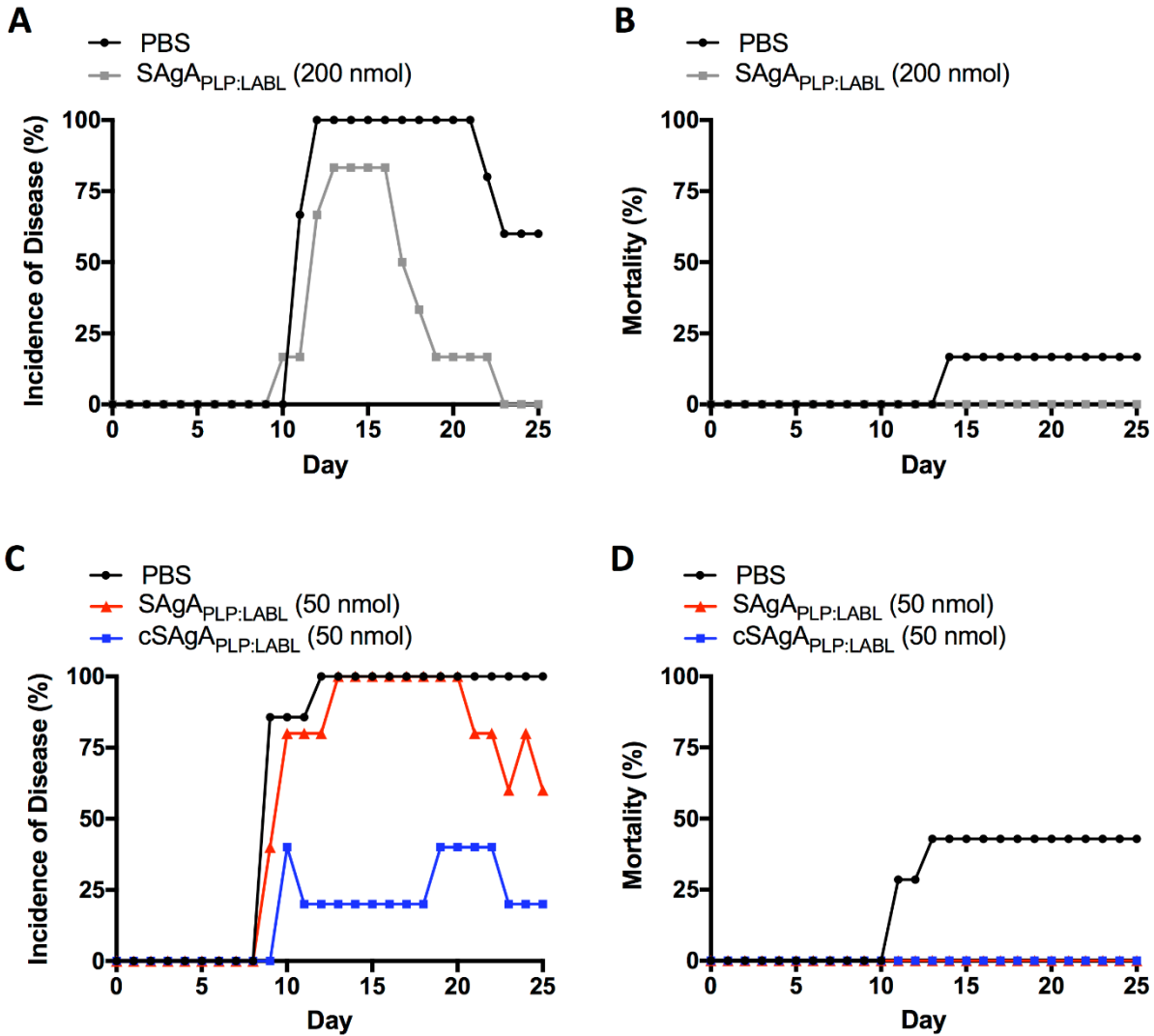


Figure 46: Comparing SAgA<sub>PLP:LABEL</sub> and cSAgA<sub>PLP:LABEL</sub> therapeutic efficacy in EAE: (A) incidence of disease and (B) mortality in mice treated with SAgA<sub>PLP:LABEL</sub> (200 nmol PLP dose) (n=6); (C) incidence of disease and (D) mortality in mice treated with cSAgA<sub>PLP:LABEL</sub> (50 nmol PLP dose) versus SAgA<sub>PLP:LABEL</sub> (50 nmol PLP dose) (n=5).

response, care must be taken to achieve an effective cumulative dose that induces tolerance without activating a severe hypersensitive response.<sup>180-182</sup> Our observation reflects the greater potency of cSAgA<sub>PLP:LABEL</sub> compared to SAgA<sub>PLP:LABEL</sub>, such that a lower dose was required to tip the immune response towards severe hypersensitivity. Therefore, a combination of lower doses was investigated in a small-scale dosing study (Figure 47). To determine whether the total cumulative dose or the number of injections caused the negative response, a group was included

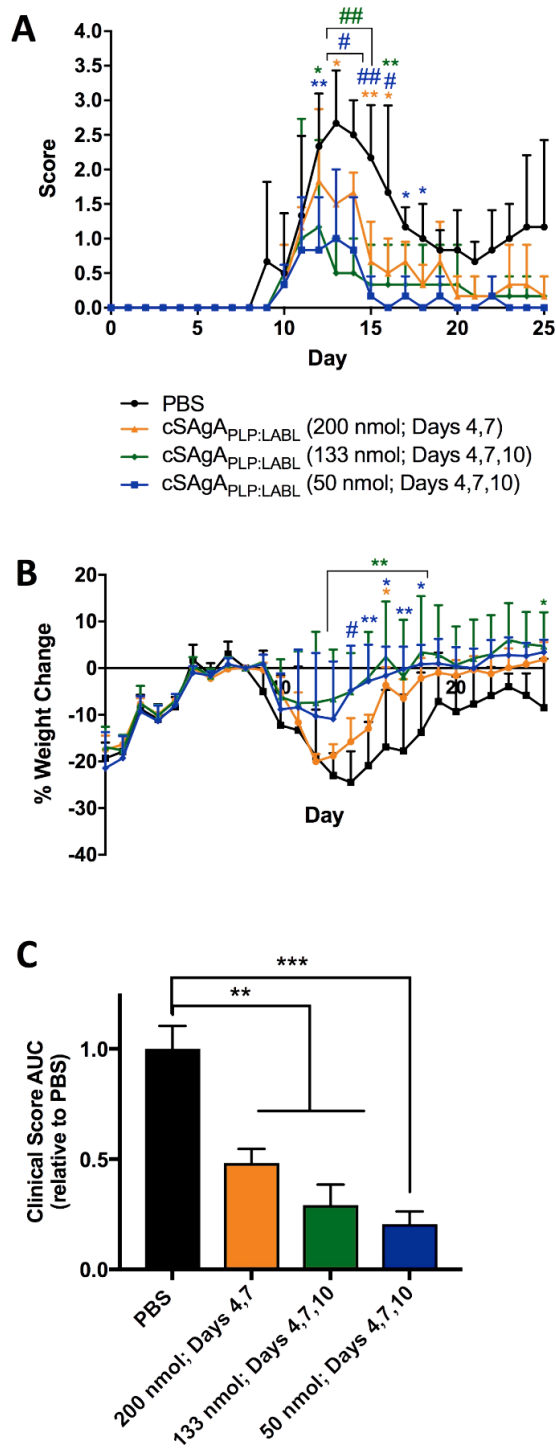


Figure 47: Clinical EAE dosing study with cSAg<sub>PLP:LABEL</sub>: cSAg<sub>PLP:LABEL</sub> was administered on days 4 and 7 at a dose equivalent to 200 nmol PLP and on days 4, 7, and 10 at a dose equivalent to 50 or 133 nmol PLP. Therapeutic efficacy evaluated by comparing (A) clinical disease score, (B) percent weight change, and (C) clinical score area under the curve (AUC). Statistical significance (compared to the negative PBS control) was determined by ANOVA followed by Tukey's post hoc test with  $p < 0.05$  and  $n = 3$  (\* $p < 0.05$ , \*\* $p < 0.01$ , #/\*\* $p < 0.001$ , ##/\*\*\*\* $p < 0.0001$ ).

with the same dose per injection (200 nmol PLP<sub>139-151</sub>) but administered only on two days (days 4, 7). In another group, an equivalent cumulative dose was administered over three days (133 nmol PLP<sub>139-151</sub> on days 4, 7, 10). A final group was included with a low dose of 50 nmol PLP<sub>139-151</sub>, administered on all three days. All dosing groups significantly alleviated disease compared to the PBS control according to clinical disease score (Figure 47A) and clinical score AUC (Figure 47C). The cSAgA<sub>PLP:LABEL</sub> dose of 50 nmol PLP<sub>139-151</sub> caused a significant reduction in clinical score on the greatest number of days (days 12-18) and exhibited the greatest reduction in clinical score AUC compared to PBS ( $p < 0.001$ ). Therefore, a cSAgA<sub>PLP:LABEL</sub> dose of 50 nmol PLP<sub>139-151</sub> was selected for studies going forward.

Next, *in vivo* efficacy of click-conjugated cSAgA<sub>PLP:LABEL</sub> was compared to hydrolyzable SAgA<sub>PLP:LABEL</sub> (Figure 48). At the original therapeutic dose equivalent to 200 nmol PLP<sub>139-151</sub>, SAgA<sub>PLP:LABEL</sub> significantly reduced clinical score on days 11-20 (Figure 48A) and significantly reduced total disease score AUC compared to PBS ( $p < 0.0001$ ) (Figure 48E). At only a quarter of the dose, cSAgA<sub>PLP:LABEL</sub> (50 nmol PLP<sub>139-151</sub>) significantly reduced total clinical score AUC to an equivalent extent as SAgA<sub>PLP:LABEL</sub> at 200 nmol PLP<sub>139-151</sub> (Figure 48E). Furthermore, cSAgA<sub>PLP:LABEL</sub> (50 nmol PLP<sub>139-151</sub>) significantly reduced clinical score on days 10-17 to a greater extent than SAgA<sub>PLP:LABEL</sub> at the 200 nmol dose (Figure 48B). In contrast, the 50 nmol dose of SAgA<sub>PLP:LABEL</sub> significantly reduced clinical score only on days 11 and 14 (Figure 48B), and reduced clinical score AUC to a significantly lesser extent ( $p < 0.001$ ) than cSAgA<sub>PLP:LABEL</sub> (50 nmol PLP<sub>139-151</sub>) (Figure 48E). While SAgA<sub>PLP:LABEL</sub> (200 nmol PLP<sub>139-151</sub>) significantly alleviated weight loss on days 11-22 (Figure 48C), cSAgA<sub>PLP:LABEL</sub> (50 nmol PLP<sub>139-151</sub>) significantly alleviated weight loss over a larger portion of the study, on days 11-25 (Figure 48D). In contrast,

SAg<sub>APLP:LABL</sub> (50 nmol PLP<sub>139-151</sub>) did not alleviate weight loss on any day of the study (Figure 48D).

Lastly, cSAg<sub>APLP:LABL</sub> (50 nmol PLP<sub>139-151</sub>) reduced incidence of disease to a greater extent than SAg<sub>APLP:LABL</sub> at either dose (Figure 46). During peak of disease, 100% of the mice treated with PBS or SAg<sub>APLP:LABL</sub> (50 nmol PLP<sub>139-151</sub>) and over 75% of the mice treated with SAg<sub>APLP:LABL</sub> (200 nmol PLP<sub>139-151</sub>) exhibited disease symptoms. In contrast, less than 25% of the mice treated with cSAg<sub>APLP:LABL</sub> (50 nmol PLP<sub>139-151</sub>) exhibited disease symptoms during peak of disease. Therefore, when considering multiple measures of efficacy, cSAg<sub>APLP:LABL</sub> achieved equivalent or greater *in vivo* efficacy as SAg<sub>APLP:LABL</sub> at one quarter of the antigen dose. We conclude that non-hydrolyzable click conjugation rendered greater therapeutic efficacy than hydrolyzable modification.

#### 4.4. Conclusion

Click-conjugated multivalent soluble antigen arrays were developed and evaluated *in vitro* and *in vivo* as therapeutic agents in a murine model of MS. Hydrolyzable SAg<sub>APLP:LABL</sub>, which we have studied extensively and shown to significantly suppress EAE,<sup>148-154</sup> employed a degradable linker to co-deliver antigen (PLP) and cell adhesion inhibitor (LABL) peptides. This approach was built upon our earlier two-signal hypothesis that SAg<sub>APLP:LABL</sub> inhibited autoimmune activation via the immunological synapse, a mechanism that would necessitate antigen uptake, processing, and presentation and motivated the design of a degradable SAgA molecule. Recent *in vitro* studies, however, pointed instead to a therapeutic mechanism whereby SAg<sub>APLP:LABL</sub> acted through

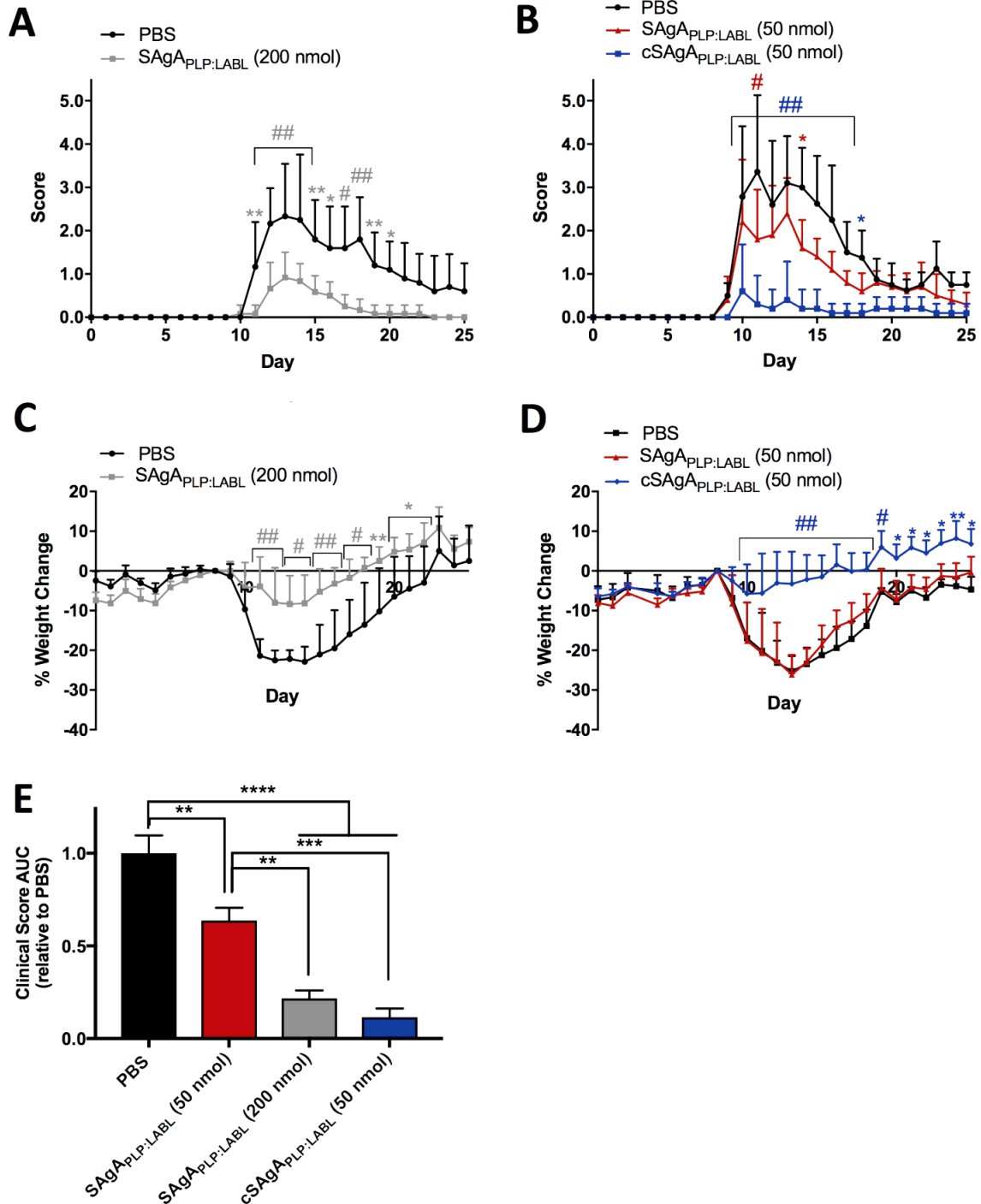


Figure 48: Comparing SAgA<sub>PLP:LABL</sub> and cSAgA<sub>PLP:LABL</sub> therapeutic efficacy in EAE: (A) SAgA<sub>PLP:LABL</sub> (200 nmol PLP dose) clinical scores (n=6), (B) cSAgA<sub>PLP:LABL</sub> versus SAgA<sub>PLP:LABL</sub> (50 nmol PLP dose) clinical scores (n=5), (C) SAgA<sub>PLP:LABL</sub> (200 nmol PLP dose) weight change, (D) cSAgA<sub>PLP:LABL</sub> versus SAgA<sub>PLP:LABL</sub> (50 nmol PLP dose) weight change, and (E) clinical score area under the curve (AUC) relative to PBS. Statistical significance was determined by ANOVA followed by Dunnett's (A-D) or Tukey's (E) post hoc test with  $p < 0.05$  (\* $p < 0.05$ , \*\* $p < 0.01$ , #/ $***p < 0.001$ , ##/ $****p < 0.0001$ ).



sustained BCR engagement, targeting BCR signaling while exhibiting prolonged residence on the cell surface.<sup>148</sup> These results motivated the development of a non-degradable SAgA molecule to enhance and maintain the molecule's surface activity, which we hypothesized would improve therapeutic efficacy. cSAgA<sub>PLP:LABL</sub> was developed as a modified version of the SAgA<sub>PLP:LABL</sub> molecule with multiple PLP<sub>139-151</sub> and LABL peptides conjugated to HA using non-hydrolyzable linker chemistry (Copper-catalyzed Azide-Alkyne Cycloaddition (CuAAC)).

Building upon previous work, these studies sought to establish therapeutic efficacy of cSAgA<sub>PLP:LABL</sub> *in vivo* while identifying a potential therapeutic mechanism by evaluating binding avidity and signaling modulation *in vitro*. Click-conjugated cSAgA<sub>PLP:LABL</sub> exhibited greatly enhanced binding in B cells compared to hydrolyzable SAgA<sub>PLP:LABL</sub>, indicating that non-hydrolyzable multivalent ligand increased the avidity of the molecule. Furthermore, cSAgA<sub>PLP:LABL</sub> exhibited greater capacity for reducing and inhibiting BCR-mediated signaling as compared to SAgA<sub>PLP:LABL</sub>. Imaging revealed that cSAgA<sub>PLP:LABL</sub> binding caused BCR clustering, another marker indicative of BCR engagement and signaling modulation. Our *in vitro* observations pointed to B cell anergy, induced by continuous BCR engagement and clustering and accompanied by reduced calcium flux signaling, as a likely cSAgA<sub>PLP:LABL</sub> therapeutic cellular mechanism. Lastly, cSAgA<sub>PLP:LABL</sub> exhibited enhanced *in vivo* efficacy against EAE, achieving equivalent therapeutic efficacy as SAgA<sub>PLP:LABL</sub> at one quarter of the dose. Taken together, these results indicated that non-hydrolyzable conjugation increased the avidity of cSAgA<sub>PLP:LABL</sub>, driving *in vivo* efficacy through modulated BCR-mediated signaling. The click-conjugated cSAgA<sub>PLP:LABL</sub> molecule shows promising potential for ASIT for the improved treatment of autoimmune disease.

**CHAPTER 5:**  
**HYALURONAN-DEXAMETHASONE CONJUGATE AS A PH-  
SENSITIVE DRUG DELIVERY SYSTEM**

## **CHAPTER 5: HYALURONAN-DEXAMETHASONE CONJUGATE AS A pH-SENSITIVE DRUG DELIVERY SYSTEM**

### **5.1. Introduction**

The antigen-specific immunotherapies described in Chapters 3 and 4 showed great promise, however, many inflammatory diseases lack a known antigen-specific autoimmune component. The construction of the hyaluronic acid (hyaluronan, HA) and dexamethasone (Dex) building blocks discussed in previous chapters provided a unique opportunity to develop an extended release delivery system capable of remaining at the site of action and releasing Dex over time. HA has seen extensive clinical use in eye surgeries in combination with Dex to manage post-surgical inflammation. This provides motivation to explore a bioconjugate to locally address post-surgical ocular inflammation.

The corneal endothelium is a monolayer of cells that acts as a barrier and active fluid pump system, functioning to maintain corneal transparency and a normal thickness of approximately 5  $\mu\text{m}$ .<sup>183-184</sup> It is widely accepted that cataract surgery results in corneal endothelial cell loss (ECL),<sup>185-187</sup> and the extent is dependent upon a number of pre-, intra-, and post-operative factors.<sup>188</sup> Complications following cataract surgeries resulting in significant ECL can lead to corneal edema or decomposition, which is associated with decreased vision.<sup>185</sup> The current standard of care is phacoemulsification which can vary by surgical technique, anterior chamber depth, and ultrasound time and energy, and has been shown to induce the formation of highly reactive free radicals,<sup>189</sup> all of which can contribute to the amount of ECL. Minimization of ECL during surgery is a priority and has been assisted by the use of ophthalmic viscoelastic devices (OVDs) to stabilize the anterior chamber at various steps in the procedure<sup>185</sup> to reduce damage by free radicals<sup>190</sup> in an effort to protect the integrity of the corneal endothelium.<sup>191-193</sup>

Viscoelastic agents used in OVDs have been employed in intraocular surgeries since the 1970's, and variant OVDs have emerged with discrete properties to fit the specific medical need, typically modifying the concentration or molecular weight (MW) of the viscoelastic substance to influence cohesive, dispersive, or other mechanical properties.<sup>194</sup> Of the viscoelastic agents commonly used in OVDs, HA is the most popular.<sup>195</sup> HA is a naturally-occurring linear disaccharide polymer present throughout the body, from the extracellular matrix of connective tissue to the aqueous humor and vitreous of the eye, totaling 15 grams for a typical individual.<sup>196</sup> It also plays an important role regulating tissue repair and disease state, such as activation of an innate inflammatory response to injury.<sup>197</sup> HA is composed of D-glucuronic acid and *N*-acetyl-D-glucosamine linked by a  $\beta$ -1,3 glucuronidic bond, and can vary widely in molecular weight, often exceeding one million daltons.<sup>198</sup> Commercially available OVDs such as Healon® 5 (2.3% HA, MW = 4 million daltons) and DisCoVisc® (1.6% HA, MW – 1.7 million daltons) employ high MW HA, but newer products such as Twinvisc® and Duovisc® contain two different MW HA.<sup>192</sup>

One primary challenge following cataract surgery is the need to manage post-operative intraocular inflammation using anti-inflammatory agents. A number of clinical studies have demonstrated the use of these agents, often included with an anti-infective drug to control the risk of infection.<sup>199-204</sup> Dex has been approved for ophthalmic use in multiple products where a risk of infection is present, including intravitreal implants,<sup>205-206</sup> topical ointments,<sup>207</sup> and suspensions. However, a setback to the effective management of post-operative inflammation is the requirement for frequent dosing, often requiring administration up to 4 times daily. This results in the potential for decreased patient compliance and reduced efficacy, especially in elderly patient populations. Here, we developed a novel HA-Dex conjugate, where Dex is linked to HA via a labile covalent

bond to enable sustained, local release of Dex as a promising alternative for management of intraocular inflammation.

## 5.2. Materials and Methods

Hyaluronic acid (HA) sodium salt (MW 16 kDa) was purchased from Lifecore Biomedical (Chaska, MN). *N*-hydroxysuccinimide, dexamethasone, *N*-(3-dimethylaminopropyl)-*N'*-ethylcarbodiimide hydrochloride (EDC), 2-(*N*-morpholino)ethanesulfonic acid sodium salt (MES), tris(3-hydroxypropyl)triazolylmethylamine (THPTA), and sodium ascorbate (NaAsc) were purchased from Sigma-Aldrich (St. Louis, MO). Copper(II) sulfate pentahydrate ( $\text{CuSO}_4 \cdot 5\text{H}_2\text{O}$ ) was purchased from Acros Organics (Geel, Belgium). 2,5-dioxopyrrolidin-1-yl 2-azidoacetate was purchased from Clickchemistrytools, LLC (Scottsdale, AZ). All other chemicals and reagents were analytical grade and were used as received without further purification.

### 5.2.1. Synthesis of azide-functionalized dexamethasone (Dex- $N_3$ )

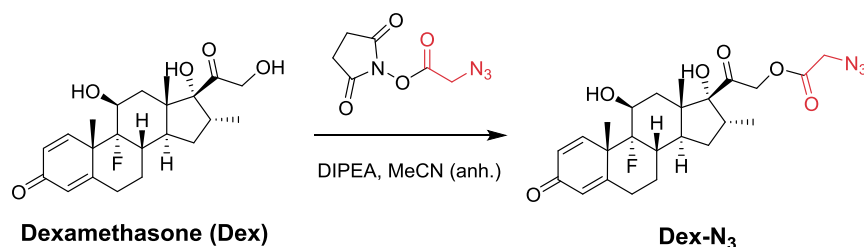


Figure 49: Reaction scheme for the synthesis of Dex- $N_3$ .

Dexamethasone was added to a flame dried 250 mL round bottom flask with a stir bar and septa. Anhydrous MeCN was added under nitrogen, then DIPEA via a glass syringe. The flask was stirred for 10 min before azidoacetic acid NHS ester was added as a powder. The reaction mixture

was stirred overnight at room temperature before being analyzed by HPLC. Additional equimolar aliquots of azidoacetic acid NHS ester were added, followed by stirring for 2 hours at room temperature and analysis by HPLC, until no additional benefit was observed. The crude reaction mixture was evaporated under reduced pressure, then dissolved in 4:6 MeCN:H<sub>2</sub>O and purified by prep HPLC. The resulting column fractions were evaporated under reduced pressure to yield the final product as a white powder. <sup>1</sup>H NMR (500 MHz, DMSO-*d*<sub>6</sub>) δ 7.30 (d, J = 10.2 Hz, 1H), 6.23 (dd, J = 10.1, 1.9 Hz, 1H), 6.01 (t, J = 1.7 Hz, 1H), 5.45 (dd, J = 5.0, 1.4 Hz, 1H), 5.23 (s, 1H), 5.17 (d, J = 17.5 Hz, 1H), 4.90 (d, J = 17.6 Hz, 1H), 4.32 – 4.19 (m, 2H), 4.19 – 4.11 (m, 1H), 2.88 (dq, J = 11.5, 7.2, 4.1 Hz, 1H), 2.62 (tdd, J = 13.6, 6.0, 1.7 Hz, 1H), 2.44 – 2.32 (m, 1H), 2.35 – 2.28 (m, 1H), 2.22 – 2.05 (m, 3H), 1.77 (dt, J = 11.2, 5.2 Hz, 1H), 1.70 – 1.58 (m, 1H), 1.56 (dd, J = 13.8, 2.0 Hz, 1H), 1.49 (s, 3H), 1.35 (qd, J = 12.9, 5.0 Hz, 1H), 1.08 (ddd, J = 12.1, 8.2, 4.1 Hz, 1H), 0.89 (s, 3H), 0.80 (d, J = 7.2 Hz, 3H). <sup>13</sup>C NMR (126 MHz, DMSO-*d*<sub>6</sub>) δ 204.36, 185.30, 168.28, 167.10, 152.77, 129.03, 124.12, 102.00, 100.61, 90.52, 70.63, 70.34, 69.00, 49.34, 48.09, 48.05, 47.87, 43.33, 35.69, 35.53, 33.67, 33.51, 31.92, 30.28, 27.32, 23.03, 22.98, 16.31, 15.15, 1.19. Expected [M+H]<sup>+</sup> = 476.2191 Da; Observed [M+H]<sup>+</sup> = 476.2067 Da.

### 5.2.2. General procedure for the synthesis of alkyne-functionalized hyaluronic acid (HA-Alk)

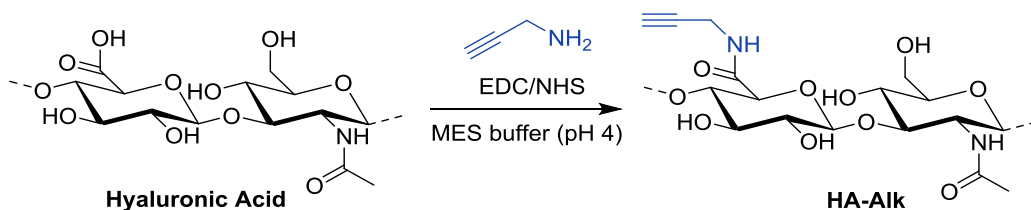


Figure 50: Reaction scheme for the synthesis of alkyne-functionalized HA.

To a solution of sodium hyaluronate (31  $\mu\text{mol}$ ) in 20 mL of 50 mM MES buffer (pH 4.0) was added *N*-hydroxysuccinimide (6.3 mmol) in 5 mL of MES buffer, then EDC (7.8 mmol) in 10 mL of MES buffer. The solution was stirred for 5 min before propargylamine (varying amounts) in MES buffer was added. The mixture was stirred for 24 hrs at room temperature before being dialyzed in 6-8 kDa cutoff dialysis tubing against a 0.9% NaCl solution for 24 hrs, then deionized water (4 x 12 hrs). The volume in the bag was frozen at  $-20^{\circ}\text{C}$ , then lyophilized to yield a white powder.

### 5.2.3. General procedure for the synthesis of HA-dexamethasone conjugates (HA-Dex)

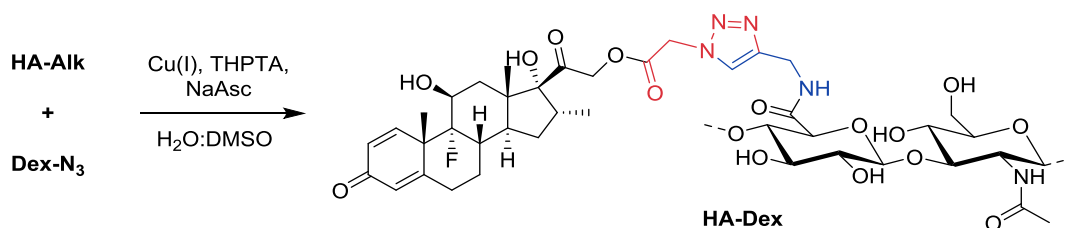


Figure 51: Reaction scheme for the synthesis of HA-Dex conjugates.

To a solution of HA-Alk (1.5  $\mu\text{mol}$ ) in deionized  $\text{H}_2\text{O}$  was added Dex- $\text{N}_3$  (23  $\mu\text{mol}$ ) in DMSO. A premixed solution of THPTA (20  $\mu\text{mol}$ ) and  $\text{CuSO}_4 \cdot 5\text{H}_2\text{O}$  (4  $\mu\text{mol}$ ) was then added

to the reaction mixture. An aliquot (“pre-NaAsc” sample) was removed for RP-HPLC analysis, then NaAsc (81  $\mu\text{mol}$ ) was added to the reaction mixture to initiate the reaction. Throughout the course of the reaction, additional aliquots were removed for RP-HPLC analysis to determine the extent of conjugation. Once the desired conjugation values were achieved, the reaction mixture was transferred to a 6-8k dialysis cassette and dialyzed against 1.0 M NaCl (2 x 12 hrs), then deionized H<sub>2</sub>O (5 x 12 hrs). The volume in the cassette was frozen at -20°C and lyophilized to yield a white powder.

#### ***5.2.4. Analytical Characterization of HA-Dexamethasone Conjugates***

All chromatographic analysis was conducted with a Waters Alliance HPLC system equipped with either a diode array detector or dual wavelength UV/Vis detector. For RP-HPLC of polymer containing samples, general chromatographic conditions employed a linear gradient from 5-70% acetonitrile in water (constant 0.05% trifluoroacetic acid) was employed over 20 min, with a Waters XBridge Protein C<sub>4</sub>, 3.5  $\mu\text{m}$ , 300 Å stationary phase (4.6 x 150 mm) with a 1.0 mL/min flow rate and detection at 214 nm. For semi-preparative HPLC, a linear elution gradient of acetonitrile in water over 20 min, with a Waters XBridge BEH C<sub>18</sub>, 5  $\mu\text{m}$ , 130 Å stationary phase (19 x 250 mm), with a 14.0 mL/min flow rate. Semi-preparative method development and reaction monitoring was completed on the identical stationary phase in a 4.6 x 250 mm configuration. For RP-HPLC analysis of Dex-N<sub>3</sub> purity, chromatographic conditions employed a linear gradient from 5-95% acetonitrile in water (constant 0.05% trifluoroacetic acid) over 60 min, with a Waters XBridge C<sub>18</sub>, 3.5  $\mu\text{m}$ , 130 Å stationary phase (4.6 x 150 mm) using a 1.0 mL/min flow rate at 35°C column temperature and detection at 214 nm.



LC/MS sample analysis with completed on a Waters Xevo G2, employing linear elution gradients of 15-100% acetonitrile in water (constant 0.1% formic acid) over 45 min, employing a Waters XBridge BEH C<sub>18</sub>, 1.7 μm, 130 Å stationary phase (0.075 x 250 mm), and a 0.5 μL/min flow rate and 50°C column temperature. Electrospray ionization, operating in the positive mode (ESI+), was used as the ionization source with a QToF mass analyzer used for detection.

NMR spectra were collected on a Bruker Avance AVIII 500 MHz spectrometer equipped with a dual carbon/proton cryoprobe. All samples were dissolved in 650 μL of D<sub>2</sub>O or DMSO-*d*<sub>6</sub>. Data processing was performed using MestReNova 11.0 (Santiago de Compostela, Spain).

### 5.2.5. Determination of Dex conjugation

For the quantitative determination of Dex conjugation by RP-HPLC, the following equation was used:

$$N_{\text{dex}} = \left[ \left( \frac{n_{\text{Dex-Az}}}{n_{\text{HA-Alk}}} \right) \left( \frac{V_{\text{pre}} - V_{\text{sam}}}{V_{\text{pre}}} \right) \right] \left( 1 - \frac{PA_t}{PA_{\text{start}}} \right) \quad \text{Equation 2}$$

where  $N_{\text{Dex}}$  = number of conjugated Dex molecules per backbone,  $n_{\text{Dex-Az}}$  = moles of Dex-N<sub>3</sub> used in reaction,  $n_{\text{HA-Alk}}$  = moles of HA-Alk used in reaction,  $V_{\text{pre}}$  = total reaction volume before NaAsc is added,  $V_{\text{sam}}$  = volume of “pre-NaAsc” sample removed from reaction mixture,  $PA_t$  = measured peak area of Dex-N<sub>3</sub> at time  $t$ , and  $PA_{\text{start}}$  = measured peak area of free Dex-N<sub>3</sub> before NaAsc is added to the reaction.

### **5.2.6. Drug release studies**

Dex release studies from HA-Dex were conducted in PBS buffer at 37°C, at a concentration of 10 mg/mL. At each time point, an aliquot of the incubated sample solution was removed and diluted to a concentration of 1 mg/mL for analysis by RP-HPLC. A linear calibration curve was used to quantify Dex release.

## **5.3. Results and Discussion**

### **5.3.1. Therapeutic design and rationale**

A polymeric system with chemistry to tune drug loading and be adapted to polymers of varying molecular weights is desirable to specifically tailor drug delivery using various OVDs. For this reason, the Copper-catalyzed Azide-Alkyne Cycloaddition (CuAAC) reaction was employed due to the breadth of literature with respect to applications and optimization,<sup>32, 34, 208</sup> in addition to previous reports of its use with HA.<sup>71-72, 209</sup> A small linker was selected to minimize the impact of the conjugation chemistry on the functional properties of HA, and to facilitate higher Dex loading. In the present work, we selected 16 kDa HA as the polymeric substrate which has an adequate balance between relevant mechanical properties in solution, while still allowing detailed analytical characterization using techniques such as heteronuclear NMR and HPLC. However, our research group has employed this same chemistry to attach payload molecules like Dex to HA with a MW in excess of a million daltons. Multiple groups have presented polymer conjugates of dexamethasone, forming a hydrazone<sup>210-211</sup> at the C<sub>3</sub> position, an ester<sup>212-215</sup> at the C<sub>21</sub> position, or thioether<sup>216</sup> at the C<sub>21</sub> position. Azide functionality was installed on Dex via esterification at the C<sub>21</sub>-OH position, yielding a degradable bond, which releases the parent Dex molecule over time. Importantly, the newly formed ester bond is short to minimize the effect of the added linker on the

mechanical properties of HA, and eventual release of Dex yields the same functional moiety, a carboxylic acid used for attachment to HA.

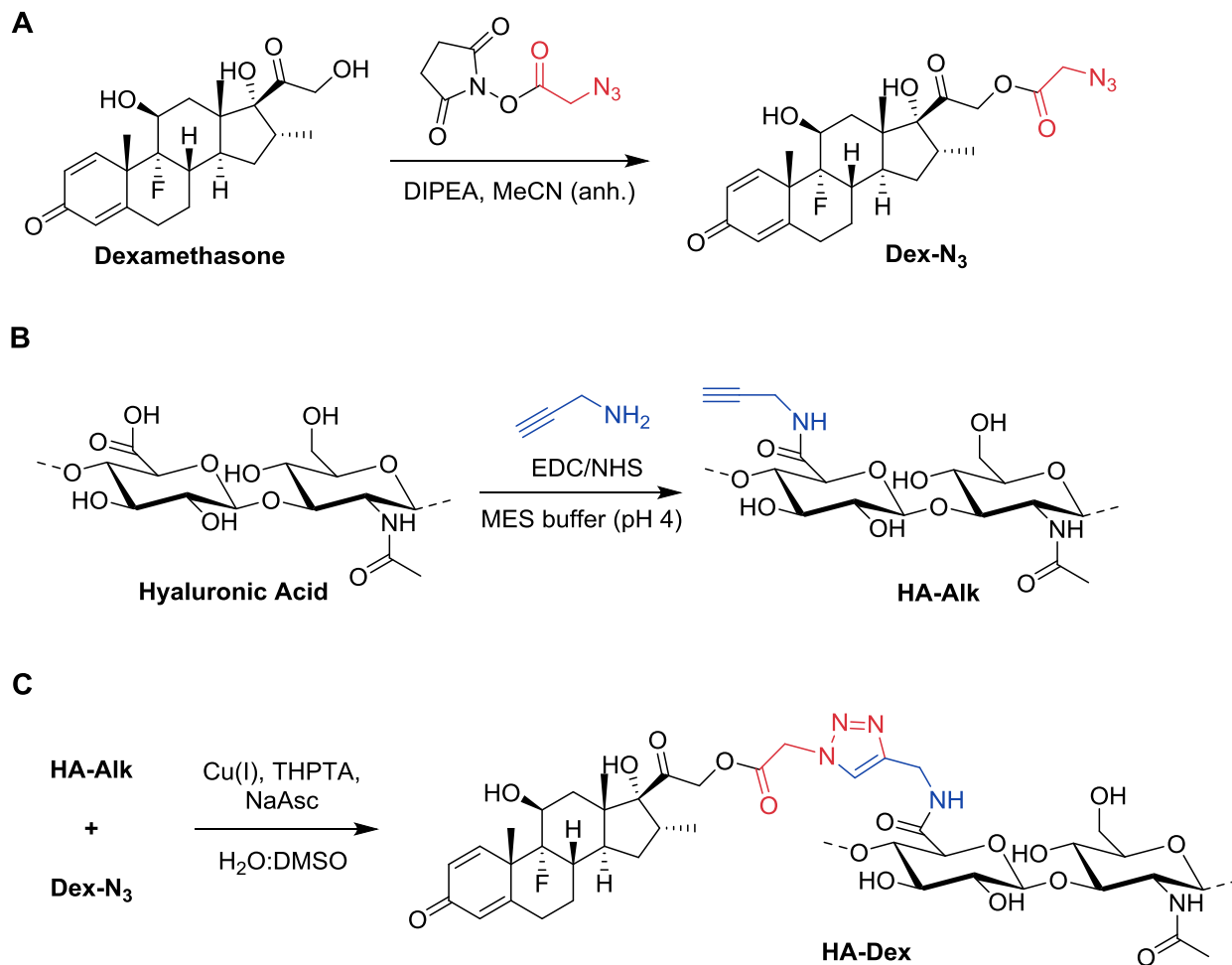


Figure 52: Reaction schemes for the synthesis of HA-dexamethasone conjugates: (A) alkyne-functionalization of hyaluronic acid, (B) azide-functionalization of dexamethasone, (C) CuAAC conjugation of HA-Alk to Dex-N<sub>3</sub>.

### 5.3.2. Synthesis and characterization of conjugates and intermediates

Azide-functionalization of Dex occurred under anhydrous conditions via esterification of the C<sub>21</sub>-OH in the presence of DIPEA (Figure 52A). The reaction was monitored by analytical RP-HPLC, and the Dex-N<sub>3</sub> product was isolated by semi-preparative RP-HPLC. Structural

confirmation of the Dex- $N_3$  product utilized  $^1\text{H}/^{13}\text{C}$  heteronuclear single quantum coherence (HSQC) NMR spectroscopy, which showed a downfield shift of the  $\text{C}_{21}$  H's with the addition of a  $\text{CH}_2$  resonance from the installed linker (Figure 53). Analysis by LC/MS confirms the expected mass, and purity analysis by RP-HPLC indicated the compound can be prepared in high purity (Figure 54).

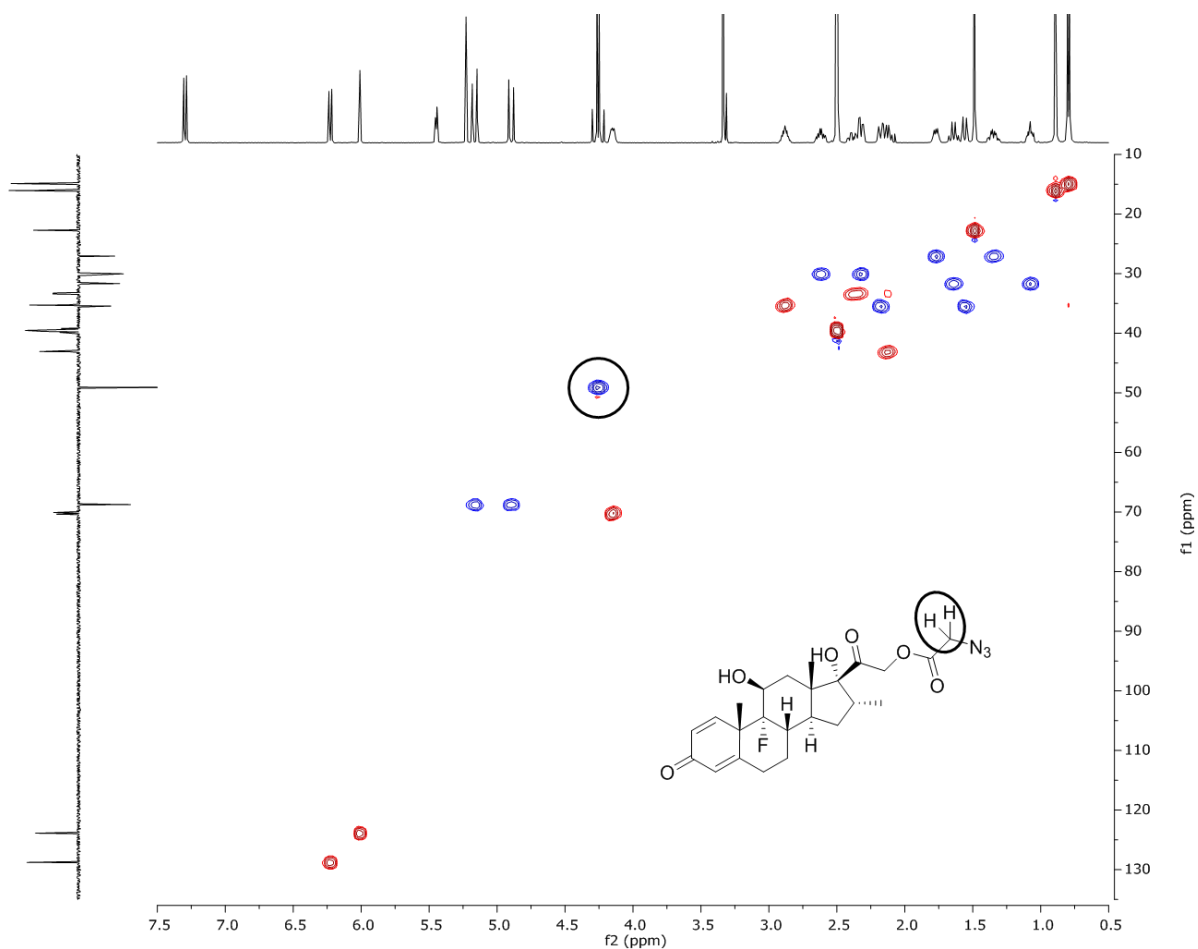


Figure 53: HSQC NMR spectrum for Dex- $N_3$  collected in  $\text{DMSO-}d_6$ , where the x-axis is a standard  $^1\text{H}$  spectrum, and the y-axis is a  $^{13}\text{C}$  DEPT-135 spectrum.

HA with an average molecular weight of 16 kDa was used in this study, which contains approximately 42 reactive carboxylic acid sites per backbone. Azide- and alkyne-functionalization of HA using heterobifunctional linkers via amidation was reported previously.<sup>209, 217</sup> Multiple

batches of HA-Alk were prepared utilizing propargylamine to install the alkyne moiety on HA (Figure 56), with varying degrees of alkyne substitution on the backbone. Dialysis was used as an effective purification process due to the significant difference in molecular weight of the functionalized HA and unreacted starting materials or reaction byproducts. HSQC NMR experiments indicated the presence of the terminal alkyne following functionalization (Figure 55), however, due to the overlapping nature of this resonance in both the  $^1\text{H}$  and  $^{13}\text{C}$  spectra (Figure 56 and Figure 57), quantitation of alkyne functionalization by NMR was not possible. RP-HPLC analysis showed an increasing degree of heterogeneity with increasing degree of substitution (Figure 58), but no unreacted material was detected following purification.

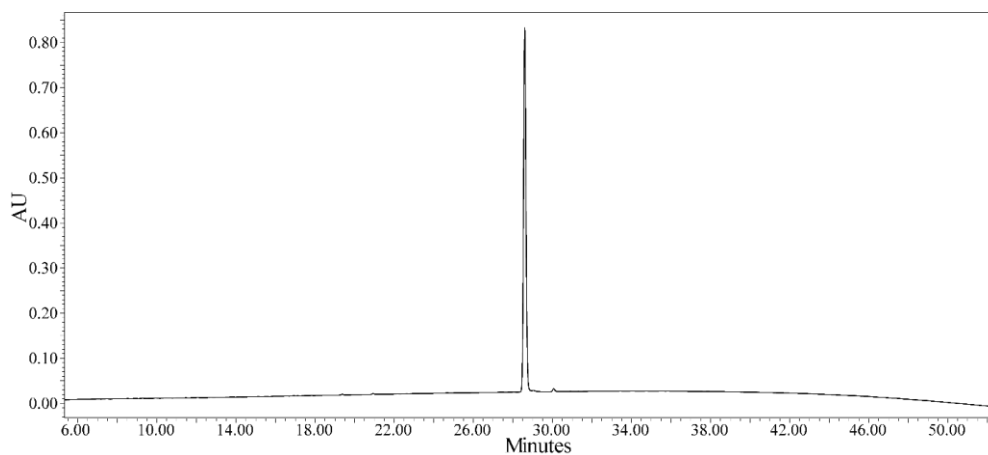


Figure 54: Analytical RP-HPLC chromatogram of Dex- $N_3$  after purification, with a purity of 98.3% (UV at 214 nm).

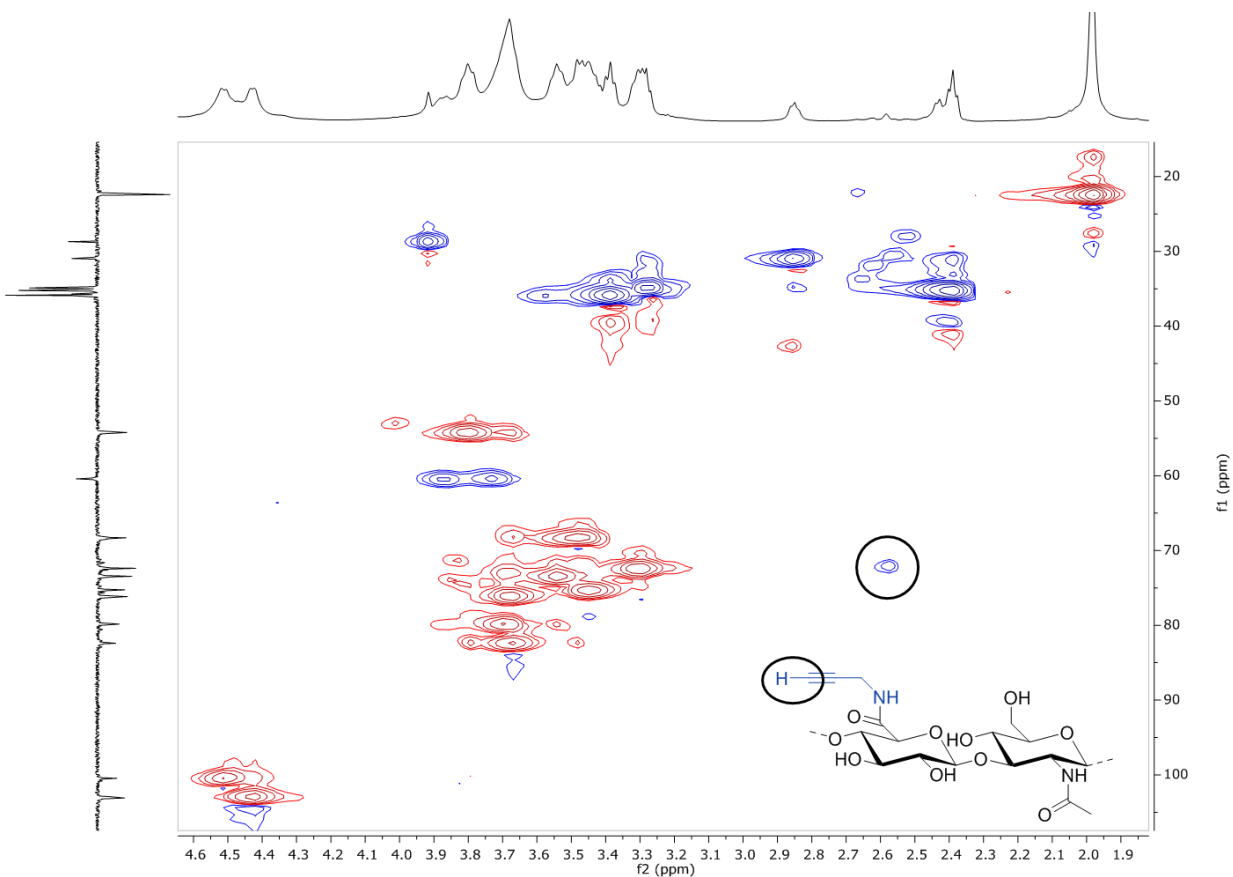


Figure 55:  $^1\text{H}/^{13}\text{C}$  HSQC NMR spectra in  $\text{D}_2\text{O}$  for alkyne-functionalized HA, highlighting the presence of a terminal alkyne resonance indicating the success of functionalization. The x-axis is a standard  $^1\text{H}$  spectrum, and the y-axis is a  $^{13}\text{C}$  DEPT-135 spectrum.

The CuAAC reaction was used for the final step to conjugate Dex- $\text{N}_3$  and HA-Alk, which requires a reducing agent to trigger the reaction through the reduction of  $\text{Cu}^{2+}$  to the active  $\text{Cu}^{1+}$ . This is an added benefit for screening numerous reaction conditions on the sub-mg scale since both HA-Alk and Dex- $\text{N}_3$  can be mixed together without the reaction proceeding. For this reason, analytical RP-HPLC could be used to determine the amount of conjugated Dex by monitoring the decrease of Dex- $\text{N}_3$  peak area before and after NaAsc was added to the reaction mixture (Figure 59). Initial multi-level reaction development studies were conducted to determine critical parameters, which impacted the level of Dex substitution in the final conjugate, varying stoichiometric ratios of Dex- $\text{N}_3$  to alkyne sites on HA (both limiting and excess), reaction time, and temperature (Table 3).

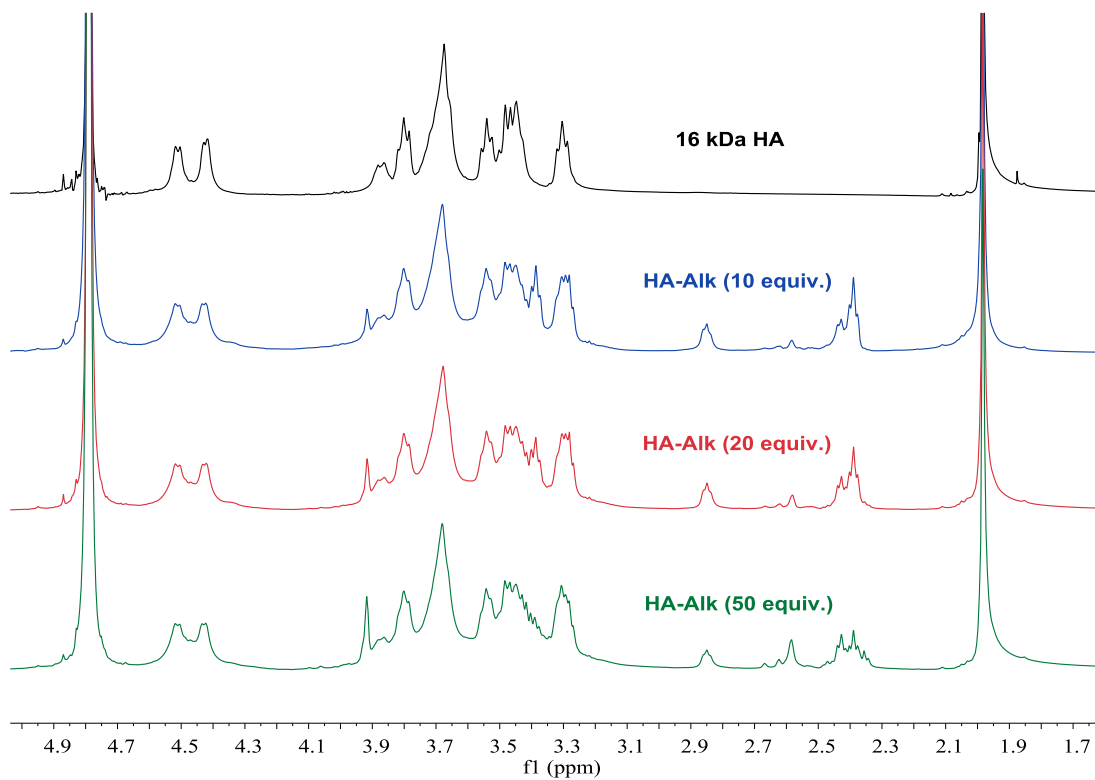


Figure 56:  $^1\text{H}$  NMR spectra of various HA-Alk batches.

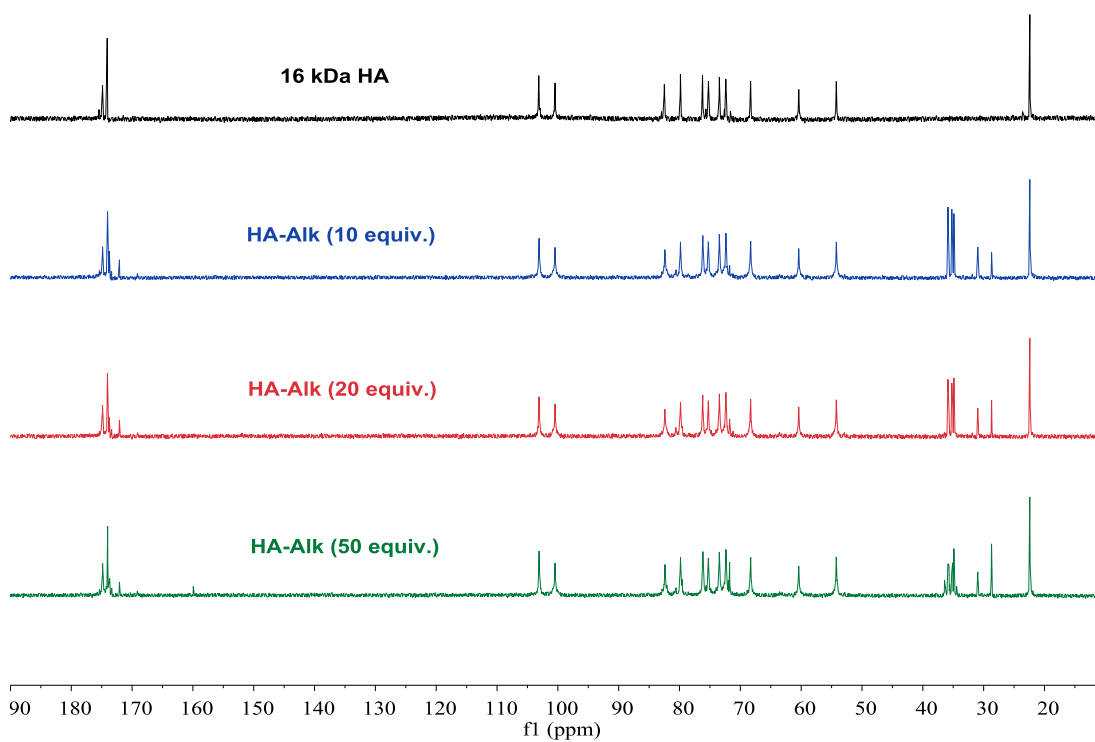


Figure 57:  $^1\text{H}$ -decoupled  $^{13}\text{C}$  NMR spectra of various HA-Alk batches.

Generally, reaction temperature and time showed less of an effect than stoichiometric ratios of the reactants, but provided a roadmap to producing HA-Dex conjugates with varying degrees of substitution. <sup>1</sup>H NMR was used as a secondary measure to quantitatively assess Dex conjugation on two larger scale batches used for subsequent studies, showing an average of 2.0 and 4.5 Dex

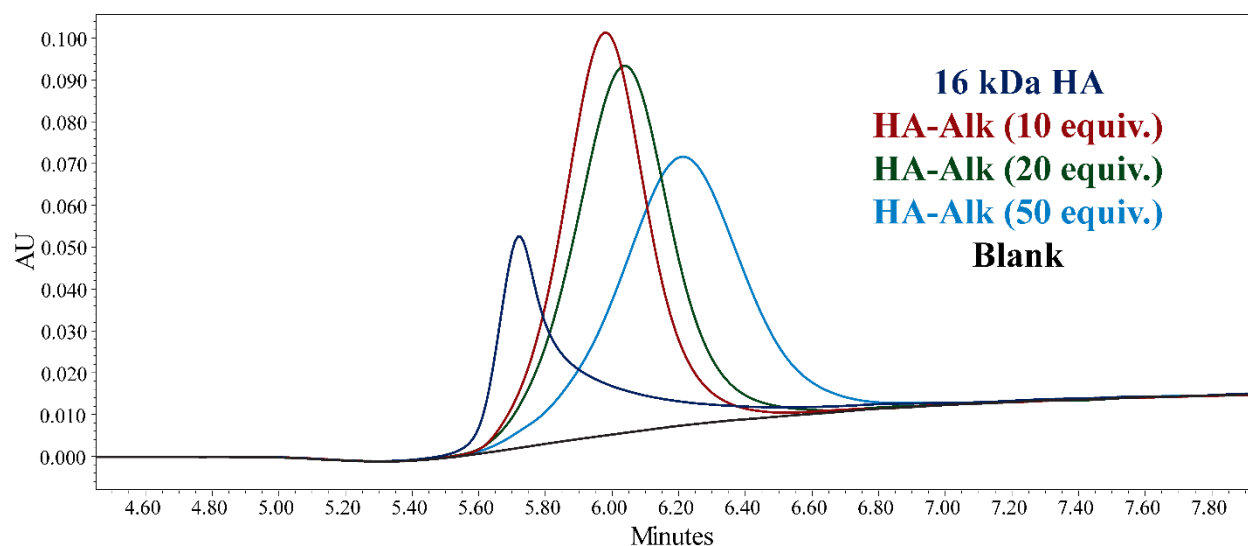


Figure 58: RP-HPLC analysis of HA-Alk batches with varying degrees of stoichiometric equivalents used in the reaction.

Table 3: Loading optimization studies of HA-Dex.

Reaction Temp	Time	Stoichiometric Equivalents <sup>1</sup>							
		10	5	10	20	40	20	40	40
Ambient	4 hrs	3.1	5	3.8	20	6.1	20	9.0	40
	24 hrs	3.0	5	7.3	20	6.3	20	13.9	40
37°C	4 hrs	2.9	5	4.5	20	6.2	20	9.0	40
	24 hrs	3.1	5	10.4	20	6.3	20	11.0	40
50°C	4 hrs	2.9	5	4.8	20	6.2	20	9.8	40
	24 hrs	3.3	5	6.6	20	6.7	20	12.2	40

<sup>1</sup>Stoichiometric equivalent values in red refer to propargylamine equivalents used to functionalize HA, and values in blue refer to Dex-N<sub>3</sub> equivalents used (relative to HA-Alk).



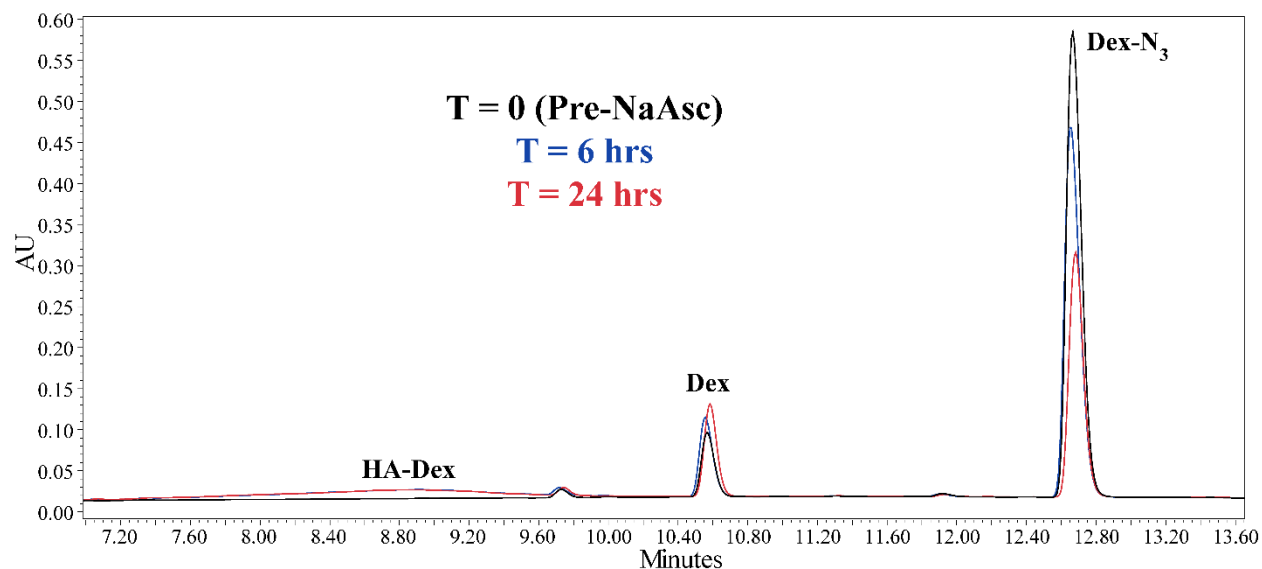


Figure 59: Representative RP-HPLC analysis employed for optimization of reaction conditions.

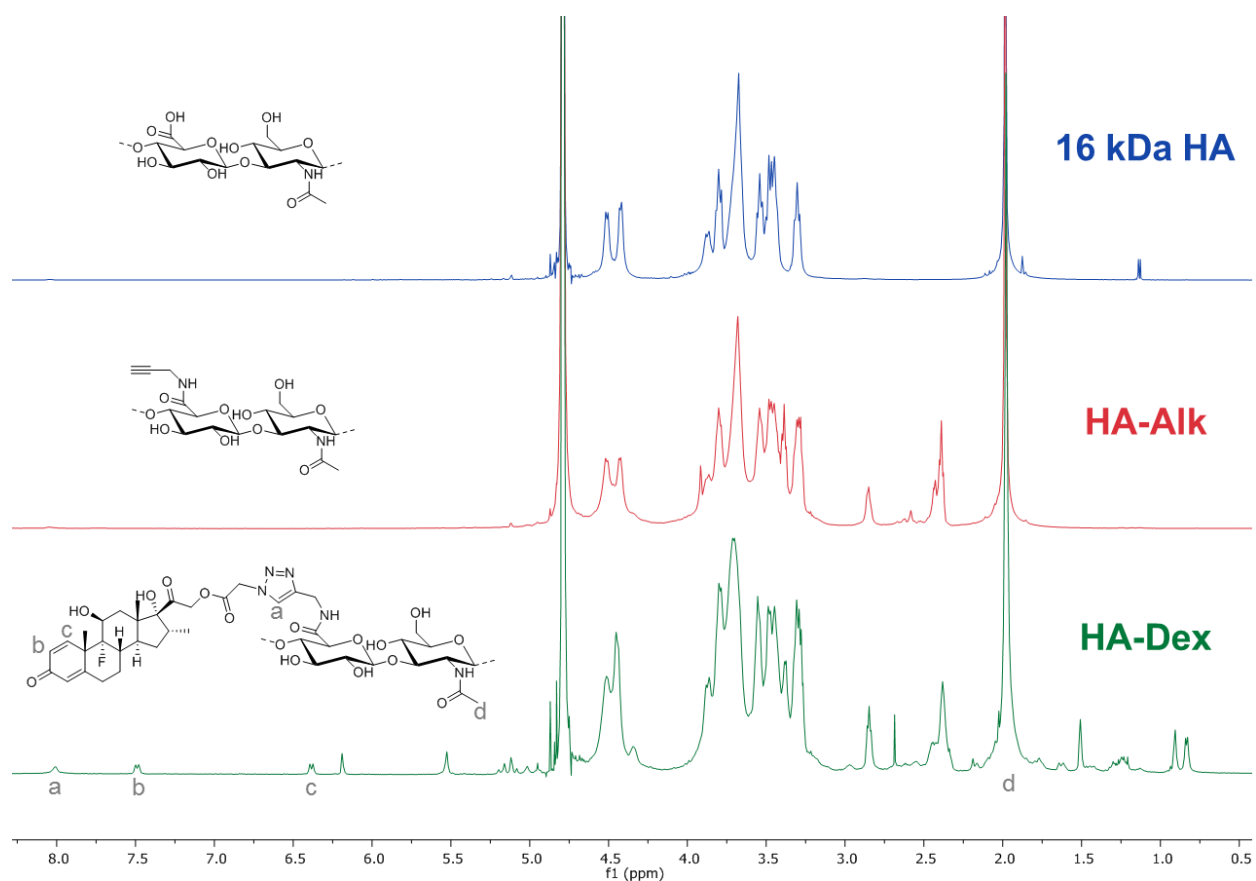


Figure 60:  $^1\text{H}$  NMR spectra of starting HA, alkyne-functionalized HA, and dexamethasone-conjugated HA. Resonances highlighted (a-d) were used for quantitative determination of dexamethasone conjugation.

per backbone in these batches. Additionally, the presence of a distinct resonance ( $\delta = 8.0$  ppm) was observed in the  $^1\text{H}$  NMR spectrum (Figure 60) corresponding to the proton on the newly-formed 5-membered ring, with the disappearance of the terminal alkyne resonance previously observed by HSQC NMR (Figure 61), confirming the success of conjugation. RP-HPLC showed dialysis was an effective method at removing unreacted Dex- $\text{N}_3$  and other reaction additives.

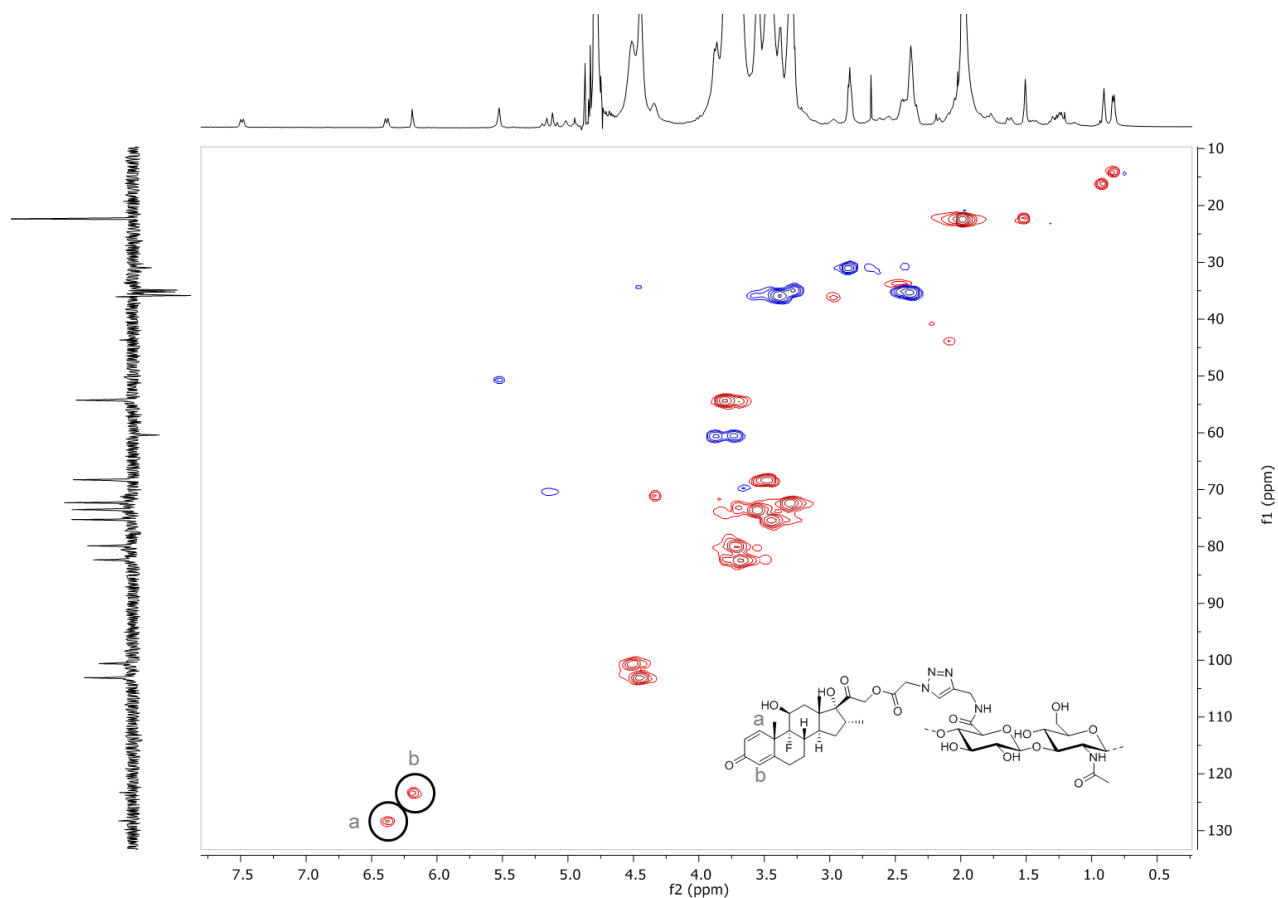


Figure 61: HSQC NMR spectrum for HA-Dex collected in  $\text{D}_2\text{O}$ , where the x-axis is a standard  $^1\text{H}$  spectrum, and the y-axis is a  $^{13}\text{C}$  DEPT-135 spectrum.

### 5.3.3. Drug release kinetics

Release studies in PBS buffer at 37°C conducted on a 2.0 Dex per HA backbone sample showed an extended release of Dex from the polymeric system over the course of approximately 24 hours (Figure 62). A total release of 201 µg Dex from the 10 mg/mL solution was observed, thus corroborating the integration values determined by <sup>1</sup>H NMR. The release rate may be further prolonged by translating to a polymeric system of higher molecular weight than the 16 kDa HA used in these studies in addition to performing release studies in more concentrated solutions. Further evidence (Section 3.3.4, **Error! Reference source not found.**) also suggested a strong correlation between release of Dex from the parent Dex-N<sub>3</sub> in the presence of phosphate buffer, which may be acting as a nucleophile to catalyze ester hydrolysis.

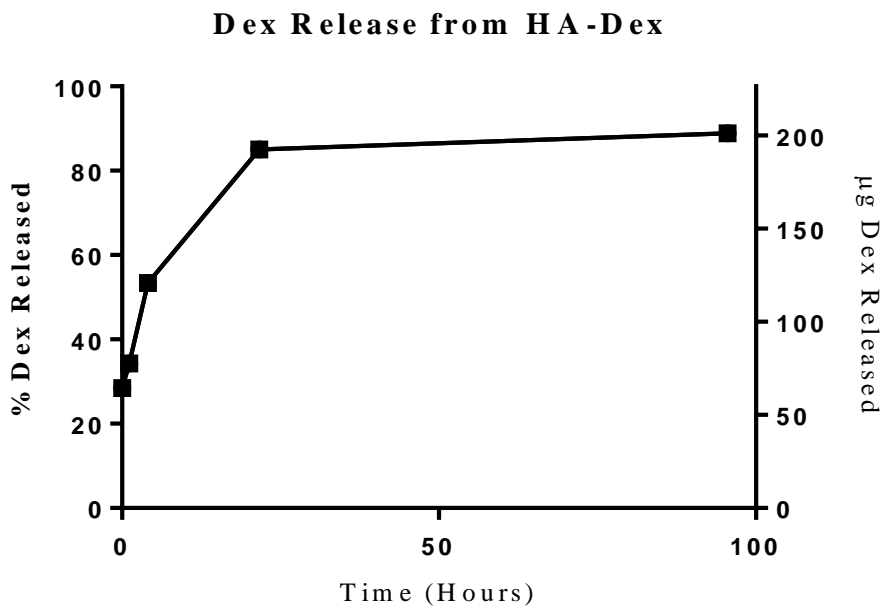


Figure 62: Release study of Dex from an HA-Dex sample containing an average of 2 Dex per HA backbone. Study conducted at 37°C in PBS buffer, at a concentration of 10 mg/mL HA-Dex.

Recent research has indicated the need for an alternative therapy in cases where HA and Dex are co-administered. Spitzer *et al.* presented the *in vitro* efficacy of a physical mixture of HA

and Dex, which released Dex for 24 hours.<sup>218</sup> Kugelberg *et al.* reported the *in vivo* use of a Dex-coated intraocular lens with post-operative sampling of the aqueous humor over 28 days. White blood cell counts and total protein levels were significantly reduced on days 1 and 3 after surgery.<sup>219</sup> Fiorica *et al.* recently presented the development of an HA-Dex hydrogel where a  $\beta$ -cyclodextrin was covalently bound to the HA backbone, enabling the formation of an inclusion complex to form with the hydrophobic Dex.<sup>220</sup> This resulted in rapid dissolution of Dex from the inclusion complex, with approximately 60% of the drug released after 24 hours.

Polymer conjugates of Dex have also been presented previously for other therapeutic indications. Liu *et al.* presented a *N*-(2-hydroxypropyl)methacrylamide (HMPA) conjugate of dexamethasone, employing a hydrazone linkage.<sup>211</sup> This conjugate showed prolonged release in pH 5.0 acetate buffer, with approximately 15% released after 14 days. Importantly, this conjugate did not display the same sensitivity to pH 7.4 phosphate buffer as was observed with HA-Dex, showing minimal release (~1%) over the same time period. Zacchigna *et al.* showed a similar conjugation strategy as with HA-Dex, by employing a succinic anhydride linker at the C<sub>21</sub> position of Dex conjugated to a 10 kDa mPEG polymer.<sup>215</sup> Interestingly, the release rate was significantly slower, with approximately 3.5% released after 24 hours in pH 7.4 phosphate buffer. The release rate was greatly enhanced, however, in the presence of porcine esterase, with approximately 45% release over the same time period. Similarly, Karkovicova *et al.* presented a Dex conjugate to HMPA, employing a heterobifunctional linker with hydrazone and ester linkages between Dex and the polymer.<sup>212</sup> The drug release studies were able to differentiate free Dex release from Dex with linker, showing approximately 20% ester cleavage over 24 hours in pH 7.4 phosphate buffer.

When considering previous reports of polymer-Dex conjugates in the context of the HA-Dex release rates observed here, there is likely a significant electronic contribution from the

adjacent triazole ring which may be accelerating the hydrolysis of the ester in the presence of phosphate buffers. The electronic properties of the triazole ring are well studied,<sup>221</sup> and the potential for modifying release rates are significant. Simply reversing the “polarity” of the components, by installing the equivalent alkyne linker on Dex and an azide linker on HA, the dipole moment reverses and the release rate may be prolonged. Similarly, by installing electron donating or withdrawing substituents at the positions  $\alpha$  to the triazole ring, the electrophilic nature of the ester carbonyl will be altered and yield a modified release rate for the Dex. Both of these approaches may allow for fine tuning of Dex release rates from polymer.

#### **5.4. Conclusions**

The emergence of ophthalmic viscoelastic devices (OVDs) used during cataract surgery have significantly improved patient outcomes with respect to minimizing endothelial cell loss. Post-operative administration of anti-inflammatory agents such as Dex have reduced the risk of inflammation, but suffer from the requirement of frequent administration, which can decrease patient compliance. The recent development of co-formulations of HA and Dex have been explored. Here, we have presented a novel azide-functionalized Dex derivative suitable for covalent conjugation to alkyne-functionalized HA, to optimize drug loading. The release rates of Dex in PBS buffer show release over the course of 24 hours in PBS buffer, which could be further modulated as desired by modifying the starting the HA molecular weight or solution concentration. Additional tuning of release rates may also be possible through modifications to the linker system installed on Dex prior to conjugation, as a consequence of the significant electronic contributions of the triazole ring.

**CHAPTER 6:**  
**CONCLUSIONS AND FUTURE DIRECTIONS**

## **CHAPTER 6: CONCLUSIONS AND FUTURE DIRECTIONS**

### **6.1. Introduction**

The construction of therapeutic bioconjugates has become an increasingly popular field, accompanied by a unique set of applications and challenges. Bioconjugates enable the combination of functionalities between multiple different molecules, and permit fine tuning of therapeutic action. Throughout this dissertation, a number of key learnings were uncovered in working with molecules with a wide range of chemical properties, summarized here in Section 6.2. Through these findings, Section 6.3 seeks to present areas of expansion with respect to different disease indications, in addition to alternate uses to repurpose molecules (Section 6.3.3) described in this dissertation.

### **6.2. Summary of dissertation chapters**

Chapter 1 presented a background and overview of the dissertation, providing the groundwork for the construction of novel bioconjugates for the treatment of antigen-specific autoimmune disorders. Autoimmune disorders affect many individuals worldwide, and are unique with respect to heterogeneous clinical manifestation and available treatment approaches. An additional complication lies in the complexity of the immune system, with a multitude of cells and biomolecules involved in disease propagation. The primary drawback to currently approved autoimmune therapies is the lack of antigen specificity, which leads to decreased efficacy in affected patient populations. This has driven the development of antigen-specific immunotherapies (ASIT) to promote improved efficacy and safety profiles for patients. By applying the framework of antibody-drug conjugates (ADCs) for targeted delivery, and leveraging the wealth of literature

surrounding ADC development, ASIT employing covalent modification to the antigen can provide a promising alternative to the available treatment options.

Chapter 2 outlined the chemistry employed throughout the dissertation, primarily focused on the azide-alkyne cycloaddition reaction, with subsequent chemistries appropriate for installation of these moieties on molecules with a range of chemical properties. In both compiling this review of the literature and presenting findings from the chemical synthesis portions of this research, this chapter highlighted the common challenges and often overlooked aspects of bioconjugate construction. When combining molecules with drastically different chemical properties, complications encountered during the development of synthetic routes and analytical methods are difficult to predict, but primarily center around solubility, stability, and reactive site availability. Additionally, properties of the final conjugate may affect key pharmacokinetic parameters, such as clearance and biodistribution, though often overcome through optimization of the structure of the bioconjugate. A fundamental understanding of key molecular properties can assist in circumnavigating downstream complications in the design and early development stages.

Chapter 3 presented the development of a novel therapeutic class for the treatment of antigen-specific autoimmune disorders, antigen-drug conjugates (AgDCs). Stemming from the previous success of ADCs, AgDCs employ the specificity of the antigen for diseased cell populations, combined with the potency of a small molecule immunomodulator, to provide an ASIT co-delivery strategy for the treatment of experimental autoimmune encephalomyelitis (EAE), a murine model of multiple sclerosis (MS). *In vivo* treatment with antigen-linked dexamethasone (PLP<sub>139-151</sub>-Dex) showed a significant and complete suppression of EAE disease symptoms when compared to the control group. This work provides the basis for expansion of this concept to include other drug molecules with different mechanisms of action, such as the



cytotoxins monomethyl auristatin E (MMAE), mertansine (DM1), and doxorubicin. The synthesis and characterization of these AgDCs is complete for potential screening in future studies. Importantly, AgDCs are a platform approach with potential to be adapted into other antigen-specific autoimmune disorders across the disease landscape (Section 6.3.1.2).

Chapter 4 built off previous research in the construction of Soluble Antigen Arrays (SAGAs), which are composed of autoantigen and cell adhesion inhibitor delivered on a polymeric support. Studies suggest SAGAs mechanism of action is involved with receptor clustering, thereby inhibiting the co-stimulatory activation required to propagate an immune response. Initial SAGA development focused on the utilization of an acid-sensitive oxime bond between the peptides and the polymer supports, and this work expanded this treatment approach by replacing the hydrolyzable bond with a stable covalent linkage, termed ‘click’ SAGAs (cSAGAs). *In vivo* results in the EAE model showed a significant improvement in efficacy of cSAGAs at 25% of the dose of SAGAs, providing an alternative to AgDCs that target a different step in the immunological cascade of reactions. While the *in vivo* results for cSAGAs are promising, further optimization of key parameters thought to be driving efficacy could provide improved therapeutic outcomes (Section 6.3.2).

Chapter 5 focused on the development of a monotherapeutic alternative to alleviate common problems observed in cataract surgery. Viscoelastic substances are solutions of high molecular weight polymers commonly employed intraoperatively to limit endothelial cell loss (ECL), which ultimately results in reduced patient outcomes. Associated with the use of viscoelastic substances is the need to manage postoperative inflammation through anti-inflammatory compounds such as dexamethasone (Dex), dosed frequently and for extended periods of time. This chapter presented the development of a bioconjugate containing covalently

linked Dex to the viscoelastic substance as an extended release approach to circumvent the need for co-therapy, which can suffer from reduced patient compliance.

## 6.3. Future directions

### 6.3.1. Continuing AgDC development

#### 6.3.1.1. Tuning MS AgDCs to alter drug release or therapeutic potency

Considering the *in vivo* success in mice presented in Chapter 3, there is still a possibility of tuning the drug release properties or therapeutic potency of the molecules. Drug release influenced by installation of electron withdrawing or electron donating groups in the R position provide the potential for tuning as desired (Figure 63).

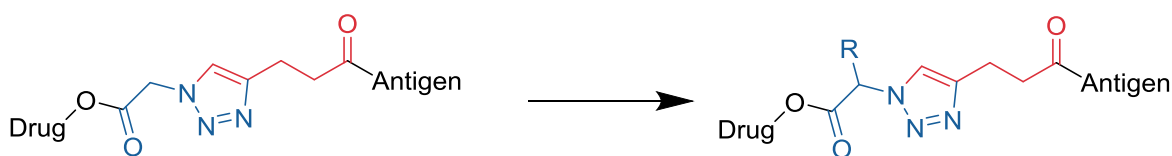


Figure 63: Potential for modulating drug release rate through installation of EWD or EDG at R.

Kuchroo *et al.* presented a study focused on identifying key residues in the PLP<sub>139-151</sub> peptide epitope sequence which were critical for binding by observing the effect of single amino acid substitutions on T cell proliferation.<sup>99</sup> Given the relatively short linker installed in the PLP<sub>139-151</sub>-Dex conjugate, using a slightly longer PEGylated linker between the antigen and drug can potentially provide additional flexibility and spacing to increase the binding affinity of the conjugate for the receptor. Additionally, modifying the peptide antigen to epitopes derived from other myelin sheath proteins known to cause disease,<sup>7</sup> such as myelin basic protein (MBP) or myelin oligodendrocyte glycoprotein (MOG) could potentially target different immune cell

populations and provide a response which is different than that based on the PLP autoantigen. Finally, utilizing cytotoxic drugs linked to the peptide, such as MMAE, DM1, or doxorubicin, have the potential to provide apoptotic cellular response as opposed to the tolerogenic response proposed with dexamethasone.

### 6.3.1.2. Adaption to other therapeutic areas

The AgDC platform approach has the potential for translation to a significant number of antigen-specific autoimmune disorders with known disease-causing autoantigens. Table 4 provides an example of the potential translation of AgDCs across the therapeutic landscape.

Table 4: Potential antigen-specific autoimmune disorders suitable for the AgDC platform

<b>Autoimmune Disease</b>	<b>Antigen</b>
Multiple Sclerosis	PLP, MBP, MOG
Type 1 Diabetes	Insulin, IA-2, GAD-65
Celiacs Disease	TG2
Graves Disease	TSHR
Myasthenia Gravis	nAChR, MuSK, LRP4
Hashimotos Encephalomyelitis	DDAHI, AKIPIAI
Neuromyelitis Optica	AQP4, MOG
Rheumatoid Arthritis	Collagen, Aggrecan

Ideally, full length protein autoantigen would be the most suitable target for the AgDC platform, but as is the case with MS, antigenic peptide epitopes are also capable of triggering an immune response.<sup>7</sup> Full length protein would follow the same internalization pathway via receptor-mediated endocytosis, then following processing by the antigen presenting cell (APC), the peptide

epitope is presented on the surface in the major histocompatibility complex (MHC class II) for subsequent T cell activation.<sup>1</sup> It is unknown whether peptide antigens would follow the same APC internalization and presentation pathway, but given that they are capable of inducing an immune response, binding in the MHC class II-T cell receptor pocket is likely. Further studies employing both peptide and full length protein autoantigens equipped with a probe molecule such as a fluorophore or radiolabel would permit tracking the cellular localization to elucidate this mechanism. Efforts to express and purify full length proteolipid protein (PLP) autoantigen used in this work were unsuccessful due to solubility issues stemming from the transmembrane  $\alpha$ -helical domains. Current efforts by other researchers in the group focus on adapting the AgDC platform to other antigen-specific autoimmune disorders.

### ***6.3.2. Continuing SAgA development***

Given the polymeric nature and accompanying heterogeneity of the therapeutic platform, (c)SAgAs have a number of key variables appropriate for tuning their activities. Peptide valency, or the number of peptides displayed on a single polymer backbone, is a critical factor in antigen binding to T cells.<sup>222</sup> Altering antigen valency through modification of reaction conditions has the potential to alter the observed immune response. Similarly, the implications of size on biodistribution of SAgA molecules has been studied,<sup>29</sup> and using polymer supports with different molecular weights could provide a varied immune response. Additionally, screening the effect of administration route on biodistribution and efficacy of cSAgA treatments, probably aided by incorporation of a tracer molecule prior to in vivo treatment, could assist in better understanding the molecular mechanisms behind increased efficacy of cSAgAs over SAgAs. Finally, as with the AgDC platform, SAgAs also have the potential for direct translation to other therapeutic

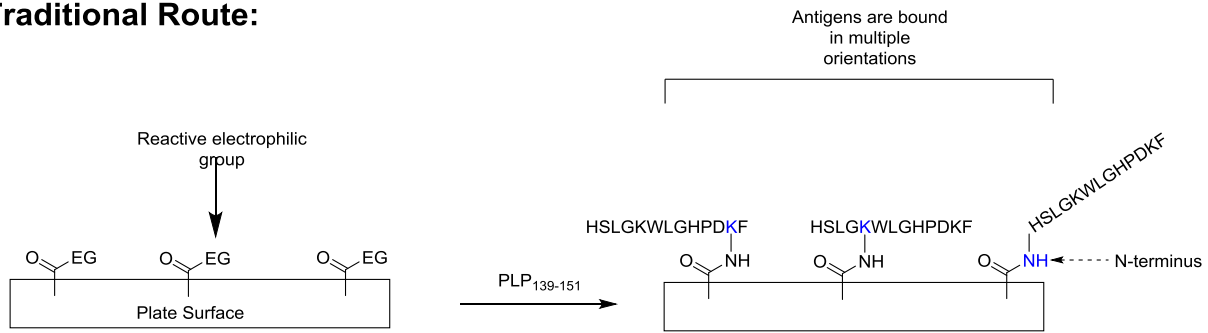
indications by modifying the sequence of the attached peptides for those applicable to another antigen-specific autoimmune disorder (Table 4). This work is currently underway on the cSAgA platform by other researchers in the group.

### ***6.3.3. Diagnostic assays: capturing antigen-specific cells or antibodies***

One of the benefits to employing click chemistry for bioconjugation applications is the large toolbox of commercial azide- and alkyne-functionalized materials available to the researcher, in addition to the significant literature precedence of the reaction across many disciplines. This section focuses on applications to repurpose molecules synthesized in this dissertation, and to present concepts to further elucidate mechanisms involved in immune responses.

Numerous groups have described the functionalization of surfaces with azide or alkyne (terminal and strained) moieties,<sup>50, 92, 223-224</sup> presenting a method of attaching the peptide antigens described here to a solid surface. Similar in concept to a sandwich ELISA assay, quantification of antigen-specific cells or autoantibodies in a mixed cell population such as those isolated from EAE mice could permit a better understanding of the cell types and biomolecules that are contributing to an immune response. Commercially available surface functionalized plates typically involve ‘proprietary’ electrophilic groups similar to the NHS ester (Section 2.3) to non-specifically attach antigens via lysine residues or the N-terminus. By using a slight modification to this procedure, antigen attachment via click chemistry ensures linkage occurs at the N-terminus, with less reduction in binding from improper orientation (Figure 64).

## Traditional Route:



## Click Route:

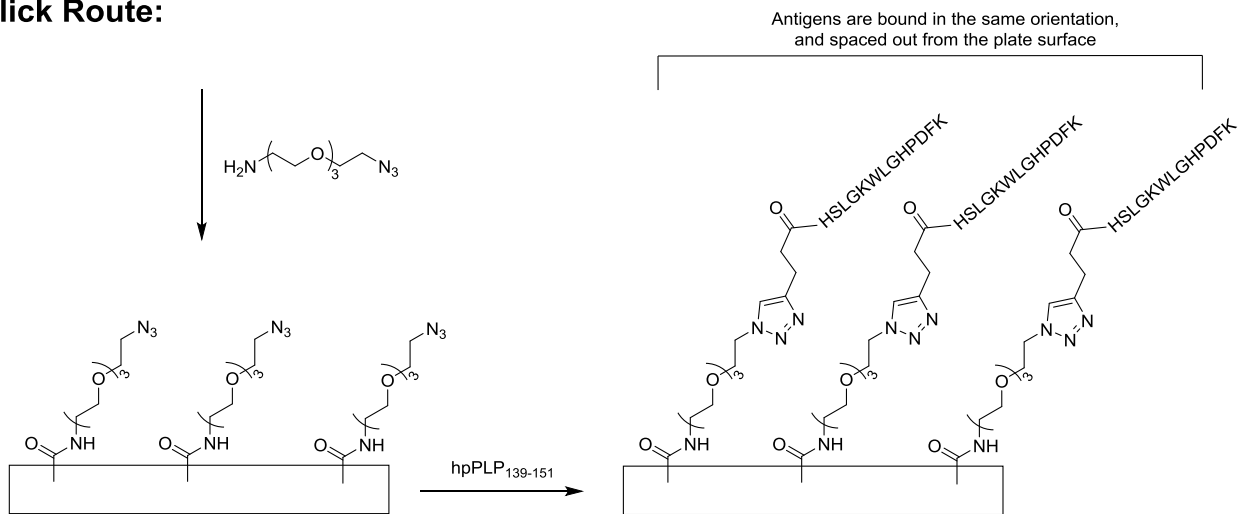


Figure 64: Overview of peptide attachment to functionalized plates, with an alternative route via click chemistry which ensures proper orientation and adequate spacing of the peptide antigen from the plate surface.

Perhaps more intriguing is a small modification to the strained alkyne approach, by synthesizing a photolabile variant which reveals the active functionality under exposure to 350 nm light (Figure 65).<sup>49</sup> This permits the site specific conjugation of the biomolecule following release of the caging group. Applying this concept to functionalized plates, the potential for a high throughput method of assaying antigen-specificity in mixed cell populations exists.

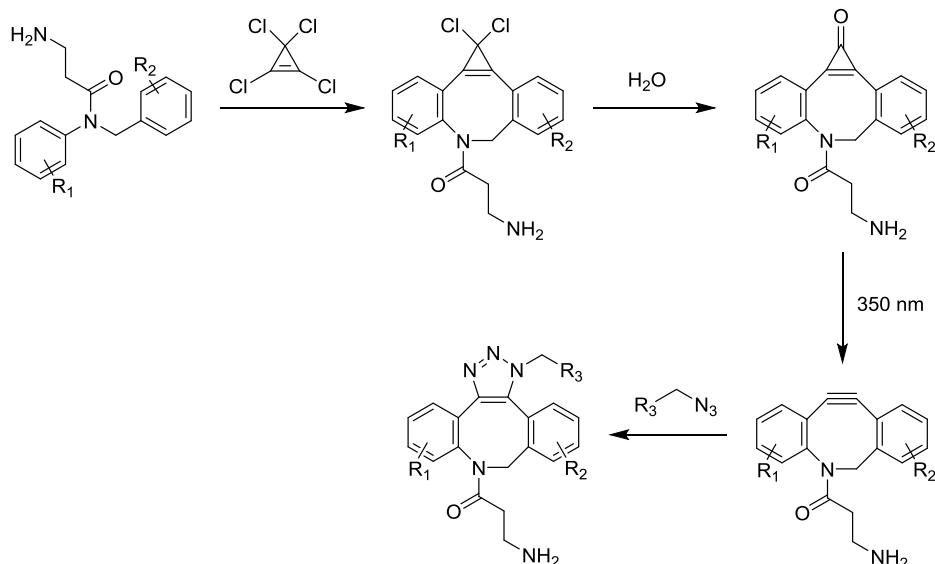


Figure 65: Synthesis of a photolabile variant of the strained alkyne, presented by Arumugam et al.<sup>49</sup>

The implementation of magnetic beads to support biomolecules for catalysis and isolation has gained recent traction, and azide- or alkyne-functionalized beads are both commercially available and presented in the literature.<sup>225</sup> After attachment of the peptide autoantigen to the magnetic bead, antigen-specific cells or autoantibodies can be isolated after mixing with a biological sample and applying a magnetic field. While techniques like flow cytometry are able to identify these antigen-specific cell populations, magnetic beads provide an attractive method of collecting these cell populations or antibodies implicated in disease for further studies.

#### 6.4. Conclusions

The work presented both in this section and throughout the dissertation provides a framework for the continued development of novel treatment approaches for antigen-specific autoimmune disorders. Utilizing the power of the azide-alkyne cycloaddition reaction and its variants, the creation of a toolbox of functionalized molecules has enabled facile access to

construction of biomolecule and materials for a variety of uses. It is hoped that further elucidation of mechanisms and tuning of molecular properties throughout these platforms leads to treatment options with improved safety profiles and therapeutic outcomes for patients affected by autoimmune disease.



## REFERENCES

1. Murphy, K. M., *Janeway's Immunobiology*. 8th ed.; Garland Science: 2012.
2. Perl, A., *Autoimmunity Methods and Protocols*. 2nd ed.; Humana Press: 2012.
3. Compston, A. C., A., Multiple Sclerosis. *Lancet* **2002**, 359, 1221-1231.
4. Dendrou, C. A.; Fugger, L.; Friese, M. A., Immunopathology of multiple sclerosis. *Nat Rev Immunol* **2015**, 15 (9), 545-58.
5. Karussis, D., The diagnosis of multiple sclerosis and the various related demyelinating syndromes: a critical review. *J Autoimmun* **2014**, 48-49, 134-42.
6. Kamm, C.; Zettl, U. K., Autoimmune disorders affecting both the central and peripheral nervous system. *Autoimmun Rev* **2012**, 11 (3), 196-202.
7. Miller, S. D.; Karpus, W. J., Experimental autoimmune encephalomyelitis in the mouse. *Curr Protoc Immunol* **2007**, Chapter 15, Unit 15 1.
8. Ransohoff, R. M., Animal models of multiple sclerosis: the good, the bad and the bottom line. *Nat Neurosci* **2012**, 15 (8), 1074-7.
9. Cross, A. H.; Naismith, R. T., Established and novel disease-modifying treatments in multiple sclerosis. *J Intern Med* **2014**, 275 (4), 350-63.
10. Carrithers, M. D., Update on disease-modifying treatments for multiple sclerosis. *Clin Ther* **2014**, 36 (12), 1938-45.
11. Northrup, L.; Christopher, M. A.; Sullivan, B. P.; Berkland, C., Combining antigen and immunomodulators: Emerging trends in antigen-specific immunotherapy for autoimmunity. *Adv Drug Deliv Rev* **2016**, 98, 86-98.
12. Pilz, G.; Wipfler, P.; Ladurner, G.; Kraus, J., Modern multiple sclerosis treatment - what is approved, what is on the horizon. *Drug Discov Today* **2008**, 13 (23-24), 1013-25.
13. Aharoni, R., Immunomodulation neuroprotection and remyelination - the fundamental therapeutic effects of glatiramer acetate: a critical review. *J Autoimmun* **2014**, 54, 81-92.
14. Larche, M.; Akdis, C. A.; Valenta, R., Immunological mechanisms of allergen-specific immunotherapy. *Nat Rev Immunol* **2006**, 6 (10), 761-71.
15. Zheng, G. Z., S.; Geng, Y.; Munirathinam, G.; Cha, I.; Reardon, C.; Getz, G.; Rooijen, N.; Kang, Y.; Wang, B.; Chen, A., Dexamethasone promotes tolerance in vivo by enriching CD11c/CD40lo tolerogenic macrophages. *Eur. J. Immunol.* **2013**, 43, 219-227.
16. Unger, W. W.; Laban, S.; Kleijwegt, F. S.; van der Slik, A. R.; Roep, B. O., Induction of Treg by monocyte-derived DC modulated by vitamin D3 or dexamethasone: differential role for PD-L1. *Eur J Immunol* **2009**, 39 (11), 3147-59.
17. Kontos, S.; Grimm, A. J.; Hubbell, J. A., Engineering antigen-specific immunological tolerance. *Curr Opin Immunol* **2015**, 35, 80-8.
18. Merten, H.; Brandl, F.; Pluckthun, A.; Zangemeister-Wittke, U., Antibody-Drug Conjugates for Tumor Targeting—Novel Conjugation Chemistries and the Promise of non-IgG Binding Proteins. *Bioconjug Chem* **2015**, 26 (11), 2176-85.
19. Beck, A.; Goetsch, L.; Dumontet, C.; Corvaia, N., Strategies and challenges for the next generation of antibody-drug conjugates. *Nat Rev Drug Discov* **2017**.
20. Kline, T.; Steiner, A. R.; Penta, K.; Sato, A. K.; Hallam, T. J.; Yin, G., Methods to Make Homogenous Antibody Drug Conjugates. *Pharm Res* **2015**, 32 (11), 3480-93.
21. Teicher, B. A., Antibody drug conjugates. *Curr Opin Oncol* **2014**, 26 (5), 476-83.
22. Agarwal, P.; Bertozzi, C. R., Site-specific antibody-drug conjugates: the nexus of bioorthogonal chemistry, protein engineering, and drug development. *Bioconjug Chem* **2015**, 26 (2), 176-92.
23. Chari, R. V.; Miller, M. L.; Widdison, W. C., Antibody-drug conjugates: an emerging concept in cancer therapy. *Angew Chem Int Ed Engl* **2014**, 53 (15), 3796-827.

24. Gordon, M. R.; Canakci, M.; Li, L.; Zhuang, J.; Osborne, B.; Thayumanavan, S., Field Guide to Challenges and Opportunities in Antibody-Drug Conjugates for Chemists. *Bioconjug Chem* **2015**, *26* (11), 2198-215.
25. McCombs, J. R.; Owen, S. C., Antibody drug conjugates: design and selection of linker, payload and conjugation chemistry. *AAPS J* **2015**, *17* (2), 339-51.
26. Baron, J. M.; Boster, B. L.; Barnett, C. M., Ado-trastuzumab emtansine (T-DM1): a novel antibody-drug conjugate for the treatment of HER2-positive metastatic breast cancer. *J Oncol Pharm Pract* **2015**, *21* (2), 132-42.
27. Garnock-Jones, K. P., Brentuximab vedotin: a review of its use in patients with hodgkin lymphoma and systemic anaplastic large cell lymphoma following previous treatment failure. *Drugs* **2013**, *73* (4), 371-81.
28. Sestak, J. O.; Sullivan, B. P.; Thati, S.; Northrup, L.; Hartwell, B.; Antunez, L.; Forrest, M. L.; Vines, C. M.; Siahaan, T. J.; Berkland, C., Codelivery of antigen and an immune cell adhesion inhibitor is necessary for efficacy of soluble antigen arrays in experimental autoimmune encephalomyelitis. *Mol Ther Methods Clin Dev* **2014**, *1*, 14008.
29. Sestak, J. O.; Fakhari, A.; Badawi, A. H.; Siahaan, T. J.; Berkland, C., Structure, size, and solubility of antigen arrays determines efficacy in experimental autoimmune encephalomyelitis. *AAPS J* **2014**, *16* (6), 1185-93.
30. Hartwell, B. L.; Martinez-Becerra, F. J.; Chen, J.; Shinogle, H.; Sarnowski, M.; Moore, D. S.; Berkland, C., Antigen-Specific Binding of Multivalent Soluble Antigen Arrays Induces Receptor Clustering and Impedes B Cell Receptor Mediated Signaling. *Biomacromolecules* **2016**, *17* (3), 710-22.
31. Hartwell, B. L.; Pickens, C. J.; Leon, M.; Berkland, C., Multivalent Soluble Antigen Arrays Exhibit High Avidity Binding and Modulation of B Cell Receptor-Mediated Signaling to Drive Efficacy against Experimental Autoimmune Encephalomyelitis. *Biomacromolecules* **2017**.
32. Hein, J. E.; Fokin, V. V., Copper-catalyzed azide-alkyne cycloaddition (CuAAC) and beyond: new reactivity of copper(I) acetylides. *Chem Soc Rev* **2010**, *39* (4), 1302-15.
33. Tang, W.; Becker, M. L., "Click" reactions: a versatile toolbox for the synthesis of peptide-conjugates. *Chem Soc Rev* **2014**, *43* (20), 7013-39.
34. Presolski, S. I.; Hong, V. P.; Finn, M. G., Copper-Catalyzed Azide-Alkyne Click Chemistry for Bioconjugation. *Curr Protoc Chem Biol* **2011**, *3* (4), 153-162.
35. Huisgen, R., 1,3-Dipolar Cycloadditions: Past and Future. *Ang. Chem. Int. Ed.* **1963**, *2* (10), 565-632.
36. Rostovtsev, V. G., L.; Folkin, V.; Sharpless, B., A Stepwise Huisgen Cycloaddition Process: Copper-Catalyzed Regioselective Ligation of Azides and Terminal Alkynes. *Angew. Chem.* **2002**, *114* (14), 2708-2711.
37. Tornøe, C. C., C.; Meldal, M., Peptidotriazoles on Solid Phase: [1,2,3]-Triazoles by Regiospecific Copper(I)-Catalyzed 1,3-Dipolar Cycloadditions of Terminal Alkynes to Azides. *J. Org. Chem.* **2002**, *67*, 3057-3064.
38. Kirchner, K. C., M.; Schmid, R.; Veiros, L., Mechanism for the Cyclotrimerization of Alkynes and Related Reactions Catalyzed by CpRuCl. *J. Am. Chem. Soc.* **2003**, *125*, 11721-11729.
39. Zhang, L. C., X.; Xue, P.; Sun, H.; Williams, I.; Sharpless, B.; Fokin, V.; Jia, G., Ruthenium-Catalyzed Cycloaddition of Alkynes and Organic Azides. *J. Am. Chem. Soc.* **2005**, *127*, 15998-15999.
40. Stanislav I. Presolski, V. H., So-Hye Cho, and M.G. Finn, Tailored Ligand Acceleration of the Cu-Catalyzed Azide-Alkyne Cycloaddition Reaction: Practical and Mechanistic Implications. *J. Am. Chem. Soc.* **2010**, *132*, 14570-14576.
41. Himo, F. L., T.; Hilgraf, R.; Rostovtsev, V.; Noodleman, L.; Sharpless, B.; Fokin, V., Copper(I)-Catalyzed Synthesis of Azoles. DFT Study Predicts Unprecedented Reactivity and Intermediates. *J. Am. Chem. Soc.* **2005**, *127*, 210-216.
42. Bock, V. D.; Hiemstra, H.; van Maarseveen, J. H., CuI-Catalyzed Alkyne-Azide "Click" Cycloadditions from a Mechanistic and Synthetic Perspective. *European Journal of Organic Chemistry* **2006**, *2006* (1), 51-68.

43. Lin, Y.; Wang, Q., Unlocking the 1,2,3-triazole ring using mechanical force. *Angew Chem Int Ed Engl* **2012**, *51* (9), 2006-7.
44. Hong, V.; Presolski, S. I.; Ma, C.; Finn, M. G., Analysis and optimization of copper-catalyzed azide-alkyne cycloaddition for bioconjugation. *Angew Chem Int Ed Engl* **2009**, *48* (52), 9879-83.
45. Besanceney-Webler, C.; Jiang, H.; Zheng, T.; Feng, L.; Soriano del Amo, D.; Wang, W.; Klivansky, L. M.; Marlow, F. L.; Liu, Y.; Wu, P., Increasing the efficacy of bioorthogonal click reactions for bioconjugation: a comparative study. *Angew Chem Int Ed Engl* **2011**, *50* (35), 8051-6.
46. Baskin, J. M.; Prescher, J. A.; Laughlin, S. T.; Agard, N. J.; Chang, P. V.; Miller, I. A.; Lo, A.; Codelli, J. A.; Bertozzi, C. R., Copper-free click chemistry for dynamic in vivo imaging. *Proc Natl Acad Sci U S A* **2007**, *104* (43), 16793-7.
47. Adronov, A.; Chadwick, R.; Van Gyzen, S.; Liogier, S., Scalable Synthesis of Strained Cyclooctyne Derivatives. *Synthesis* **2014**, *46* (05), 669-677.
48. Dommerholt, J.; Rutjes, F. P.; van Delft, F. L., Strain-Promoted 1,3-Dipolar Cycloaddition of Cycloalkynes and Organic Azides. *Top Curr Chem (J)* **2016**, *374* (2), 16.
49. Arumugam, S.; Orski, S. V.; Mbua, N. E.; McNitt, C.; Boons, G.-J.; Locklin, J.; Popik, V. V., Photo-click chemistry strategies for spatiotemporal control of metal-free ligation, labeling, and surface derivatization. *Pure and Applied Chemistry* **2013**, *85* (7).
50. Manova, R.; van Beek, T. A.; Zuilhof, H., Surface functionalization by strain-promoted alkyne-azide click reactions. *Angew Chem Int Ed Engl* **2011**, *50* (24), 5428-30.
51. Chan, A. O.; Ho, C. M.; Chong, H. C.; Leung, Y. C.; Huang, J. S.; Wong, M. K.; Che, C. M., Modification of N-terminal alpha-amino groups of peptides and proteins using ketenes. *J Am Chem Soc* **2012**, *134* (5), 2589-98.
52. Northrop, B. H.; Frayne, S. H.; Choudhary, U., Thiol-maleimide "click" chemistry: evaluating the influence of solvent, initiator, and thiol on the reaction mechanism, kinetics, and selectivity. *Polym. Chem.* **2015**, *6* (18), 3415-3430.
53. Mulder, G. E.; Kruijtzter, J. A.; Liskamp, R. M., A combinatorial approach toward smart libraries of discontinuous epitopes of HIV gp120 on a TAC synthetic scaffold. *Chem Commun (Camb)* **2012**, *48* (80), 10007-9.
54. Das, S.; Nag, A.; Liang, J.; Bunck, D. N.; Umeda, A.; Farrow, B.; Coppock, M. B.; Sarkes, D. A.; Finch, A. S.; Agnew, H. D.; Pitram, S.; Lai, B.; Yu, M. B.; Museth, A. K.; Deyle, K. M.; Lepe, B.; Rodriguez-Rivera, F. P.; McCarthy, A.; Alvarez-Villalonga, B.; Chen, A.; Heath, J.; Stratis-Cullum, D. N.; Heath, J. R., A General Synthetic Approach for Designing Epitope Targeted Macrocyclic Peptide Ligands. *Angew Chem Int Ed Engl* **2015**, *54* (45), 13219-24.
55. Empting, M.; Avrutina, O.; Meusinger, R.; Fabritz, S.; Reinwarth, M.; Biesalski, M.; Voigt, S.; Buntkowsky, G.; Kolmar, H., "Triazole bridge": disulfide-bond replacement by ruthenium-catalyzed formation of 1,5-disubstituted 1,2,3-triazoles. *Angew Chem Int Ed Engl* **2011**, *50* (22), 5207-11.
56. Nuhn, L.; Hartmann, S.; Palitzsch, B.; Gerlitzki, B.; Schmitt, E.; Zentel, R.; Kunz, H., Water-soluble polymers coupled with glycopeptide antigens and T-cell epitopes as potential antitumor vaccines. *Angew Chem Int Ed Engl* **2013**, *52* (40), 10652-6.
57. Gori, A.; Sola, L.; Gagni, P.; Bruni, G.; Liprino, M.; Peri, C.; Colombo, G.; Cretich, M.; Chiari, M., Screening Complex Biological Samples with Peptide Microarrays: The Favorable Impact of Probe Orientation via Chemoselective Immobilization Strategies on Clickable Polymeric Coatings. *Bioconjug Chem* **2016**, *27* (11), 2669-2677.
58. Maza, J. C.; McKenna, J. R.; Raliski, B. K.; Freedman, M. T.; Young, D. D., Synthesis and Incorporation of Unnatural Amino Acids To Probe and Optimize Protein Bioconjugations. *Bioconjug Chem* **2015**, *26* (9), 1884-9.
59. Kim, S.; Ko, W.; Sung, B. H.; Kim, S. C.; Lee, H. S., Direct protein-protein conjugation by genetically introducing bioorthogonal functional groups into proteins. *Bioorg Med Chem* **2016**, *24* (22), 5816-5822.
60. Zimmerman, E. S.; Heibeck, T. H.; Gill, A.; Li, X.; Murray, C. J.; Madlansacay, M. R.; Tran, C.; Uter, N. T.; Yin, G.; Rivers, P. J.; Yam, A. Y.; Wang, W. D.; Steiner, A. R.; Bajad, S. U.; Penta, K.; Yang,

- W.; Hallam, T. J.; Thanos, C. D.; Sato, A. K., Production of site-specific antibody-drug conjugates using optimized non-natural amino acids in a cell-free expression system. *Bioconjug Chem* **2014**, *25* (2), 351-61.
61. Palsuledesai, C. C.; Ochocki, J. D.; Kuhns, M. M.; Wang, Y. C.; Warmka, J. K.; Chernick, D. S.; Wattenberg, E. V.; Li, L.; Arriaga, E. A.; Distefano, M. D., Metabolic Labeling with an Alkyne-modified Isoprenoid Analog Facilitates Imaging and Quantification of the Prenylome in Cells. *ACS Chem Biol* **2016**, *11* (10), 2820-2828.
62. Neef, A. B.; Samain, F.; Luedtke, N. W., Metabolic labeling of DNA by purine analogues in vivo. *Chembiochem* **2012**, *13* (12), 1750-3.
63. Sawant, A. A.; Tanpure, A. A.; Mukherjee, P. P.; Athavale, S.; Kelkar, A.; Galande, S.; Srivatsan, S. G., A versatile toolbox for posttranscriptional chemical labeling and imaging of RNA. *Nucleic Acids Res* **2016**, *44* (2), e16.
64. Taskova, M.; Madsen, C. S.; Jensen, K. J.; Hansen, L. H.; Vester, B.; Astakhova, K., Antisense Oligonucleotides Internally Labeled with Peptides Show Improved Target Recognition and Stability to Enzymatic Degradation. *Bioconjug Chem* **2017**, *28* (3), 768-774.
65. Sivakumar, K. X., F.; Cash, B.; Long, S.; Barnhill, H.; Wang, Q., A Fluorogenic 1,3-Dipolar Cycloaddition Reaction of 3-Azidocoumarins and Acetylenes. *Org. Lett.* **2004**, *6* (24), 4603-4606.
66. Meyer, J. P.; Adumeau, P.; Lewis, J. S.; Zeglis, B. M., Click Chemistry and Radiochemistry: The First 10 Years. *Bioconjug Chem* **2016**, *27* (12), 2791-2807.
67. Li, S.; Cai, H.; He, J.; Chen, H.; Lam, S.; Cai, T.; Zhu, Z.; Bark, S. J.; Cai, C., Extent of the Oxidative Side Reactions to Peptides and Proteins During the CuAAC Reaction. *Bioconjug Chem* **2016**, *27* (10), 2315-2322.
68. van Geel, R.; Pruijn, G. J.; van Delft, F. L.; Boelens, W. C., Preventing thiol-yne addition improves the specificity of strain-promoted azide-alkyne cycloaddition. *Bioconjug Chem* **2012**, *23* (3), 392-8.
69. Fisher, S. A.; Baker, A. E. G.; Shoichet, M. S., Designing Peptide and Protein Modified Hydrogels: Selecting the Optimal Conjugation Strategy. *J Am Chem Soc* **2017**, *139* (22), 7416-7427.
70. Takahashi, A.; Suzuki, Y.; Suhara, T.; Omichi, K.; Shimizu, A.; Hasegawa, K.; Kokudo, N.; Ohta, S.; Ito, T., In situ cross-linkable hydrogel of hyaluronan produced via copper-free click chemistry. *Biomacromolecules* **2013**, *14* (10), 3581-8.
71. Huerta-Angeles, G.; Nemcova, M.; Prikopova, E.; Smejkalova, D.; Pravda, M.; Kucera, L.; Velebny, V., Reductive alkylation of hyaluronic acid for the synthesis of biocompatible hydrogels by click chemistry. *Carbohydr Polym* **2012**, *90* (4), 1704-11.
72. Hu, X.; Li, D.; Zhou, F.; Gao, C., Biological hydrogel synthesized from hyaluronic acid, gelatin and chondroitin sulfate by click chemistry. *Acta Biomater* **2011**, *7* (4), 1618-26.
73. Barrett, T. W., Solution Properties of Hyaluronic Acid. **1981**, *150*, 229-250.
74. Fakhari, A.; Berkland, C., Applications and emerging trends of hyaluronic acid in tissue engineering, as a dermal filler and in osteoarthritis treatment. *Acta Biomater* **2013**, *9* (7), 7081-92.
75. Wang, W.; Singh, S. K.; Li, N.; Toler, M. R.; King, K. R.; Nema, S., Immunogenicity of protein aggregates--concerns and realities. *Int J Pharm* **2012**, *431* (1-2), 1-11.
76. Ahn, Y. H.; Kang, H. G.; Lee, J. M.; Choi, H. J.; Ha, I. S.; Cheong, H. I., Development of antiriximab antibodies in children with nephrotic syndrome. *Pediatr Nephrol* **2014**, *29* (8), 1461-4.
77. Mazilu, D.; Opris, D.; Gainaru, C.; Iliuta, M.; Apetrei, N.; Luca, G.; Borangiu, A.; Gudu, T.; Peltea, A.; Groseanu, L.; Constantinescu, C.; Saulescu, I.; Bojinca, V.; Balanescu, A.; Predeteanu, D.; Ionescu, R., Monitoring drug and antidrug levels: a rational approach in rheumatoid arthritis patients treated with biologic agents who experience inadequate response while being on a stable biologic treatment. *Biomed Res Int* **2014**, *2014*, 702701.
78. Sun, X.; Ponte, J. F.; Yoder, N. C.; Laleau, R.; Coccia, J.; Lanieri, L.; Qiu, Q.; Wu, R.; Hong, E.; Bogalhas, M.; Wang, L.; Dong, L.; Setiady, Y.; Maloney, E. K.; Ab, O.; Zhang, X.; Pinkas, J.; Keating, T. A.; Chari, R.; Erickson, H. K.; Lambert, J. M., Effects of Drug-Antibody Ratio on Pharmacokinetics, Biodistribution, Efficacy, and Tolerability of Antibody-Maytansinoid Conjugates. *Bioconjug Chem* **2017**.

79. Lyon, R. P.; Bovee, T. D.; Doronina, S. O.; Burke, P. J.; Hunter, J. H.; Neff-LaFord, H. D.; Jonas, M.; Anderson, M. E.; Setter, J. R.; Senter, P. D., Reducing hydrophobicity of homogeneous antibody-drug conjugates improves pharmacokinetics and therapeutic index. *Nat Biotechnol* **2015**, *33* (7), 733-5.
80. Leonard, G. F., T.; Bates, S., The Role of ABC Transporters in Clinical Practice. *Oncologist* **2003**, *8*, 411-424.
81. Kovtun, Y. V.; Audette, C. A.; Mayo, M. F.; Jones, G. E.; Doherty, H.; Maloney, E. K.; Erickson, H. K.; Sun, X.; Wilhelm, S.; Ab, O.; Lai, K. C.; Widdison, W. C.; Kellogg, B.; Johnson, H.; Pinkas, J.; Lutz, R. J.; Singh, R.; Goldmacher, V. S.; Chari, R. V., Antibody-maytansinoid conjugates designed to bypass multidrug resistance. *Cancer Res* **2010**, *70* (6), 2528-37.
82. Elgersma, R. C.; Coumans, R. G.; Huijbregts, T.; Menge, W. M.; Joosten, J. A.; Spijker, H. J.; de Groot, F. M.; van der Lee, M. M.; Ubink, R.; van den Dobbelsteen, D. J.; Egging, D. F.; Dokter, W. H.; Verheijden, G. F.; Lemmens, J. M.; Timmers, C. M.; Beusker, P. H., Design, Synthesis, and Evaluation of Linker-Duocarmycin Payloads: Toward Selection of HER2-Targeting Antibody-Drug Conjugate SYD985. *Mol Pharm* **2015**, *12* (6), 1813-35.
83. van der Lee, M. M.; Groothuis, P. G.; Ubink, R.; van der Vleuten, M. A.; van Achterberg, T. A.; Loosveld, E. M.; Damming, D.; Jacobs, D. C.; Rouwette, M.; Egging, D. F.; van den Dobbelsteen, D.; Beusker, P. H.; Goedings, P.; Verheijden, G. F.; Lemmens, J. M.; Timmers, M.; Dokter, W. H., The Preclinical Profile of the Duocarmycin-Based HER2-Targeting ADC SYD985 Predicts for Clinical Benefit in Low HER2-Expressing Breast Cancers. *Mol Cancer Ther* **2015**, *14* (3), 692-703.
84. Wang, Y.; Benz, F. W.; Wu, Y.; Wang, Q.; Chen, Y.; Chen, X.; Li, H.; Zhang, Y.; Zhang, R.; Yang, J., Structural Insights into the Pharmacophore of Vinca Domain Inhibitors of Microtubules. *Mol Pharmacol* **2016**, *89* (2), 233-42.
85. Waight, A. B.; Bargsten, K.; Doronina, S.; Steinmetz, M. O.; Sussman, D.; Prota, A. E., Structural Basis of Microtubule Destabilization by Potent Auristatin Anti-Mitotics. *PLoS One* **2016**, *11* (8), e0160890.
86. Pillow, T. H.; Tien, J.; Parsons-Repointe, K. L.; Bhakta, S.; Li, H.; Staben, L. R.; Li, G.; Chuh, J.; Fourie-O'Donohue, A.; Darwish, M.; Yip, V.; Liu, L.; Leipold, D. D.; Su, D.; Wu, E.; Spencer, S. D.; Shen, B. Q.; Xu, K.; Kozak, K. R.; Raab, H.; Vandlen, R.; Lewis Phillips, G. D.; Scheller, R. H.; Polakis, P.; Sliwkowski, M. X.; Flygare, J. A.; Junutula, J. R., Site-specific trastuzumab maytansinoid antibody-drug conjugates with improved therapeutic activity through linker and antibody engineering. *J Med Chem* **2014**, *57* (19), 7890-9.
87. Hamblett, K. S., P.; Chace, D.; Sun, M.; Lenox, J.; Cerveny, C.; Kissler, K.; Bernhardt, S.; Kopcha, A.; Zabinski, R.; Meyer, D.; Francisco, J., Effects of Drug Loading on the Antitumor Activity of a Monoclonal Antibody Drug Conjugate. *Clin. Can. Res.* **2004**, *10*, 7063-7070.
88. Adem, Y. T.; Schwarz, K. A.; Duenas, E.; Patapoff, T. W.; Galush, W. J.; Esue, O., Auristatin antibody drug conjugate physical instability and the role of drug payload. *Bioconjug Chem* **2014**, *25* (4), 656-64.
89. Simon, L. C.; Sabliov, C. M., The effect of nanoparticle properties, detection method, delivery route and animal model on poly(lactic-co-glycolic) acid nanoparticles biodistribution in mice and rats. *Drug Metab Rev* **2014**, *46* (2), 128-41.
90. Nishijima, N.; Hirai, T.; Misato, K.; Aoyama, M.; Kuroda, E.; Ishii, K. J.; Higashisaka, K.; Yoshioka, Y.; Tsutsumi, Y., Human Scavenger Receptor A1-Mediated Inflammatory Response to Silica Particle Exposure Is Size Specific. *Front Immunol* **2017**, *8*, 379.
91. Kannan, R. M.; Nance, E.; Kannan, S.; Tomalia, D. A., Emerging concepts in dendrimer-based nanomedicine: from design principles to clinical applications. *J Intern Med* **2014**, *276* (6), 579-617.
92. Dirksen, A.; Madsen, M.; Dello Iacono, G.; Matin, M. J.; Bacica, M.; Stankovic, N.; Callans, S.; Bhat, A., Parallel synthesis and screening of peptide conjugates. *Bioconjug Chem* **2014**, *25* (6), 1052-60.
93. Wang, X.; Huang, B.; Liu, X.; Zhan, P., Discovery of bioactive molecules from CuAAC click-chemistry-based combinatorial libraries. *Drug Discov Today* **2016**, *21* (1), 118-32.
94. Loganzo, F.; Tan, X.; Sung, M.; Jin, G.; Myers, J. S.; Melamud, E.; Wang, F.; Diesl, V.; Follettie, M. T.; Musto, S.; Lam, M. H.; Hu, W.; Charati, M. B.; Khandke, K.; Kim, K. S.; Cinque, M.; Lucas, J.; Graziani, E.; Maderna, A.; O'Donnell, C. J.; Arndt, K. T.; Gerber, H. P., Tumor cells chronically treated

with a trastuzumab-maytansinoid antibody-drug conjugate develop varied resistance mechanisms but respond to alternate treatments. *Mol Cancer Ther* **2015**, *14* (4), 952-63.

95. Podbielska, M.; Banik, N. L.; Kurowska, E.; Hogan, E. L., Myelin recovery in multiple sclerosis: the challenge of remyelination. *Brain Sci* **2013**, *3* (3), 1282-324.

96. Karussis, D., Immunotherapy of multiple sclerosis: the state of the art. *BioDrugs* **2013**, *27* (2), 113-48.

97. Meng, Q.; Yu, M.; Zhang, H.; Ren, J.; Huang, D., Synthesis and application of N-hydroxysuccinimidyl rhodamine B ester as an amine-reactive fluorescent probe. *Dyes and Pigments* **2007**, *73* (2), 254-260.

98. Greer, J. M., Autoimmune T-cell reactivity to myelin proteolipids and glycolipids in multiple sclerosis. *Mult Scler Int* **2013**, *2013*, 151427.

99. V K Kuchroo, J. M. G., D Kaul, G Ishioka, A Franco, A Sette, R A Sobel, M B Lees, A single TCR antagonist peptide inhibits experimental allergic encephalomyelitis mediated by a diverse T cell repertoire. *J. Immunol.* **1994**, *153*, 3326-3336.

100. Doronina, S. M., B.; Bovee, T.; Cervený, C.; Alley, S.; Meyer, D.; Oflazoglu, E.; Toki, B.; Sanderson, R.; Zabinski, R.; Wahl, A.; Senter, P., Enhanced Activity of Monomethylauristatin F through Monoclonal Antibody Delivery: Effects of Linker Technology on Efficacy and Toxicity. *Bioconjugate Chem.* **2006**, *17*, 114-124.

101. Trail, P. W., D.; Lasch, S.; Henderson, A.; Hofstead, S.; Casazza, A.; Firestone, R.; Hellström, I.; Hellström, K., Cure of Xenografted Human Carcinomas by BR96-Doxorubicin Immunoconjugates. *Science* **1993**, *261* (5118), 212-215.

102. Chen, Q.; Gabathuler, R., Efficient Synthesis of Doxorubicin Melanotransferrin p97 Conjugates Through SMCC Linker. *Synthetic Communications* **2004**, *34* (13), 2407-2414.

103. Dubowchik, G. W., M., Receptor-mediated and enzyme-dependent targeting of cytotoxic anticancer drugs. *Pharmacology & Therapeutics* **1999**, *83*, 67-123.

104. Kotagiri, N.; Li, Z.; Xu, X.; Mondal, S.; Nehorai, A.; Achilefu, S., Antibody quantum dot conjugates developed via copper-free click chemistry for rapid analysis of biological samples using a microfluidic microsphere array system. *Bioconjug Chem* **2014**, *25* (7), 1272-81.

105. Gonsette, R., Self-tolerance in multiple sclerosis. *Acta Neurol. Belg.* **2012**, *112* (2), 133-140.

106. Carson, M. J.; Doose, J. M.; Melchior, B.; Schmid, C. D.; Ploix, C. C., CNS immune privilege: hiding in plain sight. *Immunol. Rev.* **2006**, *213* (1), 48-65.

107. Fletcher, J. M.; Lalor, S.; Sweeney, C.; Tubridy, N.; Mills, K., T cells in multiple sclerosis and experimental autoimmune encephalomyelitis. *Clin. Exp. Immunol.* **2010**, *162* (1), 1-11.

108. Amor, S.; Puentes, F.; Baker, D.; Van Der Valk, P., Inflammation in neurodegenerative diseases. *Immunology* **2010**, *129* (2), 154-169.

109. Herz, J.; Zipp, F.; Siffrin, V., Neurodegeneration in autoimmune CNS inflammation. *Exp. Neurol.* **2010**, *225* (1), 9-17.

110. Lassmann, H., Mechanisms of inflammation induced tissue injury in multiple sclerosis. *J. Neurol. Sci.* **2008**, *274* (1), 45-47.

111. Grakoui, A.; Bromley, S. K.; Sumen, C.; Davis, M. M.; Shaw, A. S.; Allen, P. M.; Dustin, M. L., The immunological synapse: a molecular machine controlling T cell activation. *Science* **1999**, *285* (5425), 221-227.

112. Iezzi, G.; Karjalainen, K.; Lanzavecchia, A., The duration of antigenic stimulation determines the fate of naive and effector T cells. *Immunity* **1998**, *8* (1), 89-95.

113. Baxter, A. G.; Hodgkin, P. D., Activation rules: the two-signal theories of immune activation. *Nat. Rev. Immunol.* **2002**, *2* (6), 439-446.

114. Bromley, S. K.; Iaboni, A.; Davis, S. J.; Whitty, A.; Green, J. M.; Shaw, A. S.; Weiss, A.; Dustin, M. L., The immunological synapse and CD28-CD80 interactions. *Nat. Immunol.* **2001**, *2* (12), 1159-1166.

115. Chen, L.; Flies, D. B., Molecular mechanisms of T cell co-stimulation and co-inhibition. *Nat. Rev. Immunol.* **2013**, *13* (4), 227-242.

116. Frauwirth, K. A.; Thompson, C. B., Activation and inhibition of lymphocytes by costimulation. *J. Clin. Invest.* **2002**, *109* (109 (3)), 295-299.
117. Jun, J. E.; Goodnow, C. C., Scaffolding of antigen receptors for immunogenic versus tolerogenic signaling. *Nat. Immunol.* **2003**, *4* (11), 1057-1064.
118. Zhang, Q.; Vignali, D. A., Co-stimulatory and co-inhibitory pathways in autoimmunity. *Immunity* **2016**, *44* (5), 1034-1051.
119. Mueller, D. L.; Jenkins, M. K.; Schwartz, R. H., Clonal expansion versus functional clonal inactivation: a costimulatory signalling pathway determines the outcome of T cell antigen receptor occupancy. *Annu. Rev. Immunol.* **1989**, *7* (1), 445-480.
120. Rock, K. L.; Benacerraf, B.; Abbas, A. K., Antigen presentation by hapten-specific B lymphocytes. I. Role of surface immunoglobulin receptors. *J. Exp. Med.* **1984**, *160* (4), 1102-1113.
121. Constant, S. L., B lymphocytes as antigen-presenting cells for CD4+ T cell priming in vivo. *J. Immunol.* **1999**, *162* (10), 5695-5703.
122. Kontos, S.; Grimm, A. J.; Hubbell, J. A., Engineering antigen-specific immunological tolerance. *Curr. Opin. Immunol.* **2015**, *35*, 80-88.
123. Kinzel, S.; Weber, M. S., B Cell-Directed Therapeutics in Multiple Sclerosis: Rationale and Clinical Evidence. *CNS drugs* **2016**, 1-12.
124. Jackson, S. W.; Kolhatkar, N. S.; Rawlings, D. J., B cells take the front seat: dysregulated B cell signals orchestrate loss of tolerance and autoantibody production. *Curr. Opin. Immunol.* **2015**, *33*, 70-77.
125. Khan, W. N.; Wright, J. A.; Kleiman, E.; Boucher, J. C.; Castro, I.; Clark, E. S., B-lymphocyte tolerance and effector function in immunity and autoimmunity. *Immunol. Res.* **2013**, *57* (1-3), 335-353.
126. Boster, A.; Ankeny, D. P.; Racke, M. K., The potential role of B cell-targeted therapies in multiple sclerosis. *Drugs* **2010**, *70* (18), 2343-2356.
127. Oh, S.; Cudrici, C.; Ito, T.; Rus, H., B-cells and humoral immunity in multiple sclerosis. Implications for therapy. *Immunol. Res.* **2008**, *40* (3), 224-234.
128. Bates, D., Treatment effects of immunomodulatory therapies at different stages of multiple sclerosis in short-term trials. *Neurology* **2011**, *76* (1 Supplement 1), S14-S25.
129. Feldmann, M.; Steinman, L., Design of effective immunotherapy for human autoimmunity. *Nature* **2005**, *435* (7042), 612-9.
130. Miller, S. D.; Turley, D. M.; Podojil, J. R., Antigen-specific tolerance strategies for the prevention and treatment of autoimmune disease. *Nat. Rev. Immunol.* **2007**, *7* (9), 665.
131. Jones, D. S., Multivalent compounds for antigen-specific B cell tolerance and treatment of autoimmune diseases. *Curr. Med. Chem.* **2005**, *12* (16), 1887-1904.
132. Ketchum, C.; Miller, H.; Song, W.; Upadhyaya, A., Ligand mobility regulates B cell receptor clustering and signaling activation. *Biophys. J.* **2014**, *106* (1), 26-36.
133. Batista, F. D.; Iber, D.; Neuberger, M. S., B cells acquire antigen from target cells after synapse formation. *Nature* **2001**, *411* (6836), 489-494.
134. Puffer, E. B.; Pontrello, J. K.; Hollenbeck, J. J.; Kink, J. A.; Kiessling, L. L., Activating B cell signaling with defined multivalent ligands. *ACS Chem. Biol.* **2007**, *2* (4), 252-262.
135. Tolar, P.; Sohn, H. W.; Pierce, S. K., The initiation of antigen-induced B cell antigen receptor signaling viewed in living cells by fluorescence resonance energy transfer. *Nat. Immunol.* **2005**, *6* (11), 1168-1176.
136. Harwood, N. E.; Batista, F. D., Early events in B cell activation. *Annu. Rev. Immunol.* **2009**, *28*, 185-210.
137. Getahun, A.; O'Neill, S. K.; Cambier, J. C., Establishing anergy as a bona fide in vivo mechanism of B cell tolerance. *J. Immunol.* **2009**, *183* (9), 5439-5441.
138. Gauld, S. B.; Benschop, R. J.; Merrell, K. T.; Cambier, J. C., Maintenance of B cell anergy requires constant antigen receptor occupancy and signaling. *Nat. Immunol.* **2005**, *6* (11), 1160-1167.
139. Cambier, J. C.; Gauld, S. B.; Merrell, K. T.; Vilen, B. J., B-cell anergy: from transgenic models to naturally occurring anergic B cells? *Nat. Rev. Immunol.* **2007**, *7* (8), 633-643.
140. Mueller, D. L., Mechanisms maintaining peripheral tolerance. *Nat. Immunol.* **2010**, *11* (1), 21-27.

141. Cairo, C. W.; Gestwicki, J. E.; Kanai, M.; Kiessling, L. L., Control of multivalent interactions by binding epitope density. *J. Am. Chem. Soc.* **2002**, *124* (8), 1615-1619.
142. Gestwicki, J. E.; Cairo, C. W.; Strong, L. E.; Oetjen, K. A.; Kiessling, L. L., Influencing receptor-ligand binding mechanisms with multivalent ligand architecture. *J. Am. Chem. Soc.* **2002**, *124* (50), 14922-14933.
143. Kiessling, L. L.; Gestwicki, J. E.; Strong, L. E., Synthetic multivalent ligands in the exploration of cell-surface interactions. *Curr. Opin. Chem. Biol.* **2000**, *4* (6), 696-703.
144. Hartwell, B. L.; Antunez, L.; Sullivan, B. P.; Thati, S.; Sestak, J. O.; Berkland, C., Multivalent Nanomaterials: Learning from Vaccines and Progressing to Antigen-Specific Immunotherapies. *J. Pharm. Sci.* **2015**, *104* (2), 346-361.
145. Krishnamurthy, V. M.; Estroff, L. A.; Whitesides, G. M., Multivalency in ligand design. *Fragment-based approaches in drug discovery* **2006**, *34*, 11-53.
146. Dintzis, H.; Dintzis, R.; Vogelstein, B., Molecular determinants of immunogenicity: the immunon model of immune response. *Proc. Natl. Acad. Sci. U. S. A.* **1976**, *73* (10), 3671-3675.
147. Kiessling, L. L.; Gestwicki, J. E.; Strong, L. E., Synthetic multivalent ligands as probes of signal transduction. *Angew. Chem., Int. Ed.* **2006**, *45* (15), 2348-2368.
148. Hartwell, B. L.; Martinez-Becerra, F. J.; Chen, J.; Shinogle, H.; Sarnowski, M.; Moore, D. S.; Berkland, C., Antigen-Specific Binding of Multivalent Soluble Antigen Arrays Induces Receptor Clustering and Impedes B Cell Receptor Mediated Signaling. *Biomacromolecules* **2016**, *17* (3), 710-722.
149. Hartwell, B. L.; Smalter Hall, A.; Swafford, D.; Sullivan, B. P.; Garza, A.; Sestak, J. O.; Northrup, L.; Berkland, C., Molecular Dynamics of Multivalent Soluble Antigen Arrays Support a Two-Signal Co-delivery Mechanism in the Treatment of Experimental Autoimmune Encephalomyelitis. *Mol. Pharmaceutics* **2016**, *13* (2), 330-343.
150. Northrup, L.; Sestak, J. O.; Sullivan, B. P.; Thati, S.; Hartwell, B. L.; Siahaan, T. J.; Vines, C. M.; Berkland, C., Co-delivery of autoantigen and b7 pathway modulators suppresses experimental autoimmune encephalomyelitis. *AAPS J.* **2014**, *16* (6), 1204-1213.
151. Sestak, J.; Mullins, M.; Northrup, L.; Thati, S.; Forrest, M. L.; Siahaan, T. J.; Berkland, C., Single-step grafting of aminoxy-peptides to hyaluronan: a simple approach to multifunctional therapeutics for experimental autoimmune encephalomyelitis. *J. Controlled Release* **2013**, *168* (3), 334-340.
152. Sestak, J. O.; Fakhari, A.; Badawi, A. H.; Siahaan, T. J.; Berkland, C., Structure, size, and solubility of antigen arrays determines efficacy in experimental autoimmune encephalomyelitis. *AAPS J.* **2014**, *16* (6), 1185-1193.
153. Sestak, J. O.; Sullivan, B. P.; Thati, S.; Northrup, L.; Hartwell, B.; Antunez, L.; Forrest, M. L.; Vines, C. M.; Siahaan, T. J.; Berkland, C., Codelivery of antigen and an immune cell adhesion inhibitor is necessary for efficacy of soluble antigen arrays in experimental autoimmune encephalomyelitis. *Mol. Ther.-Methods Clin. Dev.* **2014**, *1*.
154. Thati, S.; Kuehl, C.; Hartwell, B.; Sestak, J.; Siahaan, T.; Forrest, M. L.; Berkland, C., Routes of administration and dose optimization of soluble antigen arrays in mice with experimental autoimmune encephalomyelitis. *J. Pharm. Sci.* **2015**, *104* (2), 714-721.
155. Anderson, M. E.; Siahaan, T. J., Targeting ICAM-1/LFA-1 interaction for controlling autoimmune diseases: designing peptide and small molecule inhibitors. *Peptides* **2003**, *24* (3), 487-501.
156. Carrasco, Y. R.; Fleire, S. J.; Cameron, T.; Dustin, M. L.; Batista, F. D., LFA-1/ICAM-1 interaction lowers the threshold of B cell activation by facilitating B cell adhesion and synapse formation. *Immunity* **2004**, *20* (5), 589-599.
157. Tibbetts, S. A.; Jois, D. S.; Siahaan, T. J.; Benedict, S. H.; Chan, M. A., Linear and cyclic LFA-1 and ICAM-1 peptides inhibit T cell adhesion and function. *Peptides* **2000**, *21* (8), 1161-1167.
158. Badawi, A.; Kiptoo, P.; Siahaan, T., Immune Tolerance Induction against Experimental Autoimmune Encephalomyelitis (EAE) Using A New PLP-B7AP Conjugate that Simultaneously Targets B7/CD28 Costimulatory Signal and TCR/MHC-II Signal. *J Mult Scler* **2014**, *1* (131), 2376-0389.1000131.
159. Hu, X.; Li, D.; Zhou, F.; Gao, C., Biological hydrogel synthesized from hyaluronic acid, gelatin and chondroitin sulfate by click chemistry. *Acta Biomater.* **2011**, *7* (4), 1618-1626.



160. Di Meo, C.; Panza, L.; Campo, F.; Capitani, D.; Mannina, L.; Banzato, A.; Rondina, M.; Rosato, A.; Crescenzi, V., Novel Types of Carborane-Carrier Hyaluronan Derivatives via “Click Chemistry”. *Macromol. Biosci.* **2008**, *8* (7), 670-681.
161. Dintzis, R.; Middleton, M.; Dintzis, H., Studies on the immunogenicity and tolerogenicity of T-independent antigens. *J. Immunol.* **1983**, *131* (5), 2196-2203.
162. Dintzis, R. Z.; Vogelstein, B.; Dintzis, H. M., Specific cellular stimulation in the primary immune response: experimental test of a quantized model. *Proc. Natl. Acad. Sci. U. S. A.* **1982**, *79* (3), 884-888.
163. Badawi, A. H.; Kiptoo, P.; Wang, W.-T.; Choi, I.-Y.; Lee, P.; Vines, C. M.; Siahaan, T. J., Suppression of EAE and prevention of blood–brain barrier breakdown after vaccination with novel bifunctional peptide inhibitor. *Neuropharmacology* **2012**, *62* (4), 1874-1881.
164. Badawi, A. H.; Siahaan, T. J., Suppression of MOG-and PLP-induced experimental autoimmune encephalomyelitis using a novel multivalent bifunctional peptide inhibitor. *J. Neuroimmunol.* **2013**, *263* (1), 20-27.
165. Kiptoo, P.; Büyüktimkin, B.; Badawi, A.; Stewart, J.; Ridwan, R.; Siahaan, T., Controlling immune response and demyelination using highly potent bifunctional peptide inhibitors in the suppression of experimental autoimmune encephalomyelitis. *Clin. Exp. Immunol.* **2013**, *172* (1), 23-36.
166. Kobayashi, N.; Kobayashi, H.; Gu, L.; Malefy, T.; Siahaan, T. J., Antigen-specific suppression of experimental autoimmune encephalomyelitis by a novel bifunctional peptide inhibitor. *J. Pharmacol. Exp. Ther.* **2007**, *322* (2), 879-886.
167. Manikwar, P.; Tejo, B. A.; Shinogle, H.; Moore, D. S.; Zimmerman, T.; Blanco, F.; Siahaan, T. J., Utilization of I-domain of LFA-1 to Target Drug and Marker Molecules to Leukocytes. *Theranostics* **2011**, *1*, 277.
168. Tang, W.; Becker, M. L., “Click” reactions: a versatile toolbox for the synthesis of peptide-conjugates. *Chem. Soc. Rev.* **2014**, *43* (20), 7013-7039.
169. Sokolova, N. V.; Nenajdenko, V. G., Recent advances in the Cu (i)-catalyzed azide–alkyne cycloaddition: focus on functionally substituted azides and alkynes. *RSC Adv.* **2013**, *3* (37), 16212-16242.
170. Presolski, S. I.; Hong, V. P.; Finn, M., Copper-Catalyzed Azide–Alkyne Click Chemistry for Bioconjugation. *Curr. Protoc. Chem. Biol.* **2011**, 153-162.
171. Presolski, S. I.; Hong, V.; Cho, S.-H.; Finn, M., Tailored ligand acceleration of the Cu-catalyzed azide–alkyne cycloaddition reaction: practical and mechanistic implications. *J. Am. Chem. Soc.* **2010**, *132* (41), 14570-14576.
172. Delon, J.; Germain, R. N., Information transfer at the immunological synapse. *Curr. Biol.* **2000**, *10* (24), R923-R933.
173. Dang, L. H.; Rock, K. L., Stimulation of B lymphocytes through surface Ig receptors induces LFA-1 and ICAM-1-dependent adhesion. *J. Immunol.* **1991**, *146* (10), 3273-3279.
174. Symer, D. E.; Dintzis, R. Z.; Diamond, D. J.; Dintzis, H. M., Inhibition or activation of human T cell receptor transfectants is controlled by defined, soluble antigen arrays. *J. Exp. Med.* **1992**, *176* (5), 1421-1430.
175. Pierce, S. K.; Liu, W., The tipping points in the initiation of B cell signalling: how small changes make big differences. *Nat. Rev. Immunol.* **2010**, *10* (11), 767-777.
176. Penninger, J. M.; Crabtree, G. R., The actin cytoskeleton and lymphocyte activation. *Cell* **1999**, *96* (1), 9-12.
177. Monks, C. R.; Freiberg, B. A.; Kupfer, H.; Sciaky, N.; Kupfer, A., Three-dimensional segregation of supramolecular activation clusters in T cells. *Nature* **1998**, *395* (6697), 82-86.
178. Hartley, S. B.; Crosbie, J., Elimination from peripheral lymphoid tissues of self-reactive B lymphocytes recognizing membrane-bound antigens. *Nature* **1991**, *353* (6346), 765.
179. Fleming, K. K.; Bovaird, J. A.; Mosier, M. C.; Emerson, M. R.; LeVine, S. M.; Marquis, J. G., Statistical analysis of data from studies on experimental autoimmune encephalomyelitis. *J. Neuroimmunol.* **2005**, *170* (1), 71-84.

180. Akdis, M.; Akdis, C. A., Mechanisms of allergen-specific immunotherapy: multiple suppressor factors at work in immune tolerance to allergens. *Journal of Allergy and Clinical Immunology* **2014**, *133* (3), 621-631.
181. Burks, A. W.; Calderon, M. A.; Casale, T.; Cox, L.; Demoly, P.; Jutel, M.; Nelson, H.; Akdis, C. A., Update on allergy immunotherapy: American academy of allergy, asthma & immunology/European academy of allergy and clinical immunology/PRACTALL consensus report. *Journal of Allergy and Clinical Immunology* **2013**, *131* (5), 1288-1296. e3.
182. Sabatos-Peyton, C. A.; Verhagen, J.; Wraith, D. C., Antigen-specific immunotherapy of autoimmune and allergic diseases. *Curr. Opin. Immunol.* **2010**, *22* (5), 609-615.
183. Ho, J. W.; Afshari, N. A., Advances in cataract surgery: preserving the corneal endothelium. *Curr Opin Ophthalmol* **2015**, *26* (1), 22-7.
184. Dikstein, S. M., D., The Metabolic Basis to the Fluid Pump in the Cornea. *J. Physiol.* **1972**, *221*, 29-41.
185. Rosado-Adames, N.; Afshari, N. A., The changing fate of the corneal endothelium in cataract surgery. *Curr Opin Ophthalmol* **2012**, *23* (1), 3-6.
186. Mencucci, R.; Ponchiotti, C.; Virgili, G.; Giansanti, F.; Menchini, U., Corneal endothelial damage after cataract surgery: Microincision versus standard technique. *J Cataract Refract Surg* **2006**, *32* (8), 1351-4.
187. Sugar, J. M., J.; Kraff, M., The Effect of Phacoemulsification on Corneal Endothelial Cell Density. *Arch Ophthalmol* **1978**, *96*, 446-448.
188. Chan, E.; Mahroo, O. A.; Spalton, D. J., Complications of cataract surgery. *Clin Exp Optom* **2010**, *93* (6), 379-89.
189. Cameron, M. P., J.; Aust, S., Identification of free radicals produced during phacoemulsification. *J. Cataract Refract. Surg.* **2001**, *27*, 463-470.
190. Augustin, A. J. D., H. B., Oxidative tissue damage after phacoemulsification: Influence of ophthalmic viscosurgical devices. *J. Cataract Refract. Surg.* **2004**, *30*, 424-427.
191. Espindola, R. F.; Castro, E. F.; Santhiago, M. R.; Kara-Junior, N., A clinical comparison between DisCoVisc and 2% hydroxypropylmethylcellulose in phacoemulsification: a fellow eye study. *Clinics* **2012**, *67* (9), 1059-1062.
192. Auffarth, G. U.; Auerbach, F. N.; Rabsilber, T.; Gegundez, J. A.; Cuina, R.; Renard, Y.; Vinciguerra, P.; Camesasca, F.; Van Cauwenberge, F.; Amzallag, T.; Van Setten, G.; Holzer, M. P., Comparison of the performance and safety of 2 ophthalmic viscosurgical devices in cataract surgery. *J Cataract Refract Surg* **2017**, *43* (1), 87-94.
193. Storr-Paulsen, A.; Norregaard, J. C.; Farik, G.; Tarnhoj, J., The influence of viscoelastic substances on the corneal endothelial cell population during cataract surgery: a prospective study of cohesive and dispersive viscoelastics. *Acta Ophthalmol Scand* **2007**, *85* (2), 183-7.
194. Tognetto, D. C., P.; Ravalico, G., Survey of ophthalmic viscosurgical devices. *Curr Opin Ophthalmol* **2004**, *15*, 29-32.
195. Tomomi Higashide, K. S., Use of viscoelastic substance in ophthalmic surgery – focus on sodium hyaluronate. *Clin Ophthalmol* **2008**, *2* (1), 21-30.
196. Stern, R., Hyaluronan catabolism: a new metabolic pathway. *Eur J Cell Biol* **2004**, *83* (7), 317-25.
197. Slevin, M.; Krupinski, J.; Gaffney, J.; Matou, S.; West, D.; Delisser, H.; Savani, R. C.; Kumar, S., Hyaluronan-mediated angiogenesis in vascular disease: uncovering RHAMM and CD44 receptor signaling pathways. *Matrix Biol* **2007**, *26* (1), 58-68.
198. Liang, J.; Jiang, D.; Noble, P. W., Hyaluronan as a therapeutic target in human diseases. *Adv Drug Deliv Rev* **2016**, *97*, 186-203.
199. Mohan, N. G., V.; Tandon, R.; Gupta, S.; Vajpayee, R., Topical ciprofloxacin–dexamethasone combination therapy after cataract surgery. *J. Cataract Refract. Surg.* **2001**, *27*, 1975-1978.
200. Notivol, R. B., D.; Amin, D.; Whitling, A.; Kennedy, M.; Cockrum, P., Comparison of Topical Tobramycin-Dexamethasone with Dexamethasone-Neomycin-Polymyxin and NeomycinPolymyxin-Gramicidin for Control of Inflammation After Cataract Surgery: Results of a Multicenter,

Prospective, Three-Arm, Randomized, Double-Masked, Controlled, Parallel-Group Study *Clin. Therapeutics* **2004**, *26* (8), 1274-1285.

201. Wang, Q. W.; Yao, K.; Xu, W.; Chen, P. Q.; Shentu, X. C.; Xie, X.; Weng, Y.; Zhang, L.; Jin, C. F.; Wu, W.; Zhu, Y. N.; Yu, Y. H., Bromfenac sodium 0.1%, fluorometholone 0.1% and dexamethasone 0.1% for control of ocular inflammation and prevention of cystoid macular edema after phacoemulsification. *Ophthalmologica* **2013**, *229* (4), 187-94.

202. Saari, K. M.; Nelimarkka, L.; Ahola, V.; Loftsson, T.; Stefansson, E., Comparison of topical 0.7% dexamethasone-cyclodextrin with 0.1% dexamethasone sodium phosphate for postcataract inflammation. *Graefes Arch Clin Exp Ophthalmol* **2006**, *244* (5), 620-6.

203. Faraldi, F.; Papa, V.; Rasa, D.; Santoro, D.; Russo, S., Netilmicin/dexamethasone fixed combination in the treatment of conjunctival inflammation. *Clin Ophthalmol* **2013**, *7*, 1239-44.

204. Russo, S.; Papa, V.; Di Bella, A.; Favero, A.; Radulescu, C.; Gafencu, O.; Carstocea, B.; Milazzo, G., Dexamethasone-netilmicin: a new ophthalmic steroid-antibiotic combination. Efficacy and safety after cataract surgery. *Eye (Lond)* **2007**, *21* (1), 58-64.

205. Larochelle, M. B.; Smith, J.; Dacey, M. S., Dexamethasone Intravitreal Implant in the Treatment of Uveitic Macular Edema in the Perioperative Cataract Setting: A Case Series. *Am J Ophthalmol* **2016**, *166*, 149-53.

206. Augustin, A. J.; Kuppermann, B. D.; Lanzetta, P.; Loewenstein, A.; Li, X. Y.; Cui, H.; Hashad, Y.; Whitcup, S. M.; Ozurdex, M. S. G., Dexamethasone intravitreal implant in previously treated patients with diabetic macular edema: subgroup analysis of the MEAD study. *BMC Ophthalmol* **2015**, *15*, 150.

207. Cagini, C.; Cometa, F.; Torroni, G.; Pellegrino, A.; Pellegrino, R.; Cavallini, G. M., Dexamethasone Disodium Phosphate Penetration Into the Human Aqueous Humor After Topical Application. *Curr Eye Res* **2016**, *41* (7), 897-9.

208. Sokolova, N. V.; Nenajdenko, V. G., Recent advances in the Cu(I)-catalyzed azide-alkyne cycloaddition: focus on functionally substituted azides and alkynes. *RSC Advances* **2013**, *3* (37), 16212.

209. Di Meo, C.; Panza, L.; Campo, F.; Capitani, D.; Mannina, L.; Banzato, A.; Rondina, M.; Rosato, A.; Crescenzi, V., Novel types of carborane-carrier hyaluronan derivatives via "click chemistry". *Macromol Biosci* **2008**, *8* (7), 670-81.

210. Liu, X. Q., L.; Tian, J.; Laquer, F.; Ciborowski, P.; Wang, D., Syntheses of Click PEG-Dexamethasone Conjugates for the Treatment of Rheumatoid Arthritis. *Biomacromolecules* **2010**, *11*, 2621-2628.

211. Liu, X. M.; Quan, L. D.; Tian, J.; Alnouti, Y.; Fu, K.; Thiele, G. M.; Wang, D., Synthesis and evaluation of a well-defined HPMA copolymer-dexamethasone conjugate for effective treatment of rheumatoid arthritis. *Pharm Res* **2008**, *25* (12), 2910-9.

212. Krakovicova, H.; Etrych, T.; Ulbrich, K., HPMA-based polymer conjugates with drug combination. *Eur J Pharm Sci* **2009**, *37* (3-4), 405-12.

213. Choksi, A.; Sarojini, K. V.; Vadnal, P.; Dias, C.; Suresh, P. K.; Khandare, J., Comparative anti-inflammatory activity of poly(amidoamine) (PAMAM) dendrimer-dexamethasone conjugates with dexamethasone-liposomes. *Int J Pharm* **2013**, *449* (1-2), 28-36.

214. Sun, J.; Xiao, C.; Tan, H.; Hu, X., Covalently crosslinked hyaluronic acid-chitosan hydrogel containing dexamethasone as an injectable scaffold for soft tissue engineering. *Journal of Applied Polymer Science* **2013**, *129* (2), 682-688.

215. Zacchigna, M.; Cateni, F.; Di Luca, G.; Voinovich, D.; Perissutti, B.; Drioli, S.; Bonora, G. M., Synthesis of a new mPEG-dexamethasone conjugate and preliminary bioavailability studies in rabbits. *Journal of Drug Delivery Science and Technology* **2008**, *18* (3), 155-159.

216. Bae, Y. C., Y.; Lee, S.; Kang, S.; Kim, Y.; Nam, K.; Park, J.; Lee, M.; Choi, J., Dexamethasone-Conjugated Low Molecular Weight Polyethylenimine as a Nucleus-Targeting Lipopolymer Gene Carrier. *Bioconjugate Chem.* **2007**, *18*, 2029-2036.

217. Crescenzi, V. C., L.; Meo, C.; Nardecchia, S.; Lamanna, R., Novel Hydrogels via Click Chemistry: Synthesis and Potential Biomedical Applications. *Biomacromolecules* **2007**, *8*, 1844-1850.

218. Spitzer, M. S.; Yoeruek, E.; Kaczmarek, R. T.; Sierra, A.; Aisenbrey, S.; Grisanti, S.; Bartz-Schmidt, K. U.; Szurman, P., Sodium hyaluronate gels as a drug-release system for corticosteroids: release kinetics and antiproliferative potential for glaucoma surgery. *Acta Ophthalmol* **2008**, *86* (8), 842-8.
219. Kugelberg, M.; Shafiei, K.; van der Ploeg, I.; Zetterstrom, C., Intraocular lens as a drug delivery system for dexamethasone. *Acta Ophthalmol* **2010**, *88* (2), 241-4.
220. Fiorica, C.; Palumbo, F. S.; Pitarresi, G.; Bongiovi, F.; Giammona, G., Hyaluronic acid and beta cyclodextrins films for the release of corneal epithelial cells and dexamethasone. *Carbohydr Polym* **2017**, *166*, 281-290.
221. Schulze, B.; Schubert, U. S., Beyond click chemistry - supramolecular interactions of 1,2,3-triazoles. *Chem Soc Rev* **2014**, *43* (8), 2522-71.
222. Siliciano, R. C., R.; Keegan, A.; Dintzis, R.; Dintzis, H.; Shin, H., Antigen Valence Determines the Binding of Nominal Antigen to Cytolytic T Cell Clones. *J. Exp. Med.* **1985**, *162*, 768-773.
223. Orski, S. V.; Sheppard, G. R.; Arumugam, S.; Arnold, R. M.; Popik, V. V.; Locklin, J., Rate determination of azide click reactions onto alkyne polymer brush scaffolds: a comparison of conventional and catalyst-free cycloadditions for tunable surface modification. *Langmuir* **2012**, *28* (41), 14693-702.
224. Laradji, A. M.; McNitt, C. D.; Yadavalli, N. S.; Popik, V. V.; Minko, S., Robust, Solvent-Free, Catalyst-Free Click Chemistry for the Generation of Highly Stable Densely Grafted Poly(ethylene glycol) Polymer Brushes by the Grafting To Method and Their Properties. *Macromolecules* **2016**, *49* (20), 7625-7631.
225. Bayramoglu, G.; Celikbicak, O.; Arica, M. Y.; Salih, B., Trypsin Immobilized on Magnetic Beads via Click Chemistry: Fast Proteolysis of Proteins in a Microbioreactor for MALDI-ToF-MS Peptide Analysis. *Industrial & Engineering Chemistry Research* **2014**, *53* (12), 4554-4564.